LBL-2701
c.2 Repl.

LARGE AMPLITUDE MOTION IN MOLECULES

Lawrence Steven Bernstein
(Ph.D. thesis)

May 1974

Prepared for the U. S. Atomic Energy Commission
under Contract 7405-ENG-48

TWO-WEEK LOAN COPY

This is a Library Circulating Copy which may be borrowed for two weeks. For a personal retention copy, call Tech. Info. Division, Ext. 5545

LAWRENCE BERKELEY LABORATORY
UNIVERSITY OF CALIFORNIA
BERKELEY

LBL-2701
c.2 Repl.

DISCLAIMER

This document was prepared as an account of work sponsored by the United States Government. While this document is believed to contain correct information, neither the United States Government nor any agency thereof, nor the Regents of the University of California, nor any of their employees, makes any warranty, express or implied, or assumes any legal responsibility for the accuracy, completeness, or usefulness of any information, apparatus, product, or process disclosed, or represents that its use would not infringe privately owned rights. Reference herein to any specific commercial product, process, or service by its trade name, trademark, manufacturer, or otherwise, does not necessarily constitute or imply its endorsement, recommendation, or favoring by the United States Government or any agency thereof, or the Regents of the University of California. The views and opinions of authors expressed herein do not necessarily state or reflect those of the United States Government or any agency thereof or the Regents of the University of California.

LARGE AMPLITUDE MOTION IN MOLECULES

Contents

ABSTRACT v

I. INTRODUCTION 1

II. INVERSION POTENTIAL FOR A MX_3 (C_{3v}) MOLECULE 4

A. Derivation of the Inversion Potential 4

B. Calculation: Definition of Potential Parameters and Presentation of Computations 18

C. Discussion: Discussion of Computational Results and Comparison to Previous Work 21

III. EQUILIBRIUM AND AXIAL-EQUATORIAL INTERCHANGE POTENTIAL IN $MX_5(D_{3h})$ MOLECULES 27

A. Theory: Derivation of Axial-Equatorial Interchange Potential 27

B. Calculation: Definition of Potential Parameters and Presentation of Results 45

C. Discussion: Discussion of Computational Results and Comparison to Previous Work on Axial-Equatorial Interchange 48

D. Theory: Derivation of Equilibrium Potential and Application to Interpretation of $MX_5(D_{3h})$ Spectra . . 50

IV. RING PUCKERING IN FOUR-MEMBERED, PSEUDO FOUR-MEMBERED, AND FIVE-MEMBERED RINGS 66

A. Derivation of Puckering Potentials for Four-Membered, Pseudo Four-Membered, and Five-Membered Rings 66

B. Comparison of Theoretically Derived Puckering Potentials to Empirically Derived Puckering Potentials 78

V. PSEUDOROTATION IN IF_7 AND ReF_7 87

A. Derivation of Pseudorotation Potentials for IF_7 and ReF_7 87

B. Definition of Coordinate System and Estimate of Some Potential Parameters 99

C. Discussion of Other Work on IF_7 and ReF_7 104

VI. PSEUDOROTATION IN XENON HEXAFLUORIDE (XeF_6) 113

A. Theory: Derivation of the Pseudorotational Potential Function (XeF_6) 113

B. Calculations 132

C. Discussion of the Previous Experimental Work and Refinement of the Potential Function 134

1. Electron Diffraction 134

2. Infrared and Raman Spectra of XeF_6 144

3. Ultraviolet Spectrum of XeF_6 164

4. Thermodynamics of XeF_6 174

5. Electric Field Deflection of XeF_6 182

6. Comparison to Other Theoretical Approaches 182

VII. ELECTRIC FIELD DEFLECTION OF MOLECULES WITH LARGE AMPLITUDE MOTIONS 195

A. Introduction to Electric Field Deflection 195

B. Stark Effect for MX_3 Molecules Undergoing a Double Minimum Vibration 201

C. Stark Effect in MX_7 (IF_7, ReF_7) Molecules 206

D. Stark Effect in XeF_6 (Free Pseudorotation Limit) 209

E. Stark Effect in XeF_6 (Low Angular Barrier Limit) 211

F. Comparison of Theory to Experiment 213

ACKNOWLEDGEMENTS 222

APPENDICES 223

REFERENCES 228

LARGE AMPLITUDE MOTION IN MOLECULES

Lawrence Steven Bernstein

Inorganic Materials Research Division, Lawrence Berkeley Laboratory and Department of Chemistry; University of California, Berkeley, California

ABSTRACT

A pseudo Jahn-Teller formalism is used to construct potential functions for molecules with large amplitude internal motions. The types of molecules studied are MX_3 (C_{3v}, inversion), MX_5 (D_{3h}, axial-equatorial interchange), XeF_6 (distorted O_h, pseudorotation), MX_7 (distorted D_{5h}, pseudorotation), and four-membered, pseudo four-membered, and five-membered rings (ring puckering).

The potential functions for the MX_3 (C_{3v}) molecules have the form

$$V(S) = \frac{1}{2}\Delta\varepsilon_o\,[1-(1+4\alpha^2S^2)^{1/2}] + \frac{1}{2}KS^2$$

where S is the inversion coordinate, and $\Delta\varepsilon_o$, α, K are parameters which are related to structural and electronic factors. With this potential we have determined the barriers to planarity in NH_3(2179 cm^{-1}), PH_3(15736 cm^{-1}), AsH_3(14154 cm^{-1}), and SbH_3(16649 cm^{-1}).

The potential functions for the MX_5 (D_{3h}) molecules have the form

$$V(S) = \frac{1}{2}\Delta\varepsilon_o\,[1-(1+4\alpha^2S^2(1+\beta S)^{1/2}] + \frac{1}{2}KS^2$$

where S is the axial-equatorial interchange coordinate, and $\Delta\varepsilon_o$, α, β, K are parameters related to structural and electronic factors. We have used this potential to calculate the axial-equatorial interchange barriers in PF_5(1224 cm^{-1}), AsF_5(913 cm^{-1}), NbF_5(1210 cm^{-1}), TaF_5(942 cm^{-1}), and VF_5(592 cm^{-1}).

The potential function for XeF_6 (distorted O_h) has the form

$$V(R,\theta,\phi) = -aR^2 + bR^4 - cR^4 \left[\sin^4\theta \left(\frac{\sin^2 2\phi}{4} - 1\right) + \sin^2\theta\right]$$

where R,θ,ϕ are pseudorotational coordinates, and a,b,c are parameters which were determined using experimental data (electron diffraction, infrared and Raman spectra, heat capacity, electric field deflection). The calculated radial barrier in XeF_6 is approximately 1650 cm^{-1}, while the angular barriers fall in the neighborhood of 120 cm^{-1} ($C_{3v} \leftrightarrow C_{2v}$), 240 cm^{-1} ($C_{2v} \leftrightarrow C_{4v}$), and 360 cm^{-1} ($C_{3v} \leftrightarrow C_{4v}$).

For the MX_7 (distorted D_{5h}) molecules the potential has the form

$$V(\rho,\theta) = \frac{1}{2}\Delta\varepsilon_o \left[1-(1+4\alpha^2\rho^2 \ (1+\delta^2\rho^2))^{1/2}\right] + \frac{1}{2}K\rho^2$$

where ρ,θ are pseudorotational coordinates, and $\Delta\varepsilon_o$, α, δ, K are parameters related to structural and electronic factors. The barriers to planarity of the equatorial fluorines were determined for IF_7 (1481 cm^{-1}) and ReF_7 (2236 cm^{-1}).

The potential functions for the four-membered, and pseudo four-membered rings have the form

$$V(S) = \frac{1}{2}\Delta\varepsilon_o\,[1 - (1+4\alpha^2S^2)^{1/2}] + \frac{1}{2}KS^2$$

where S is the puckering coordinate and $\Delta\varepsilon_o$, α, K are parameters related to electronic and structural factors.

The potential function for cyclopentane (five-membered ring) has the form

$$V(\rho,\theta) = \frac{1}{2}\Delta\varepsilon_o\,[1-(1+4\alpha^2\rho^2)^{1/2}] + \frac{1}{2}K\rho^2$$

where ρ,θ are pseudorotational coordinates, and $\Delta\varepsilon_o$, K, α are related to electronic and structural parameters. The barrier to planarity in cyclopentane was calculated to be in the region of 2,300-2,600 cm^{-1}.

The behavior of these molecules with large amplitude motion in inhomogeneous electric fields is also discussed.

I. INTRODUCTION

In recent years, several molecules (XeF_6, IF_7, ReF_7, VF_5) have been synthesized, which exhibit unusual molecular motions not normally expected from relatively simple, highly symmetric inorganic molecules. There has been considerable speculation, particularly for XeF_6, about the nature and the origin of the behavior of these molecules. It has even been proposed that commonly accepted ideas on structure and bonding might have to be abandoned or at least modified to account for the properties of these molecules.

The purpose of this thesis is to demonstrate that these molecules can be adequately, in fact, quantitatively dealt with in the conventional Born-Oppenheimer approximation to molecular theory. The basis of the Born-Oppenheimer approximation is that the nuclear motion is so much slower than the motions of the electrons about the nuclei that the molecular Hamiltonian, H, can be expanded in any desired, complete set of nuclear coordinates (S).

$$H = H_{S_o} + \sum_i \left(\frac{\partial H}{\partial S_i}\right)_{S_o} S_i + \frac{1}{2} \sum_i \sum_j \left(\frac{\partial^2 H}{\partial S_i \partial S_j}\right) S_i S_j + \ldots$$

The first term, H_{So}, is a purely electronic Hamiltonian which represents electrons moving in the potential field due to a fixed nuclear frame (S_o). Once the electronic ground state wavefunction is derived from H_{So}, it can be used to average the complete Hamiltonian, H, over the electronic motion and thus define the effective potential for the

nuclear motion in the ground electronic state. If we assume that H has been expanded about the potential minimum (equilibrium geometry) then averaging H over the ground electronic state will cause the linear terms in S_i to vanish. This is obvious since there would not be a true potential minimum if there were linear terms in S_i. It is the quadratic terms, S_iS_j, which are the leading terms to survive this averaging process. Normally, the description of the nuclear potential stops at these quadratic terms. However, a positive quadratic form for the potential is not adequate to explain large amplitude motions or the existence of several identical potential minima separated by large displacements in coordinate space.

The approach taken in this work is to include the effects of excited electronic states which can couple to the ground electronic state via the linear term in the expanded form of H. Although the linear term vanishes in its average over the ground electronic state, it will contribute second order and higher order terms to the nuclear potential because of nonzero, off diagonal terms between the ground electronic state and excited electronic states used as electronic basis functions in which to evaluate the matrix of the linear terms, $(\partial H/\partial S_i)_{So}$ Si. It will be seen that the contribution of the linear terms to the nuclear potential accounts nicely for the unusual aspects of the molecules mentioned previously. This treatment of the linear terms is often referred to as the pseudo Jahn-Teller approach.[1,2,3,4]

In order to demonstrate the validity, and the generality of the pseudo Jahn-Teller approach we have treated the more familiar double minimum problem of the NH_3 like molecules (NH_3, AsH_3, PH_3, SbH_3) from this point of view. We have also applied it to a quite different type of large amplitude nuclear motion, puckering of four-membered, pseudo four-membered, and five-membered rings. The fact that this formalism accounts so well for the properties of these more completely understood systems lends a large measure of credibility to its application in the more novel molecules (IF_7, ReF_7, XeF_6, VF_5).

II. INVERSION POTENTIAL FOR A MX_3 (C_{3v}) MOLECULE

A. Derivation of the Inversion Potential

The inversion potential for MX_3 (C_{3V}) molecules can be determined as follows. Expand the vibronic Hamiltonian (H_v) about a D_{3h} reference configuration in a complete set of symmetry coordinates (Fig. 2).

$$H_v = H_{vS_o} + \sum_K \left(\frac{\partial H_v}{\partial S_K}\right)_{S_o} S_K + \frac{1}{2}\sum_K\sum_L \left(\frac{\partial^2 H_v}{\partial S_K \partial S_L}\right)_{S_o} S_K S_L + \ldots \qquad (1)$$

Determine the eigenstates of H_{vS_o}, which is a pure electronic Hamiltonian representing electrons moving in a D_{3h} potential due to a fixed nuclear framework.

$$H_{vS_o}|\psi_n\rangle = \varepsilon_n|\psi_n\rangle \qquad n = 0,1,2,\ldots \qquad (2)$$

The zeroeth order vibrational potential can be determined for the electronic ground state, $|\psi_o\rangle$.

$$V_o(S) = \langle\psi_o|H_v|\psi_o\rangle = \varepsilon_o + \sum_K \langle\psi_o|\left(\frac{\partial H_v}{\partial S_K}\right)_{S_o}|\psi_o\rangle S_K + \frac{1}{2}\sum_K\sum_L \langle\psi_o|\left(\frac{\partial^2 H_v}{\partial S_K \partial S_L}\right)_{S_o}|\psi_o\rangle S_K S_L + \ldots \qquad (3)$$

For nondegenerate electronic states the linear term in S_K vanishes. This can be understood by finding the representations generated by $|\psi_o\rangle$ and $\left(\frac{\partial H_v}{\partial S_K}\right)_{S_o}$ in the D_{3h} point group. We have

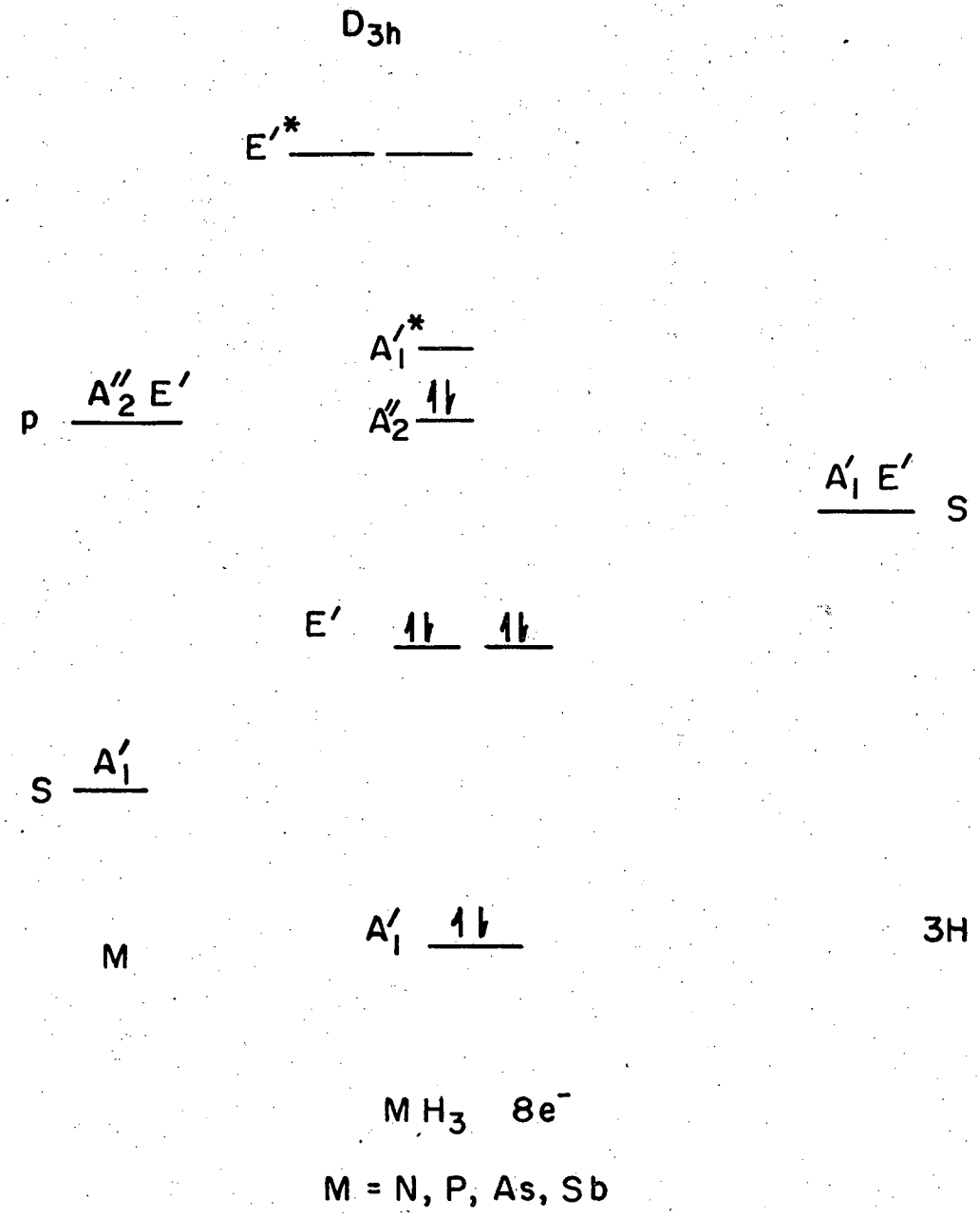

XBL744-6143

Fig. 1. Molecular orbital diagram for MH_3 molecules.

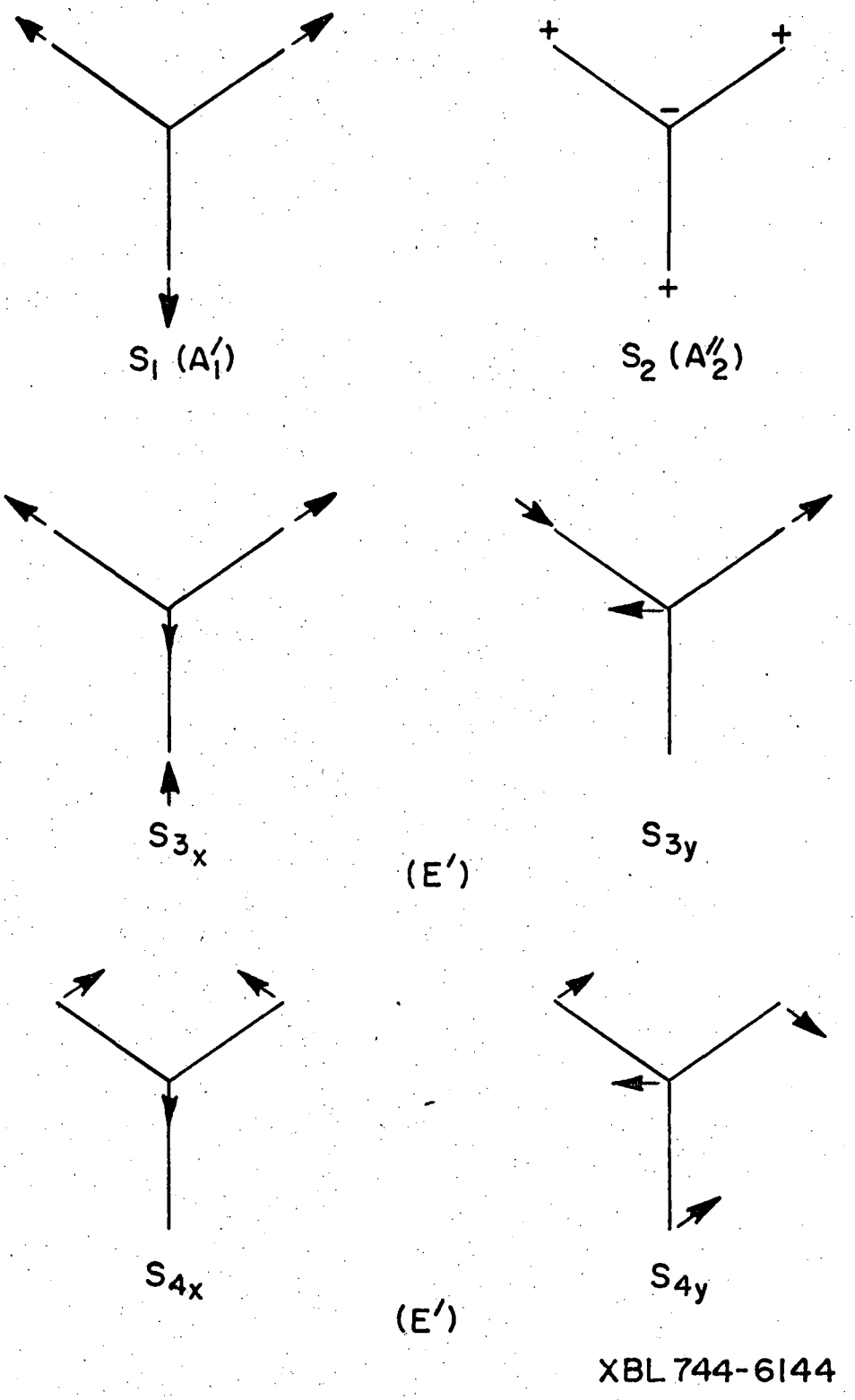

Fig. 2. Symmetry coordinates for $MX_3(D_{3h})$ molecules.

$$\Gamma_{\left(\frac{\partial H_v}{\partial S_K}\right)_{S_o}} = \Gamma_{S_K} \qquad \Gamma_{\psi_o} = \Gamma_{A_1'} \quad \text{(Fig. 1)} \tag{4}$$

where Γ is an irreducible representation of the D_{3h} point group. For the linear matrix element to be nonvanishing requires that the direct product of the representations involved contain A_1' .

$$\Gamma_{\psi_o} \times \Gamma_{\left(\frac{\partial H_v}{\partial S_K}\right)_{S_o}} \times \Gamma_{\psi_o} = A_1' \times \Gamma_{S_K} \times A_1' = \Gamma_{S_K} \tag{5}$$

We can conclude that the only possible nonzero linear matrix elements can occur when Γ_{S_K} equals A_1' . Because totally symmetric motions ($S_{A_1'}$) change only the dimensions but not the symmetry of the molecule we can arbitrarily move along a totally symmetric coordinate ($S_{A_1'}$) without affecting the results of the preceeding discussion. We can take advantage of this by choosing the dimensions of the reference configuration to yield,

$$\langle \psi_{A_1'} | \left(\frac{\partial H_v}{\partial S_{A_1'}}\right)_{S_o} | \psi_{A_1'} \rangle = 0 \tag{6}$$

where for symmetry reasons alone a zero result is not required. This now makes all the linear terms vanish and the potential (3) simplifies to

$$V_o(S) = \varepsilon_o + \frac{1}{2} \sum_K \sum_L C_{KL} S_K S_L \tag{7}$$

where

$$C_{KL} = \langle \psi_o | \left(\frac{\partial^2 H_v}{\partial S_K \partial S_L} \right)_{S_o} | \psi_o \rangle \tag{7a}$$

This is nothing more than the quadratic approximation used as the starting point for a normal coordinate analysis. Since we are seeking a potential of the double minimum type, and the purely quadratic potential in Eq. (7) is not of that form, the zeroeth order approximation to the ground state potential (3) is clearly not adequate. The next step is to include the effect of higher electronic states on the linear term. We are interested in terms of the form

$$\langle \psi_{A_1'} | \left(\frac{\partial H_v}{\partial S_K} \right)_{S_o} | \psi_n \rangle \quad n > 0 \tag{8}$$

One might expect that the most important contributions come from the lowest electronic states of the proper symmetry. The proper symmetry is defined by

$$\Gamma_{\psi_{A_1'}} \times \Gamma_{\left(\frac{\partial H_v}{\partial S_K}\right)_o} \times \Gamma_{\psi_n} = A_1' \times \Gamma_{S_K} \times \Gamma_{\psi_n} = \Gamma_{S_K} \times \Gamma_{\psi_n} = A_1' \tag{9}$$

This will only be true when Γ_{S_K} equals Γ_{ψ_n}. From the molecular orbital diagram (Fig. 1) we see that the first excited state is $\Psi_{1_{A_2''}}$, where the triplet state $\Psi_{3_{A_2''}}$ is excluded from consideration

because of the orthogonality of its spin function to the singlet spin of the ground state. The $\psi_{1A_1'}$ and $\psi_{1A_2''}$ can be coupled by any symmetry coordinate transforming as $\Gamma_{S_{A_2''}}$ (9). Examining the symmetry coordinates for $MX_3(D_{3h})$ molecules (Fig. 2) shows that there is a mode transforming as A_2''. Furthermore, this is identical to the motion involved in the inversion of $MX_3(C_{3v})$ molecules. The contribution of this excited electronic state to the potential can now be calculated by diagonalizing the following matrix

$$\begin{array}{c c} & \begin{array}{cc} |\psi_{1A_1'}\rangle & |\psi_{1A_2''}\rangle \end{array} \\ \begin{array}{c} |\psi_{1A_1'}\rangle \\ |\psi_{1A_2''}\rangle \end{array} & \begin{pmatrix} -\varepsilon & a\,S_2 \\ a\,S_2 & bS_1 + \Delta\varepsilon_o - \varepsilon \end{pmatrix} \end{array} \tag{10}$$

where a, b, and $\Delta\varepsilon_o$ are defined by

$$a = \langle \psi_{1A_1'} | \left(\frac{\partial H_v}{\partial S_2}\right)_{S_o} | \psi_{1A_2''} \rangle \tag{11a}$$

$$b = \langle \psi_{1A_2''} | \left(\frac{\partial H_v}{\partial S_1}\right)_{S_o} | \psi_{1A_2''} \rangle \tag{11b}$$

$$\Delta\varepsilon_o = \varepsilon_{1A_2''} - \varepsilon_{1A_1'} = \varepsilon_{1A_2''} \tag{11c}$$

where we can define $\varepsilon_{1A_1'} = 0$

The eigenvalues of Eq. (10) are

$$\varepsilon = \frac{1}{2}\,[(\Delta\varepsilon_o+bS_1) \pm (\Delta\varepsilon_o+bS_1)(1+4a^2S_2^2/(\Delta\varepsilon_o+bS_1)^2)^{1/2}] \qquad (12)$$

The presence of the symmetrical stretching coordinate S_1 in addition to the inversion mode S_2 allows an analytic description of the change in bond length (M-X) in going from the planar to the pyramidal form. Only a small change in bond length would be expected, since the symmetry and nature of the bonding do not change much during the inversion. This assumption is quantitatively justified by SCF calculations on NH_3 [5] and PH_3.[6]. If we now ignore the coupling of S_1 to S_2 by setting b equal to zero the eigenvalue simplifies to

$$\varepsilon_L = (\tfrac{1}{2})\ [\Delta\varepsilon_o - \Delta\varepsilon_o\ (1+4\alpha^2S_2^2] \qquad \alpha = \frac{a}{\Delta\varepsilon_o} \qquad (13)$$

where ε_L represents the lower root of Eq. (12) because we are interested in the ground state vibrational potential. The augmented ground state potential is

$$V(S) = \varepsilon_L + V_o(S) \qquad (14)$$

Because ε_L involves only S_2 the other coordinates in $V_o(S)$ can be ignored, leaving just the inversion potential,

$$V(S_2) = \frac{1}{2}\,[\Delta\varepsilon_o - \Delta\varepsilon_o(1+4\alpha^2S_2^2)^{1/2}] + (\tfrac{1}{2})C_2\ S_2^2 \qquad (15)$$

Expansion of the first term in Eq. (15) yields

$$\varepsilon_L \approx -\alpha^2 \Delta\varepsilon_o \, S_2^{\,2} + \alpha^4 \Delta\varepsilon_o \, S_2^{\,4} + \ldots \tag{16}$$

We can define a truncated potential by

$$V_{Trunc}(S_2) = (-\alpha^2 \Delta\varepsilon_o + \frac{C_2}{2}) \, S_2^{\,2} + \alpha^4 \Delta\varepsilon_o S_2^{\,4} \tag{17}$$

If the following situation occurs

$$\alpha^2 \Delta\varepsilon_o > C_2/2 \tag{18}$$

the truncated potential has the special form

$$V_{Trunc}(S_2) = -aS_2^{\,2} + bS_2^{\,4} \tag{19}$$

with

$$a = \alpha^2 \Delta\varepsilon_o - C_2/2 \tag{19a}$$

and

$$b = \alpha^4 \Delta\varepsilon_o \tag{19b}$$

This shows both that the more complicated potential (15) has the proper symmetry (double minima) to express the inversion, and also that in the limit of $1 \gg 4\alpha^2 S_2^{\,2}$ the expansion (17) is valid and the potential takes a very simple form (19).

Now that the form of the inversion potential has been established in Eqs. (15 and 19) it remains to give the various parameters a quantitative meaning. Working first with Eq. (15), values are needed for $\Delta\varepsilon_o$, α, and C_2. $\Delta\varepsilon_o$ can be found from the ultraviolet absorption spectrum of the MH_3 molecules[7,8,9] and is just the $^1A_1' \rightarrow {}^1A_2''$ transition. Strictly speaking $\Delta\varepsilon_o$ is the excitation with respect to the planar form (D_{3h}) and what is observed experimentally is $\Delta\varepsilon_o^{C_{3v}}$. The correction of $\Delta\varepsilon_o^{C_{3v}}$ to $\Delta\varepsilon_o^{D_{3h}}$ will be discussed later. Values for C_2, the force constant for the A_2'' motion in the (hypothetical) D_{3h} configuration, and α, the linear matrix element, can be established by the following procedure. Take the first derivative of the potential (15) and set it equal to zero at the minimum (C_{3v}) and maximum (D_{3h}) (Fig. 3).

$$\frac{\partial V}{\partial S_2} = -2\,\Delta\varepsilon_o\alpha^2(1 + 4\alpha^2 S_2^{\,2})^{-1/2}\, S_2 + C_2 S_2 = 0 \qquad (20)$$

This yields

$$S_2 = 0 \qquad D_{3h} \text{ maximum} \qquad (20a)$$

$$-2\Delta\varepsilon_o\alpha^2(1 + 4\alpha^2 S_2^{\,2})^{-1/2} + C_2 = 0 \quad \text{at the } C_{3v} \text{ minimum } (S_2 = S_o) \qquad (20b)$$

The second derivative must equal the curvature (K_o) at the C_{3v} configuration (S_o).

$$\frac{\partial^2 V}{\partial S_2^{\,2}} = -2\Delta\varepsilon_o\alpha^2(1+4\alpha^2 S_2^{\,2})^{-1/2} + 8\Delta\varepsilon_o\alpha^4(1+4\alpha^2 S_2^{\,2})^{-3/2}\, S_2^{\,2} + C_2 = K_o \qquad (21)$$

$$\text{at } S_2 = S_o$$

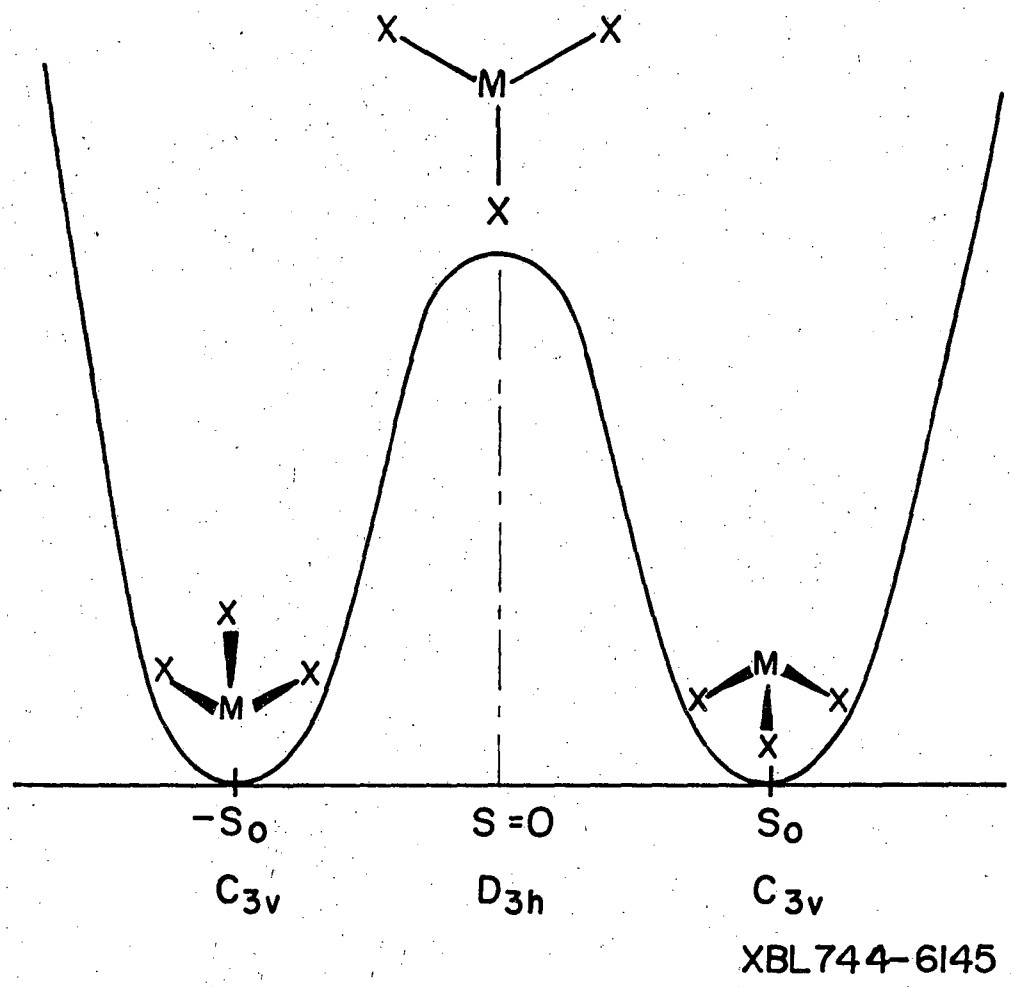

Fig. 3. Double minimum potential along the $S_2(A_2'')$ path.

K_o can be approximated by the A_2'' force constant in the actual C_{3v} conformation. To obtain the true K_o, the force constant, which is based on a normal coordinate analysis, must be corrected for anharmonicity effects. This correction will be discussed later. Equations (20b) and (21) can be solved simultaneously to yield α and C_2.

$$\frac{\alpha^4}{(1 + 4\alpha^2 S_o^2)^{3/2}} = \frac{K_o}{8\Delta\varepsilon_o S_o^2} \tag{22a}$$

Solve Eq. (22a) iteratively for α, then C_2 is

$$C_2 = 2\Delta\varepsilon_o \alpha^2 \, (1 + 4\alpha^2 S_o^2)^{-1/2} \tag{22b}$$

The same analysis can be applied to the truncated potential (19) to define the constants a, and b.

$$a = \frac{K_o}{4} \qquad b = \frac{K_o}{8S_o^2} \tag{23}$$

We return now to the correction of $\Delta\varepsilon_o^{D_{3h}}$ and K_o. The relationship between $\Delta\varepsilon_o^{D_{3h}}$ and $\Delta\varepsilon_o^{C_{3v}}$ can be visualized as in Fig. 5. NH_3 is known to have a planar excited state[3] ($^1A_2''$) while the remaining molecules have a pyramidal excited state.[3] Then the correction for NH_3 is

$$\Delta\varepsilon_o^{D_{3h}} = \Delta\varepsilon_o^{C_{3v}} - \delta_1 - \delta_2 \tag{24}$$

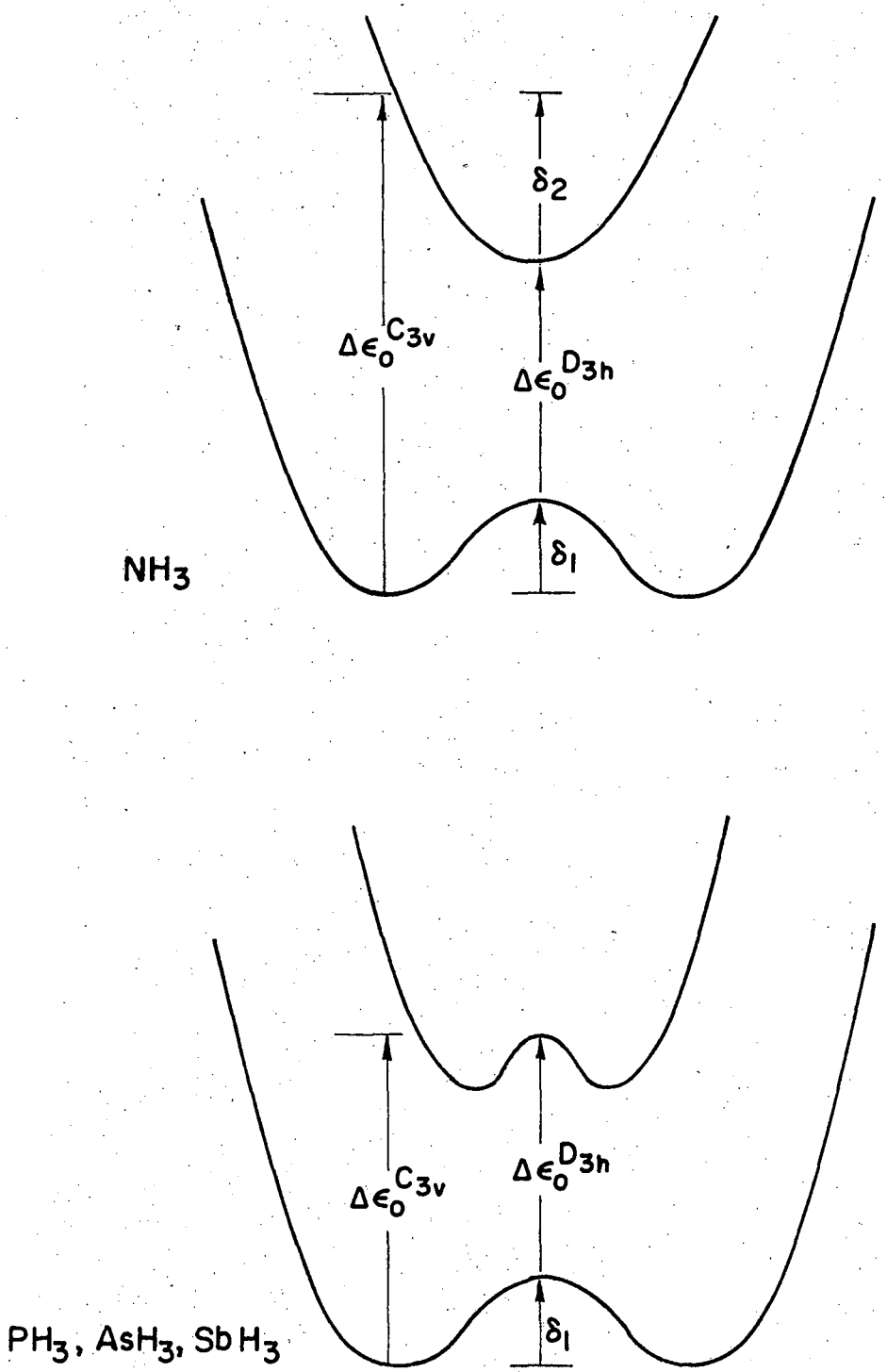

XBL 744-6147

Fig. 5. Relationship of $\Delta\varepsilon_o^{C_{3v}}$ to $\Delta\varepsilon_o^{D_{3h}}$ in MH_3 molecules.

where δ_1 is just the barrier height and δ_2 is the energy required to bend the excited state from the ground state pyramidal geometry to the planar form. δ_2 is known from spectroscopic measurements[7] and has a value of 5400 cm^{-1}. For PH_3, AsH_3, SbH_3 we have

$$\Delta\varepsilon_o^{D_{3h}} \approx \Delta\varepsilon_o^{C_{3v}} - \delta_1 \tag{25}$$

where we have assumed δ_2 is less important than in the NH_3 case due to the nonplanar excited state. $\Delta\varepsilon_o^{D_{3h}}$ can now be corrected in an iterative manner. Using the initial guess of the potential, where it was assumed $\Delta\varepsilon_o^{D_{3h}} = \Delta\varepsilon_o^{C_{3v}}$, calculate the barrier height and apply Eq. (25). This can be repeated until the correction becomes negligible. The justification for this procedure is that $\Delta\varepsilon_o^{C_{3v}}(\sim 10^4\ cm^{-1})$ is roughly an order of magnitude larger than the barrier height ($\sim 10^3\ cm^{-1}$) in MH_3 molecules.

The correction of K_o for anharmonicity is more involved than the $\Delta\varepsilon_o^{D_{3h}}$ adjustment. The initial assumption is that

$$K_o = C_2^{C_{3v}} \tag{26}$$

where $C_2^{C_{3v}}$ is the A_2'' force constant in the actual C_{3v} configuration. The usual method of calculating $C_2^{C_{3v}}$ is by a normal coordinate analysis in which the $0 \rightarrow 1$ ($V_{A_2''}$) transition is assumed to be entirely harmonic. Using this K_o in the potential and calculating $V_{0\rightarrow1}^{calc}$ one would find $V_{0\rightarrow1}^{calc} < V_{0\rightarrow1}^{exp}$ because of the anharmonicity of the potential.

An iterative correction procedure is possible if we assume the true harmonic contribution to $V_{0\to1}^{exp}$ is given by

$$V_{0\to1}^{har(1)} = V_{0\to1}^{exp} + (V_{0\to1}^{exp} - V_{0\to1}^{calc(1)}) \quad \text{for the first iteration} \tag{27a}$$

thereafter

$$V_{0\to1}^{har(i)} = V_{0\to1}^{har(i-1)} + (V_{0\to1}^{exp} - V_{0\to1}^{calc(i)}) \quad \text{for the i'th iteration } (i>1) \tag{27b}$$

We can now correct k_o.

$$k_o = C_2^{C_{3v}} \frac{(V_{0\to1}^{har(i)})^2}{(V_{0\to1}^{exp})^2} \tag{28}$$

This adjustment can be repeated until the difference $(V_{0\to1}^{exp} - V_{0\to1}^{calc(i)})$ is negligible. It should be stressed that after each iteration on either k_o or $\Delta\varepsilon_o^{D_{3h}}$ one must re-evaluate Eqs. (22a, 22b) or (23) to obtain the corrected potential function.

B. Calculation: Definition of Potential Parameters and Presentation of Computations

The inversion coordinate S_2 is defined by[10]

$$S_2^{\beta} = \sqrt{3}\ r\ (\beta-\beta_{D_{3h}}) = \sqrt{3}\ r\Delta\beta \tag{29}$$

where r is the M-X bond length and β is the angle of an M-X bond with respect to a planar configuration (Fig. 4). Because the literature values of the C_{3v} force constant ($C_2^{C_{3v}}$) are based on the coordinate[10]

$$S_2^{\alpha} = \sqrt{3}\ r\ (\alpha-\alpha_{C_{3v}}) = \sqrt{3}\ r\Delta\alpha \quad \text{(Fig. 4)} \tag{30}$$

we must adjust $C_{2_{\Delta\alpha}}^{C_{3v}}$ to our inversion coordinate S_2^{β}. The reason for changing coordinates from S_2^{α} to S_2^{β} is the anomalous behavior of Δα in the neighborhood of the planar conformation. Δα does not change sign in passing through the planar form, which means it does not have the proper symmetry to express the inversion process. However, if the equilibrium structure is not too close to D_{3h}, Δα is suitable for expressing small equilibrium displacements. The relationship between $C_{2_{\Delta\alpha}}^{C_{3v}}$ and $C_{2_{\Delta\beta}}^{C_{3v}}$ in the region of the equilibrium structure (C_{3v}) is

$$C_{2_{\Delta\beta}}^{C_{3v}} = C_{2_{\Delta\alpha}}^{C_{3v}} \left(\frac{d\Delta\alpha}{d\Delta\beta}\right)^2_{C_{3v}} \tag{31}$$

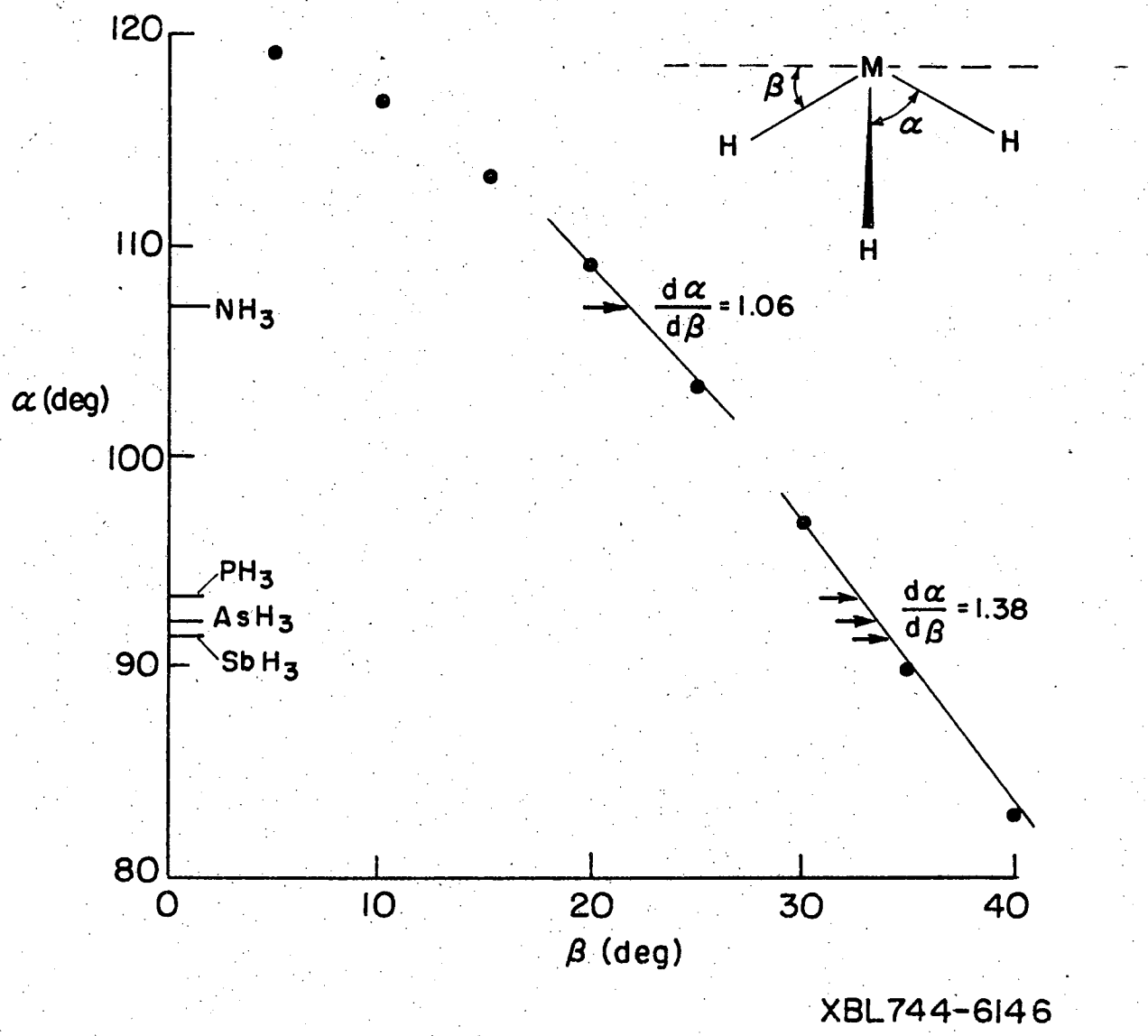

Fig. 4. Plot of α versus β for MX_3 molecules.

A similar relationship exists between the reduced mass based on the two coordinates.

$$m_2^{\Delta\beta} = m_2^{\Delta\alpha} \left(\frac{d\Delta\alpha}{d\Delta\beta}\right)^2_{C_{3v}} \tag{32}$$

The value of $(d\Delta\alpha/d\Delta\beta)_{C_{3v}}$ for a specific molecule can be determined from the slope of a plot of α versus β (Fig. 4). The reduced masses used in the calculations were based on Wilson's[11,12] high frequency approximation. In this case the high frequency was taken as the A_1 stretch and the low frequency as the A_1 bend, relative to the C_{3v} form (App. 1). The actual force constants ($C_{2\Delta\beta}^{C_{3v}}$) used in the calculations were based on the derived masses (32).

$$C_{2\Delta\beta}^{C_{3v}} = (5.9 \times 10^{-7})\ (\nu_{0\to1}^{exp})^2 m_2^{\Delta\beta} \tag{33}$$

$\nu_{0\to1}^{exp}$ is entered in (cm^{-1}), and $m_2^{\Delta\beta}$ in (amu) then $C_{2\Delta\beta}^{C_{3v}}$ will be in (mdyn/A^o). Formula (33) is just a rearrangement of the familiar $h\nu = \frac{1}{2}\ (\frac{K}{m})^{1/2}$, which shows how the frequency of a harmonic oscillator is determined by its force constant (K) and mass (m). The appropriate experimental[13] information used as input to the potential function can be found in Table 1.

The energy levels calculated from the potential were obtained by computer diagonalization of the vibrational Hamiltonian in a 40-member harmonic oscillator basis set. The final results can be found in Tables 2 and 3. In Table 2 we see that it took 3 iterations to converge on the final NH_3 potential, while for all the other

molecules almost exact agreement between $\nu_{0\to1}^{calc}$ and $\nu_{0\to1}^{exp}$ was obtained on the first iteration. Because of the relatively small barrier in NH_3 compared to $\nu_{0\to1}^{exp}$ we would expect a large anharmonicity correction while for the other molecules the well is so deep that it is very nearly harmonic about the potential minima. A small correction (3 cm^{-1}) to $\nu_{0\to1}^{calc}$ in PH_3 could be made, however it would not significantly alter the indicated parameters.

C. Discussion: Discussion of Computational Results and Comparison to Previous Work

For the MH_3 series we have found that the parameters α, and S_o^{β} are very close to unity (Table 2). Therefore the condition for using the truncated potential ($1 \gg 4\alpha^2 S_2^{\,2}$) is not met. This is why only the full potential (16) was used in the calculations.

It is interesting to compare the various potentials used to describe NH_3 inversion[14,15,16] with the one derived in this work. These include

$$V(S) = \frac{1}{2}\,[\Delta\varepsilon_o - \Delta\varepsilon_o(1 + \alpha^2 S^2)^{1/2}] + \frac{1}{2}\,C_2 S^2 \quad \text{(This work)} \tag{34a}$$

$$V(S) = -\,C\,\mathrm{sech}^2\left(\frac{S}{2p}\right) + D\,\mathrm{sech}^4\left(\frac{S}{2p}\right) \quad \text{(Manning)}^{14} \tag{34b}$$

$$V(S) = K(a + bS^2)^2/(1 + S^2)^2 \quad \text{(Newton)}^{15} \tag{34c}$$

$$V(S) = \frac{1}{2}\,a\,S^2 + \frac{1}{2}\,b\,S^4 + \nu\,\exp(-cS^2) \quad \text{(Swalen)}^{16} \tag{34d}$$

where S is the inversion coordinate. In Manning's potential C, p and D are arbitrary constants which were adjusted to obtain the best fit to the available experimental energy levels. The arbitrary constants K, a, and b in Newton's potential were fit to the first four levels of NH_3 with extra weighting given to the $0_S \rightarrow 0_A$ splitting. This accounts for Newton's success at fitting $0_S \rightarrow 0_A$ while not managing as well with the $1_S \rightarrow 1_A$ transition (Table 3). In Swalen's potential the four constants a, b, v, and c, and also the reduced mass were least squares fit to the first fourteen energy levels in NH_3.

The potential used here (34a) differs greatly in form and concept from its predecessors (34b,c,d). Both Manning and Newton picked their particular form to obtain a reasonably easy to solve form for the Schrödinger equation. Swalen chose his very flexible potential in order to get a very exact fit to the energy levels (Table 3), and hence closely approximate the true potential. In this work the parameters of the potential have a direct physical interpretation (see theory p.12), and more importantly the form of the potential is not arbitrary but derived, with various approximations, from the exact non-relativistic Hamiltonian. This suggests that if one treated the constants $m_{\Delta\beta}^{C_{3v}}$, α, $\Delta\varepsilon_o$ and $C_2^{D_{3h}}$ as arbitrary one could probably obtain a fit as good or better than Swalen's five parameter potential.

We have focused our discussion primarily on NH_3 simply because a comparable amount of experimental and theoretical information is not available for the other MH_3 (PH_3, AsH_3, SbH_3) molecules. The absence of an observable inversion splitting in the lower levels of these

molecules makes it impossible to fit an arbitrary double minimum potential to the data in order to obtain an estimate of the barrier height. In this work detailed experimental information (inversion splittings) is not needed and we have calculated the inversion potentials for the entire MH_3 series (Table 2). The best available data on the inversion potential in the molecules other than NH_3 is an SCF calculation on PH_3 [6] in which the barrier height was calculated to be 13,012 cm^{-1}. We calculate the PH_3 barrier to be 15,736 cm^{-1} (Table 2). A recent SCF calculation on NH_3 [5] placed the barrier at 2,589 cm^{-1} compared to the best experimental determination (Swalen) of 2,018 cm^{-1}. This is a difference of about 25%. In view of the NH_3 case it is not unreasonable that the two calculated barriers for PH_3 differ by approximately 20%.

Table 1. Experimental Data for MH_3 Molecules

	$\Delta\beta_{C_{3v}}$ (DEG)	r_{M-H} (Å)	s_o^{β} (Å)	$V_{0\to1}^{exp}$ (cm^{-1})	$m_2^{\Delta\beta}$ (amu)	$C_{2_{\Delta\beta}}^{C_{3v}}$ ($\frac{mdyn}{Å}$)	$\Delta\varepsilon_o^{C_{3v}}$ (mdyn-Å)
NH_3	21.8	1.011	.669	950	.832	.443	1.024
PH_3	32.4	1.419	1.390	991	.951	.551	1.103
AsH_3	33.6	1.523	1.549	906	.951	.412	1.085
SbH_3	34.0	1.712	1.764	782	.951	.343	1.008

Table 2. Refined Parameters for MH_3 Potential Function

	$\alpha(Å^{-1})$	$\varepsilon_o^{D_{3h}}$(mdyn-Å)	$k_o(\frac{mdyn}{Å})$	$C_2^{D_{3h}}(\frac{mdyn}{Å})$	$E_{Barrier}(cm^{-1})$	$V_{0\to1}^{calc}(cm^{-1})$	$V_{0\to1}^{exp}(cm^{-1})$
	.826	.881	.443	.806	1,787	859.5	950
NH_3	.897	.873	.531	.890	2,226	961.6	950
	.890	.873	.522	.890	2,179	951.4	950
PH_3	1.121	.792	.551	.608	15,736	988	991
AsH_3	.936	.807	.412	.461	14,154	904	906
SbH_3	1.010	.671	.343	.370	16,649	782	782

Table 3. Comparison of Observed and Computed Properties of NH_3

	Obs.	This Work	Manning[14]	Swalen[15]	Newton[16]
Barrier (cm^{-1})		2179	2072	2018	2225
0_S	0.00	0.00	0.00	0.00	0.00
0_A	0.79	0.78	0.83	0.83	0.79
1_S	932.5	938	935	930	933
1_A	968.3	965	961	966	956
2_S	1597.6	1660	1610	1596	
2_A	1910	1892	1870	1882	
3_S	2383.5	2410	2360	2385	
3_A	2895.5	2891	2840	2897	

III. EQUILIBRIUM AND AXIAL-EQUATORIAL INTERCHANGE POTENTIAL IN $MX_5(D_{3h})$ MOLECULES

A. Theory: Derivation of Axial-Equatorial Interchange Potential

In this chapter on MX_5 molecules our attention will be focused on two areas. The first is the axial-equatorial interchange potential. The second is the nature of the potential in the neighborhood of the equilibrium structure and its relation to interpretation of infrared and Raman spectra.

The symmetry coordinates for a MX_5 molecule of D_{3h} symmetry are shown in Fig. 1. From an examination of these coordinates we might expect that a proper combination of the axial bend (S_7) with the equatorial bend (S_6) would lead to interchange of the axial X atoms with two equatorial X atoms. This path is indicated in Fig. 2. By symmetry there are two more paths equivalent to the one in Fig. 2, which can be constructed by ± 120° rotations about the C_3 axis. Therefore, from any given D_{3h} structure there are three neighboring equivalent structures differing only in the permutation of the X atoms. Altogether there are ten identical D_{3h} structures differing only by permutation of X. The relationship of these ten conformations to one another is schematically outlined in Fig. 3.

The construction of the potential energy surface corresponding to Fig. 3 is accomplished in a similar manner to that discussed in the first chapter. By analogy the major consideration becomes - what excited electronic states are coupled to the ground state via an E' symmetry coordinate? The key to unlocking this question lies in

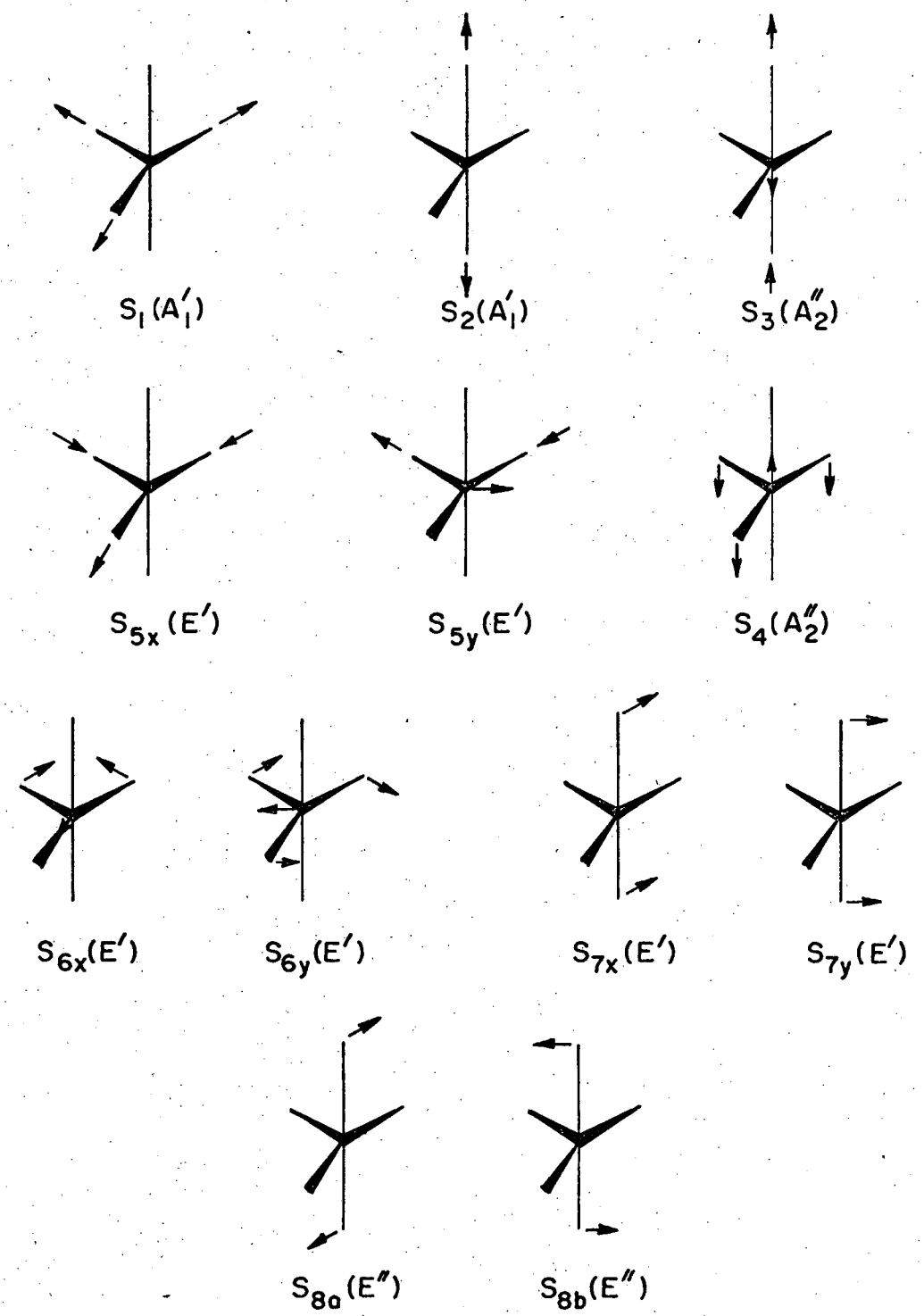

Fig. 1. Symmetry coordinates for $MX_5(D_{3h})$ molecules.

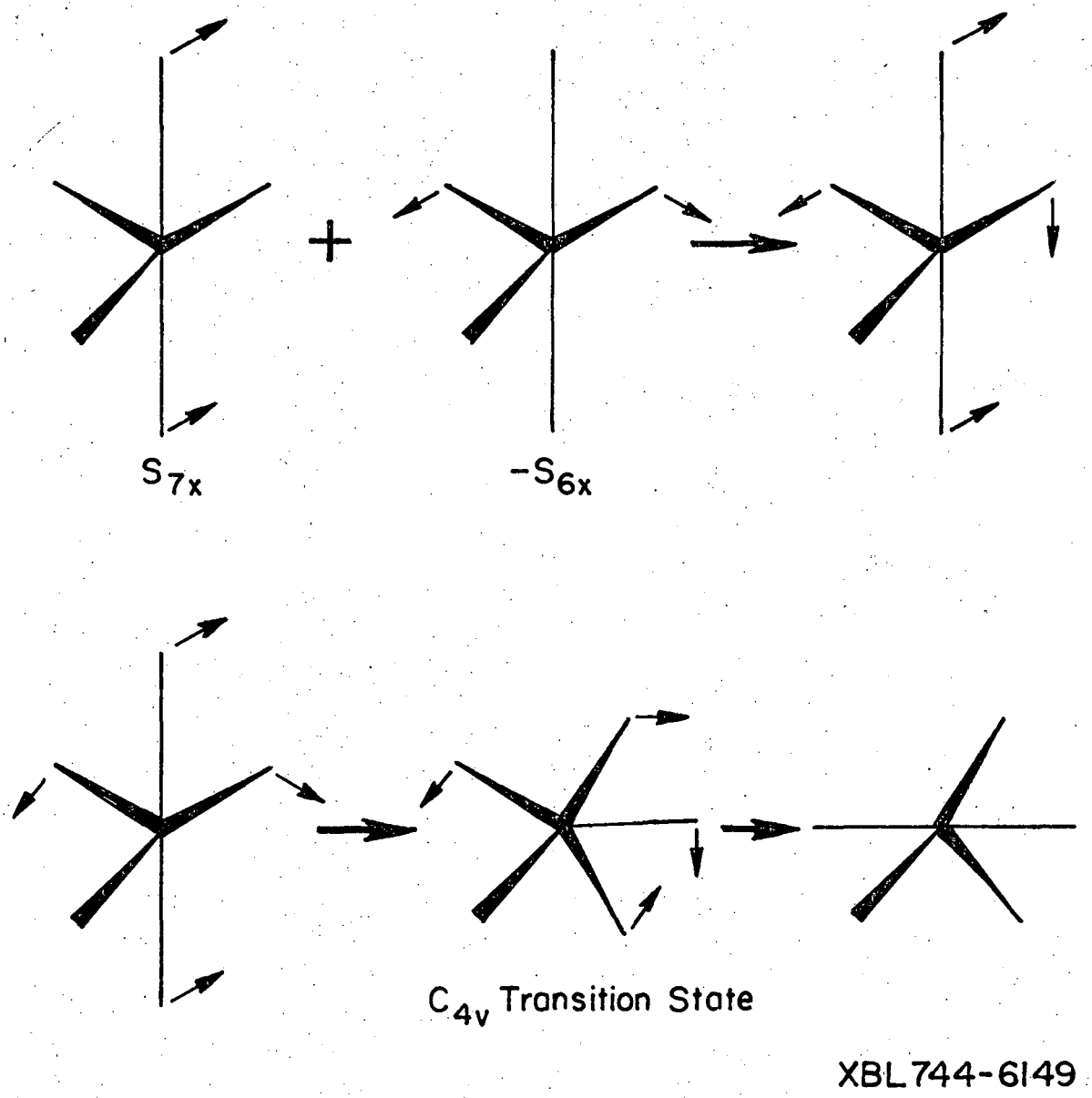

Fig. 2. Path of axial-equatorial interchange in $MX_5(D_{3h})$ molecules.

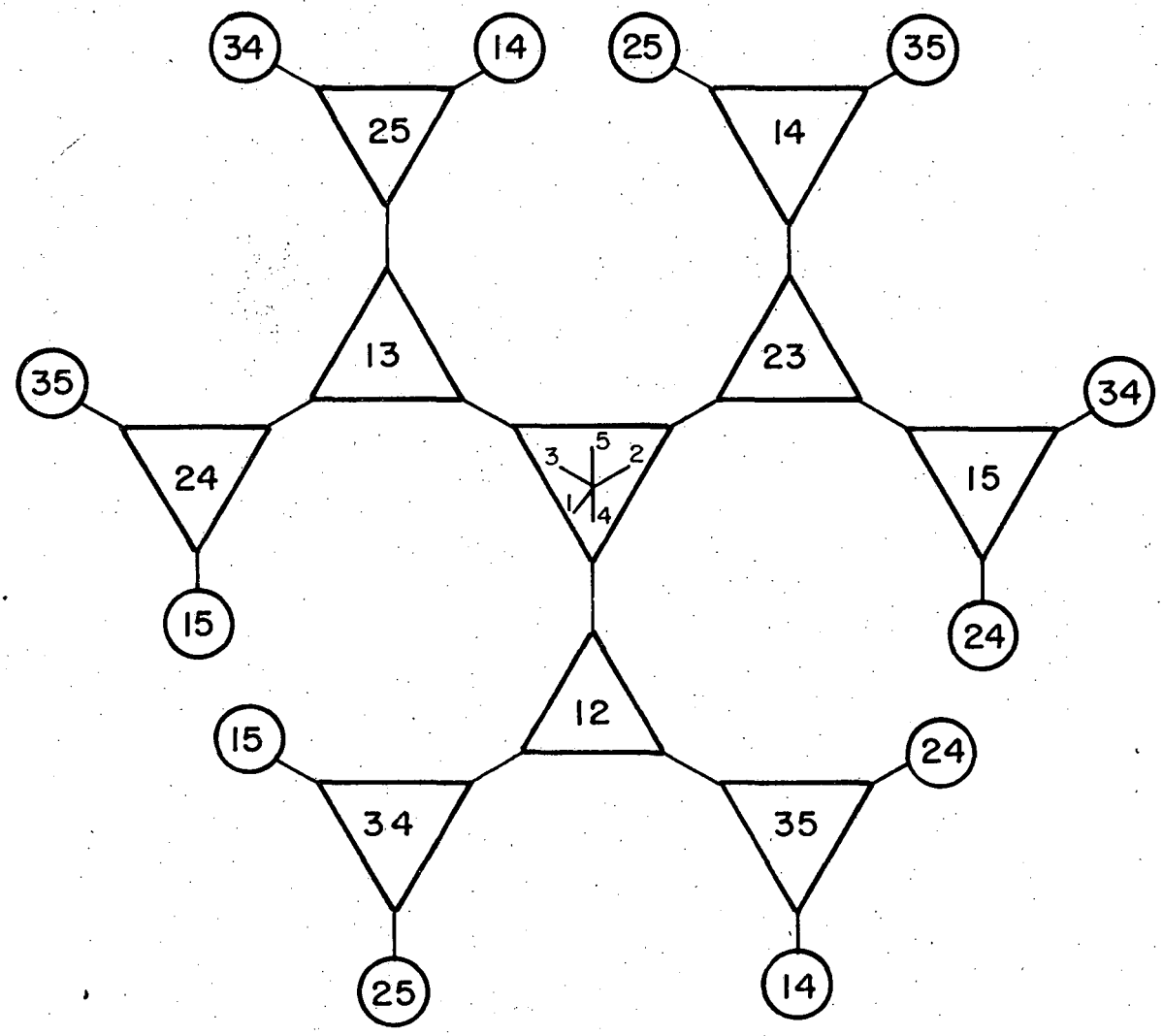

XBL 744-6150

Fig. 3. Relationship of the ten equivalent D_{3h} configurations obtained by interchanging axial and equatorial X atoms. Each new configuration is represented by its two axial atoms. Numbers in the circles show that after the ten unique permutations (triangles) are exhausted previous permutations are obtained.

studying the molecular orbital diagrams found in Figs. 4 and 5. We see that in both cases (Figs. 4,5) the ground state has symmetry $^1A_1'$, which means only excited states of $^1E'$ symmetry can couple to the ground state via the E' coordinate. From the molecular orbital diagrams it is clear that there are many possible excited states of $^1E'$ symmetry. Our task is to find the one that contributes the most to the interchange process. We can narrow the possibilities if we consider the interchange path in more detail than indicated in Fig. 2. From normal coordinate analysis[17,18] it is found that the axial bend (ν_7) occurs at much lower frequency than the equatorial bend (ν_6) in all of the MX_5 molecules (Table 1). This implies that up to the C_{4v} transition state (Fig. 2) the axial bend contributes most to the exchange mode. Past the C_{4v} intermediate the other motion (S_6) must predominate in order to reach another D_{3h} configuration. However, we can view the S_6 coordinate as an axial bend originating from the neighboring D_{3h} configuration. In this sense the axial bend is the predominant motion on either side of the C_{4v} intermediate. From a molecular orbital viewpoint we are looking for excited molecular orbitals which can lend bonding character to the axial fluorines as they progress to the C_{4v} transition state. That is, we seek to increase the overlap of the wavefunctions localized on the axial fluorines with orbitals localized on the central atom. With these considerations the most reasonable choice is the $A_2'' \rightarrow E''$ transition. The A_2'' orbital is mainly the antisymmetric combination of $2p_z$ functions on the axial fluorines. The E'' orbitals are the d_{xz} and d_{yz} orbitals on the central atom, which

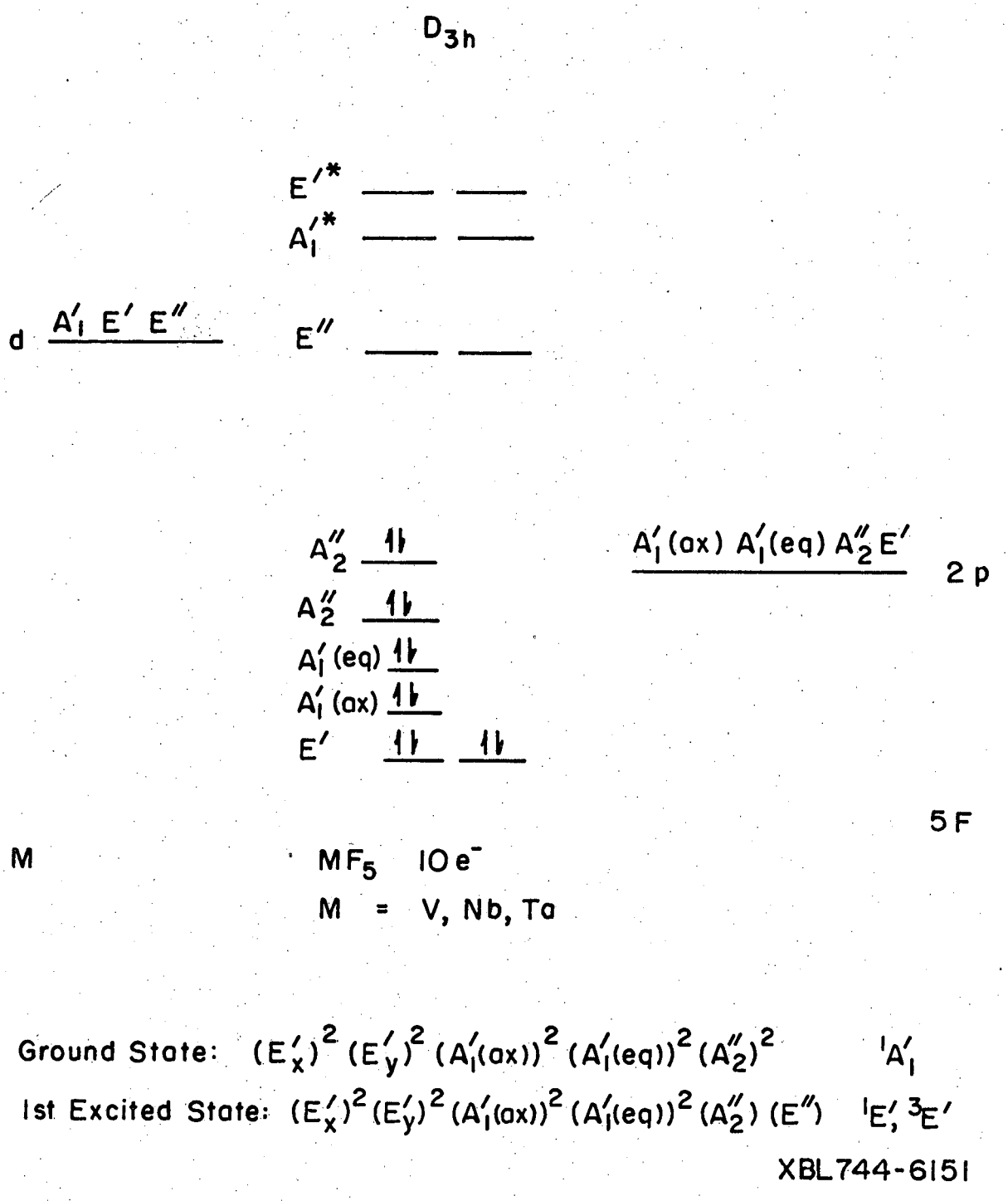

Fig. 4. Molecular orbital diagram for MF_5 molecules of the VF_5 type.

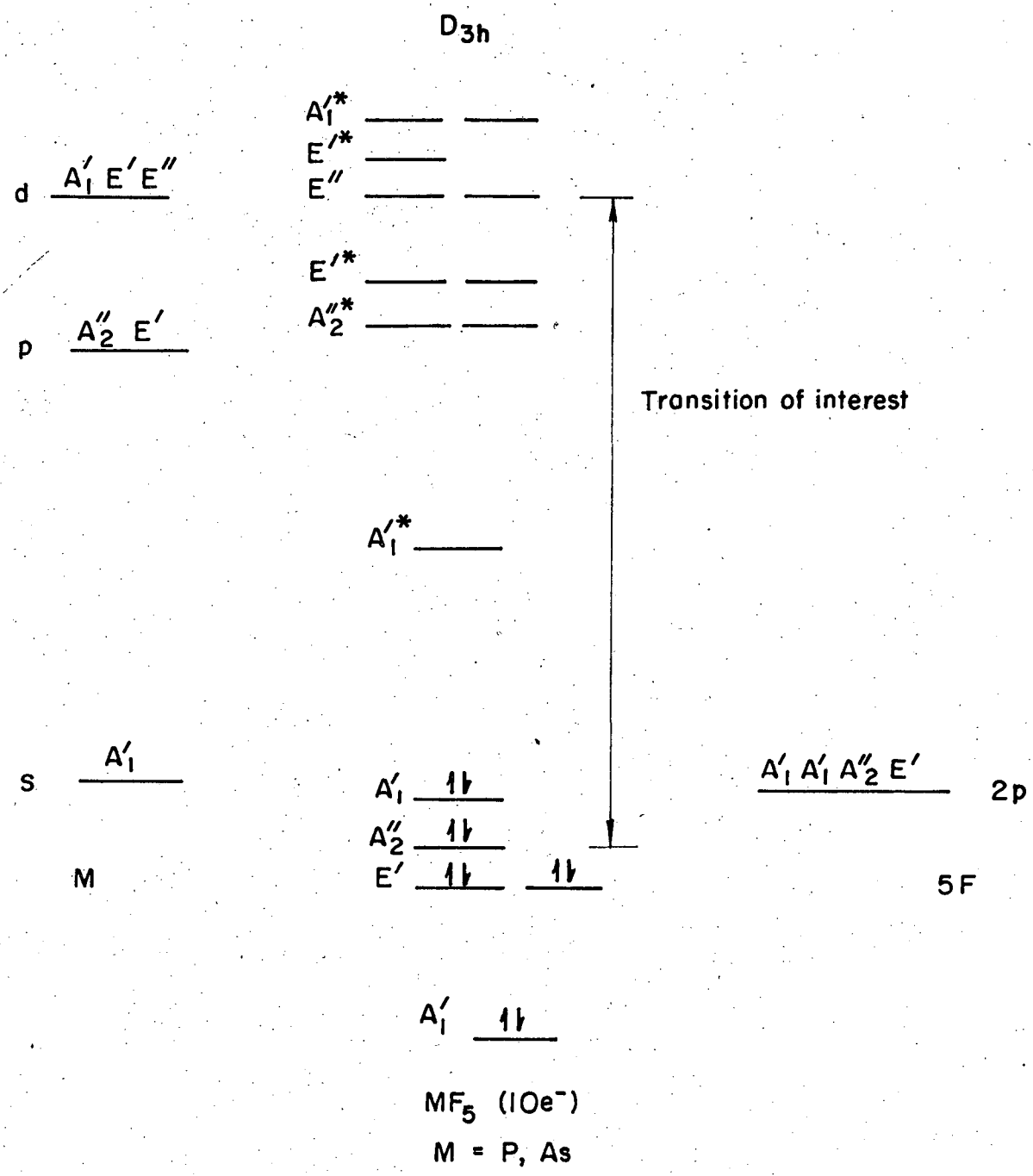

Ground State: $(A_1')^2(E_x')^2(E_y')^2(A_2'')^2(A_1')^2$ $^1A_1'$

Excited State of "Interest": $(A_1')^2(E_x')^2(E_y')^2(A_2'')^2(A_1')^2(E'')$ $^1E''$, $^3E''$

XBL744-6152

Fig. 5. Molecular orbital diagram for MF_5 molecules of the PF_5 type.

can provide some bonding character to intermediate configurations. This is shown pictorially in Fig. 6.

Using the states, $|^1A_1'\rangle$, $|^1E_x'\rangle$, $|^1E_x'\rangle$, and $|^1E_y'\rangle$ as our basis states we can construct the matrix of the linear term.

$$H_{linear} = \frac{\partial H_v}{\partial S_{E_x'}} S_{E_x'} + \frac{\partial H_v}{\partial S_{E_y'}} S_{E_y'} \tag{1}$$

Recalling that there are four coorindates of E' symmetry, S_{6x}, S_{7x} transforming as E_x' and S_{6y}, S_{7y} as E_y', we can cast the matrix in the form

$$\begin{array}{c} \\ |^1A_1'\rangle \\ |^1E_x'\rangle \\ |^1E_y'\rangle \end{array} \begin{array}{c} \begin{array}{ccc} |^1A_1'\rangle & |^1E_x'\rangle & |^1E_y'\rangle \end{array} \\ \begin{pmatrix} -\varepsilon & aS_{7x}+bS_{6x} & aS_{7y}+bS_{6y} \\ aS_{7x}+bS_{6x} & cS_{7x}+dS_{6x}+\Delta\varepsilon_o-\varepsilon & eS_{7y}+fS_{6y} \\ aS_{7y}+bS_{6y} & eS_{7y}+fS_{6y} & -cS_{7x}-dS_{6x}+\Delta\varepsilon_o-\varepsilon \end{pmatrix} \end{array} \tag{2}$$

where a, b, c, d, e, f and $\Delta\varepsilon_o$ are defined by

$$a = \langle {}^1A_1'| \left(\frac{\partial H_v}{\partial S_{7x}}\right)_{S_o} |^1E_x'\rangle = \langle {}^1A_1'| \left(\frac{\partial H_v}{\partial S_{7y}}\right)_{S_o} |^1E_y'\rangle \tag{2a}$$

$$b = \langle {}^1A_1'| \left(\frac{\partial H_v}{\partial S_{6x}}\right)_{S_o} |^1E_x'\rangle = \langle {}^1A_1'| \left(\frac{\partial H_v}{\partial S_{6y}}\right)_{S_o} |^1E_y'\rangle \tag{2b}$$

$$c = \langle {}^1E_x'| \left(\frac{\partial H_v}{\partial S_{7x}}\right)_{S_o} |^1E_x'\rangle = \langle {}^1E_y'| \left(\frac{\partial H_v}{\partial S_{7x}}\right)_{S_o} |^1E_y'\rangle \tag{2c}$$

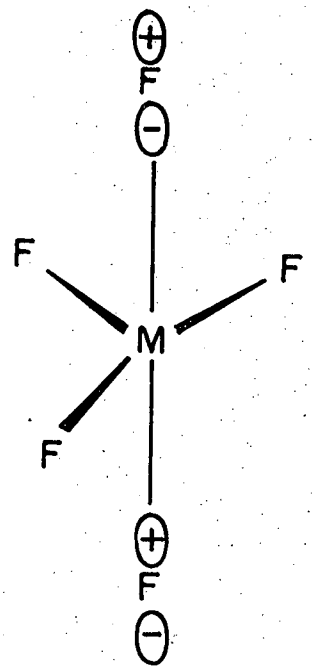

A_2'' (F_{2p_z})

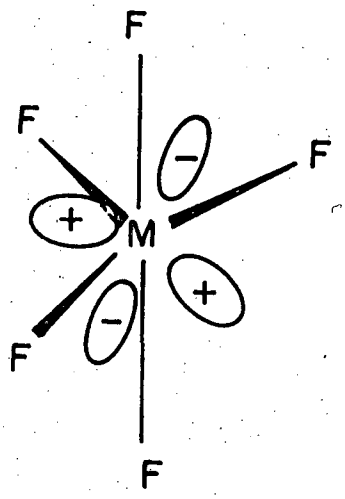

E'' (d_{xz})

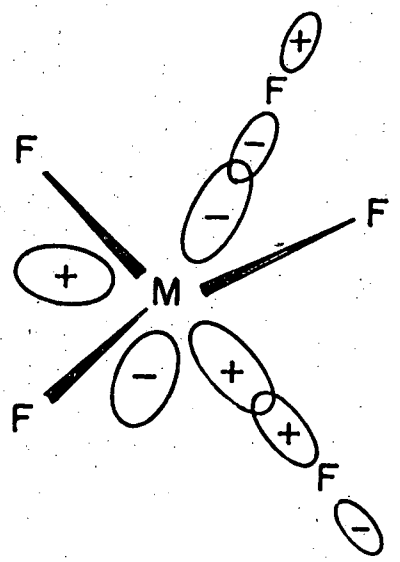

Stabilized Intermediate

XBL744-6153

Fig. 6. Stabilization of intermediate forms by mixing of A_2'' and E" orbitals.

$$d = \langle {}^1E'_x | \left(\frac{\partial H_v}{\partial S_{6x}}\right)_{S_o} | {}^1E'_x \rangle = \langle {}^1E'_y | \left(\frac{\partial H_v}{\partial S_{6x}}\right)_{S_o} | {}^1E'_y \rangle \tag{2d}$$

$$e = \langle {}^1E'_x | \left(\frac{\partial H}{\partial S_{7y}}\right)_{S_o} | {}^1E'_y \rangle \quad f = \langle {}^1E'_x | \left(\frac{\partial H}{\partial S_{6_y}}\right)_{S_o} | {}^1E'_y \rangle \tag{2e}$$

$$\Delta\varepsilon_o = \varepsilon_{{}^1E'} - \varepsilon_{{}^1A'_1} = \varepsilon_{{}^1E'} \tag{2f}$$

where we can define $\varepsilon_{{}^1A'_1} = 0$. Although they have not been included in Eq. (2) there are nonvanishing matrix elements involving the totally symmetric coordinate $S_{A'_1}$. Since we do not expect a large change in bond length during the interchange process the dependence on $S_{A'_1}$ will be ignored. Because of the threefold symmetry about each configuration (Fig. 3) we can confine our attention to one of the three equivalent paths connecting a particular permutation to its neighbors. For convenience we will choose the path diagrammed in Fig. 2, which means we can set S_{6y}, and S_{7y} equal to zero. The matrix Eq. (2) becomes

$$\begin{array}{c} \\ |{}^1A'_1\rangle \\ |{}^1E'_x\rangle \\ |{}^1E'_y\rangle \end{array} \begin{array}{c} \begin{array}{ccc} |{}^1A'_1\rangle & |{}^1E'_x\rangle & |{}^1E'_y\rangle \end{array} \\ \begin{pmatrix} -\varepsilon & aS_{7x} + bS_{6x} & 0 \\ aS_{7x} + bS_{6x} & cS_{7x} + dS_{6x} + \Delta\varepsilon_o - \varepsilon & 0 \\ 0 & 0 & -cS_{7x} - dS_{6x} + \Delta\varepsilon_o - \varepsilon \end{pmatrix} \end{array} \tag{3}$$

Because this matrix is block factored we can focus on the upper submatrix which contains the lowest root.

$$\begin{array}{cc} & \begin{array}{cc} |^1A_1'\rangle & |^1E_x'\rangle \end{array} \\ \begin{array}{c} |^1A_1'\rangle \\ |^1A_x'\rangle \end{array} & \begin{pmatrix} -\varepsilon & aS_{7x} + bS_{6x} \\ aS_{7x} + bS_{6x} & cS_{7x} + dS_{6x} + \Delta\varepsilon_o - \varepsilon \end{pmatrix} \end{array} \tag{4}$$

The eigenvalues of Eq. (4) are

$$\varepsilon = \frac{1}{2}\left[(\Delta\varepsilon_o + cS_{7x} + dS_{6x}) \pm (\Delta\varepsilon_o + cS_{7x} + dS_{6x})\left(1 + \frac{4(aS_{7x}+bS_{6x})^2}{(\Delta\varepsilon_o + cS_{7x} + dS_{6x})^2}\right)^{1/2}\right] \tag{5}$$

If the assumption is made that $\Delta\varepsilon_o \gg (cS_{7x}+dS_{6x})$ over the range of the distortions involved, Eq. (5) simplifies to

$$\varepsilon_{low} = \frac{1}{2}\Delta\varepsilon_o\left[1 - \left(1 + \frac{4}{\Delta\varepsilon_o^2}(aS_{7x}+bS_{6x})^2\left(1 - \frac{2}{\Delta\varepsilon_o}(cS_{7x}+dS_{6x})\right)\right)^{1/2}\right] \tag{6}$$

where we have displayed the lowest eigenvalue, because we are interested in the ground state vibrational potential. Including the quadratic terms the full interchange potential becomes

$$V(S_{6x}, S_{7x}) = \varepsilon_{low} + \frac{1}{2}C_7 S_{7x}^2 + \frac{1}{2}C_6 S_{6x}^2 \tag{7}$$

If we expand ε_{low} about S_{7x}, S_{6x} equal to zero, the leading term coupling S_{6x} to S_{7x} has the form

$$-\frac{ab}{\Delta\varepsilon_o} S_{7x} S_{6x} \tag{8}$$

This implies that close to the origin S_{6x} follows S_{7x} in a linear fashion. We can see this by requiring the interchange potential (7) to be at a minimum in S_{6x} for each value of S_{7x}.

$$\frac{\partial V}{\partial S_{6x}} \approx -\frac{ab}{\Delta\varepsilon_o} S_{7x} + C_6 S_{6x} = 0$$

$$S_{6x} = \frac{ab}{\Delta\varepsilon_o C_6} \tag{9}$$

The linear coupling approximation in Eq. (9) is physically reasonable because (i) it is the leading term coupling S_{6x} to S_{7x} and (ii) it should dominate higher order coupling terms close to the equilibrium position (in the region before the C_{4v} intermediate). Substitution of the linear coupling approximation (9) back into the potential (7) leads to the final form

$$V(S_{7x}) = (\tfrac{1}{2})\Delta\varepsilon_o [1 - (1 + 4\alpha^2 S_{7x}^2 (1 + \beta S_{7x}))^{1/2}] + (\tfrac{1}{2}) K S_{7x}^2 \tag{10}$$

where α, β, and K are constants to be determined later.

We have succeeded in reducing what was originally a four dimensional problem, Eq. (2), to a parametric potential in one dimension (S_{7x}). The interplay between S_{6x} and S_{7x} is visually displayed in Fig. 7. We see that P_1 is the shortest path between adjacent D_{3h} conformations. This path is one in which both the S_{6x} and S_{7x} coordinates change at equal rates throughout the interchange. This path can be eliminated from consideration because it is experimentally determined that the axial bend is energetically lower than the equatorial bend (Table 1). Thus, at least close to the D_{3h} configuration the slope must be smaller than that indicated for P_1. P_3 represents the opposite extreme in which S_{7x} changes completely to its new D_{3h} value while S_{6x} remains static. This, of course, is physically unreasonable. The actual path is determined by the coupling of S_{6x} and S_{7x}, Eq. (9), and is linear insofar as the coupling is dominated by the first term in the expansion of

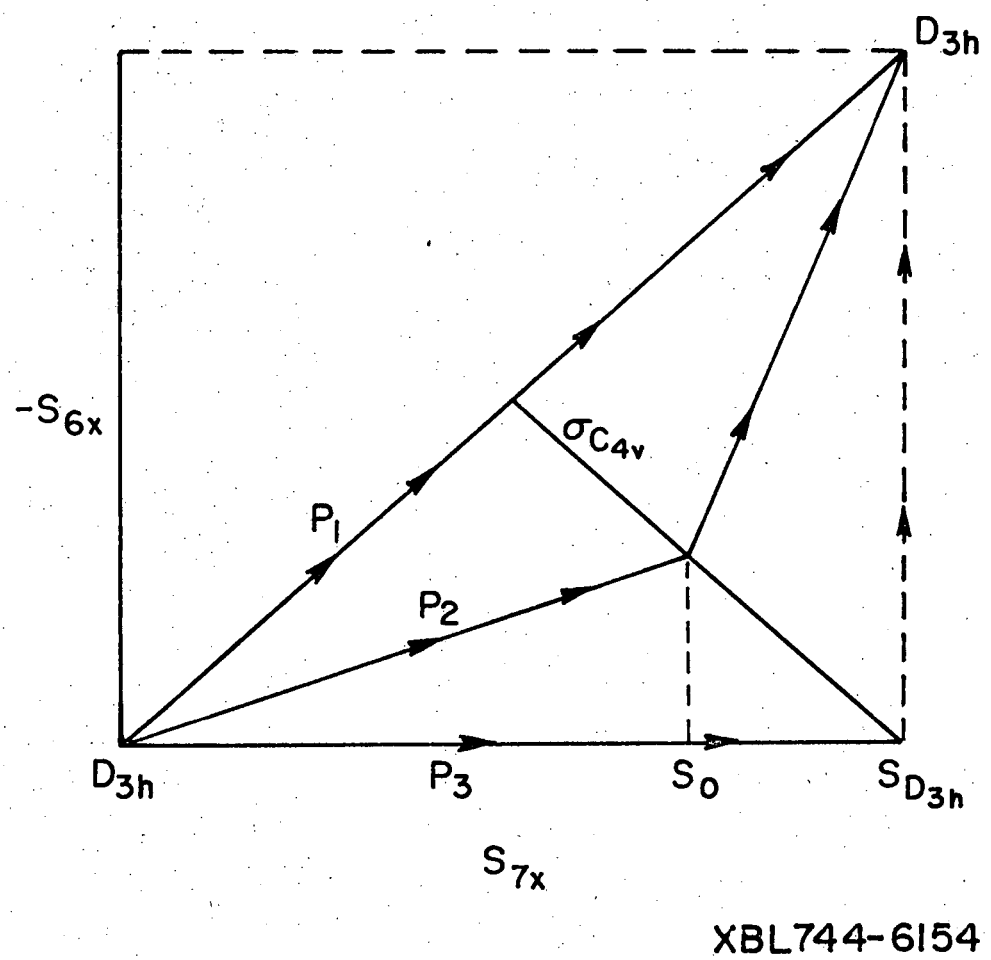

Fig. 7. Possible interchange paths (P_1,P_2,P_3) linking two neighboring D_{3h} forms. The line labeled $\sigma_{C_{4v}}$ represents the location of all possible C_{4v} transition states.

ε_{low} in Eq. (8). Since this coupling depends on quantities which are difficult to determine we cannot calculate it directly. However, by consideration of the previous arguments we can make a physically reasonable guess. This guess is represented by the path P_2, located midway between P_1 and P_3. For the purposes of later calculations we will let P_2 define the C_{4v} intermediate structure by

$$S_o = .75\ S_{D_{3h}} \tag{11}$$

In contrast to the MX_3 molecules we have chosen not to expand the MX_5 potential about the symmetrical C_{4v} transition state but rather about the D_{3h} equilibrium position. The reason for not expanding about the C_{4v} configuration is that the exact location of this intermediate form is not known, in contrast to the well defined geometry of the planar MX_3 intermediate. Because of this and the linear coupling approximation we should not expect the potential to be reasonable beyond the C_{4v} transition state. This is no real problem because we can assume an identical potential extending from the other D_{3h} form to the C_{4v} transition state. The justification for this is the interchange of S_{6x} and S_{7x} beyond the C_{4v} form (see page 31).

We can define a truncated form of the full potential (10) by first expanding ε_{low} about the equilibrium D_{3h} configuration.

$$\varepsilon_{low} \approx -\Delta\varepsilon_o\alpha^2\ S_{7x}^2\ (1 + \beta S_{7x}) + \Delta\varepsilon_o\ \alpha^4\ S_{7x}^4\ (\ 1 + \beta\ S_{7x})^2 + \cdots \tag{12}$$

Retaining terms of order four or less the truncated potential is

$$V_{trunc}(S_{7x}) = (-\ \Delta\varepsilon_o\alpha^2 + \tfrac{1}{2}K)\,S_{7x}^2 - \Delta\varepsilon_o\alpha^2\ \beta\,S_{7x}^3 + \Delta\varepsilon_o\alpha^4\ S_{7x}^4 \tag{13}$$

For simplicity we can rewrite Eq. (13) as

$$V_{trunc}(S_{7x}) = a\, S_{7x}^2 - b\, S_{7x}^3 + c\, S_{7x}^4 \quad \text{with } b,\ c > 0 \tag{14}$$

where

$$a = -\Delta\varepsilon_o \alpha^2 + \frac{1}{2} K \tag{14a}$$

$$b = \Delta\varepsilon_o \alpha^2 \beta \tag{14b}$$

$$c = \Delta\varepsilon_o \alpha^4 \tag{14c}$$

The constant "c" is greater than zero because $\Delta\varepsilon_o$ and α^4 are both positive. The parameter "b" is assumed positive in order that cubic term can counterbalance the positive quartic term to produce a potential maximum, $\left(\frac{\partial V}{\partial S_{7x}}\right)_{S_o} = 0$, at the C_{4v} transition state. "a" can be either positive or negative and its sign has interesting implications as to the shape of the potential. The effect "a" has on the potential is explored in Fig. 8. The case $a \lesssim 0$ leads to a symmetrical quadruple minimum potential with two different types of equilibrium positions. These correspond to a slight bending of the axial atoms (Fig. 9). We might predict a distorted equilibrium position in cases where the d orbitals on the central atom are not too high in energy above the ground MF_5 state. This would allow "enhanced" mixing of the $E'(d_{xz})$ and the $A_2''(F_{2P_z})$ orbitals, thereby stabilizing the distorted configuration (Fig. 6). The symmetry of the E' and A_2'' orbitals is such as to allow another stabilized geometry not pictured in Fig. 6 but equivalent to the form S_1 in Figs. 8 and 9. S_1 is presumably higher in energy than S_2 due to increased F-F repulsion as the axial atoms directly approach an equatorial F atom in the motion $S_{7x} < 0$ (Fig. 9).

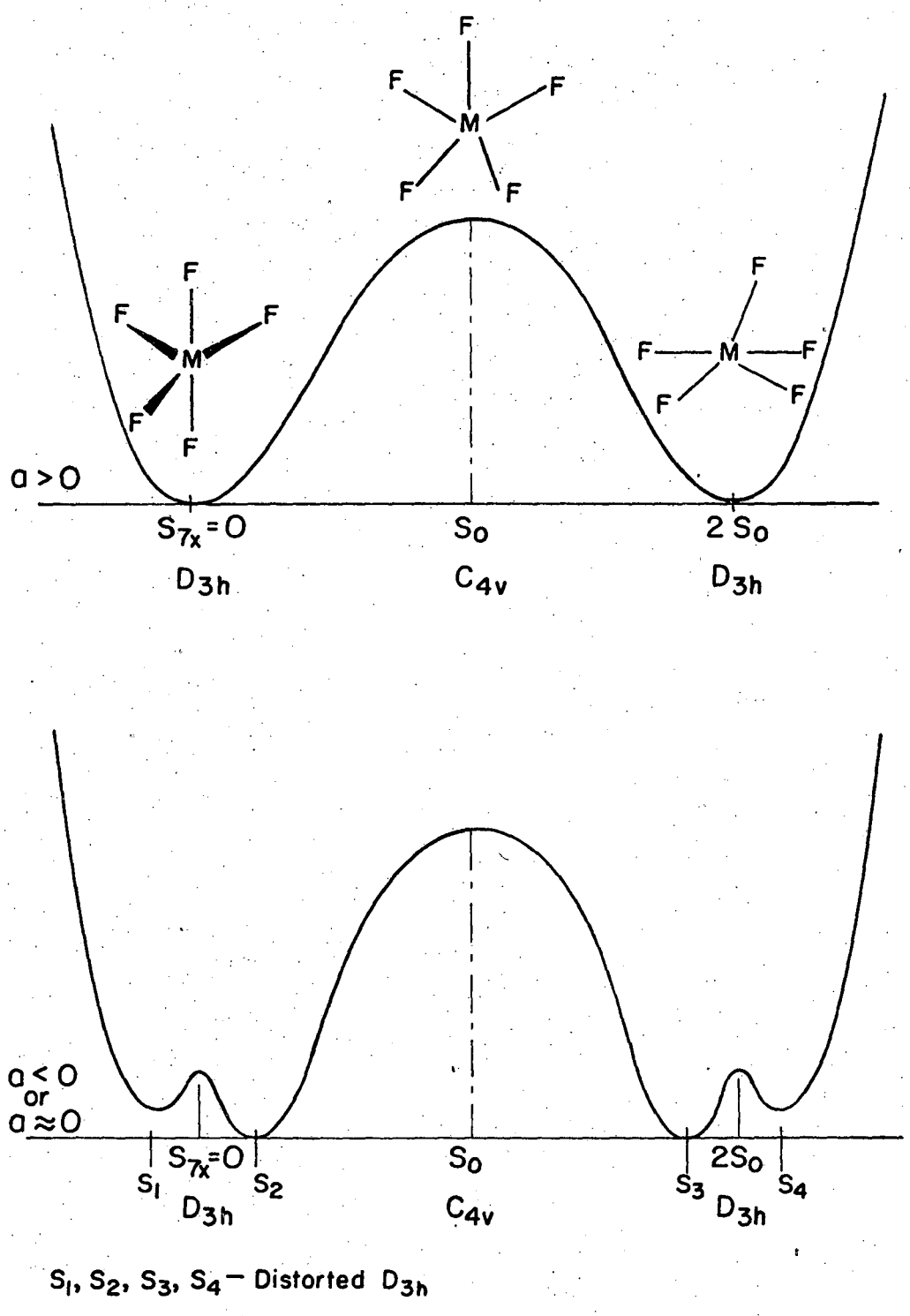

XBL 744-6155

Fig. 8. Possible potential functions for MF_5 molecules.

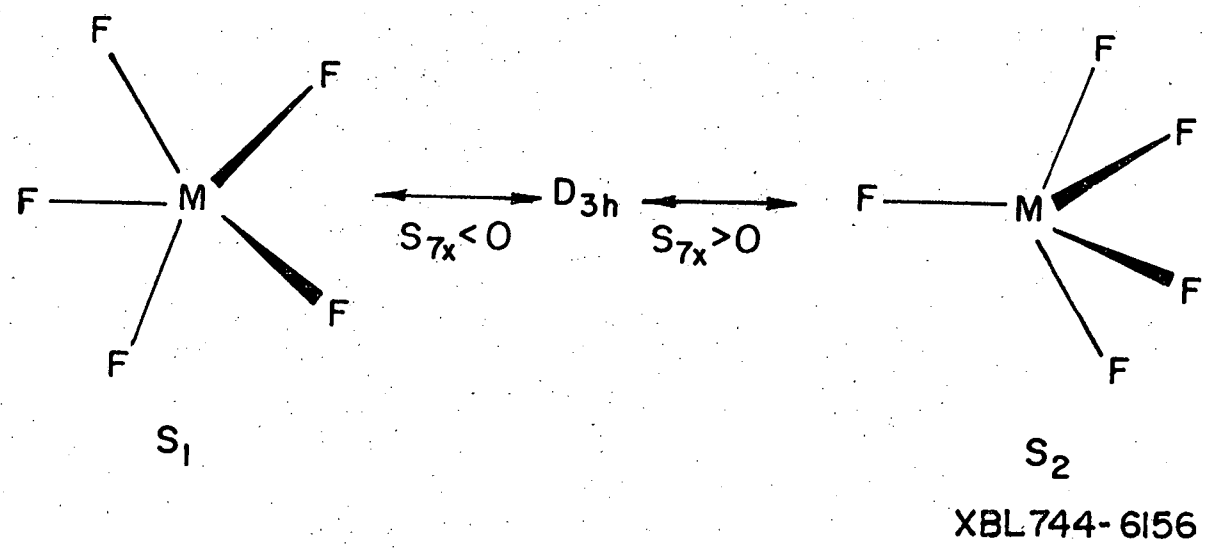

Fig. 9. Distorted D_{3h} equilibrium structures for MF_5 molecules.

A comparison of the molecular orbital diagrams (Figs. 4 and 5) reveals that d orbitals play a more important role in the VF_5 series than in the PF_5 series because they are energetically more accessible. Within the VF_5 series the "atomic" d orbitals of TaF_5 and NbF_5 are considerably higher in energy than for VF_5.[19] Therefore VF_5 is the most likely pentafluoride to undergo the type of distortion just discussed. There is experimental evidence[20] that VF_5 is slightly distorted from a D_{3h} configuration, while the remaining pentafluorides display a D_{3h} equilibrium structure.[20,21] The unusual behavior of VF_5 will be dealt with in the following discussion section. For now we will treat VF_5 as an ordinary D_{3h} molecule because our present concern is only in determining the interchange potential, not the details of the potential in the equilibrium region.

Although Fig. 8 and the preceding discussion are based on the truncated potential (14) the full potential (10) will display the same behavior in both cases ($a > 0$, $a \lesssim 0$). We can make both potential forms (10,14) quantitative in the same manner as in the MH_3 chapter. This involved taking various derivatives of the potential and relating them to structural and equilibrium parameters. The resulting simultaneous equations were solved for the unknown quantities in the potential function. Without displaying the intermediate steps the final sets of equations are presented for both the full and truncated potentials.

For the full potential based on a D_{3h} equilibrium position we have

$$K = k_o + 2\alpha^2 \Delta\varepsilon_o \tag{15a}$$

$$\alpha^2 \left(\frac{(1+1.5\beta S_o)}{(1+4\alpha^2 S_o^2(1+\beta S_o))^{1/2}} - 1 \right) = \frac{k_o}{2\Delta\varepsilon_o} \qquad (15b)$$

$$\frac{(2+6\beta S_o)(4\alpha^2 S_o+6\alpha^2\beta S_o^2)}{(1+4\alpha^2 S_o^2(1+\beta S_o))^{3/2}} - \frac{.5\alpha^4(4S_o+6\beta S_o^2)^3}{(1+4\alpha^2 S_o^2\ (1+\beta S_o))^{5/2}} - \frac{2\beta}{(1+4\alpha^2 S_o^2(1+\beta S_o))^{1/2}} = 0 \qquad (15c)$$

where k_o is equal to the curvature (2nd derivative) at the D_{3h} equilibrium position. Equations (15b) and (15c) can be solved for α, and β by an iterative procedure.

For the truncated potential based on a D_{3h} minimum we

$$a = \frac{k_o}{2} \qquad (16a)$$

$$b = \frac{k_o}{2S_o} \qquad (16b)$$

$$c = \frac{k_o}{8S_o^{\ 2}} \qquad (16c)$$

B. Calculation: Definition of Potential Parameters and Presentation of Results

The interchange coordinate (S_{7x}) used in the calculations was defined by[22]

$$S_{7x} = \frac{1}{\sqrt{12}}\ r(2\Delta\beta_{15}-\Delta\beta_{25}-\Delta\beta_{35}+\ 2\Delta\beta_{16}-\Delta\beta_{26}-\Delta\beta_{36}) \qquad (17)$$

where $\Delta\beta$ is the change in angle between the axial fluorines (labeled 5,6) and the equatorial fluorines (labeled 1,2,3), and r is the M-F bond distance. If we use the relationship, $S_o = .75\ S_{D_{3h}}$ (11), which

defines the C_{4v} intermediate (S_o), and the fact that $\Delta\beta_{15} = 30°$ for $S_{D_{3h}}$ (Fig. 7), we can employ the definition of S_{7x} (Eq. 17) to find S_o.

$$S_o = .680\ r_{M-F} \tag{18}$$

The initial value for k_o was taken as the force constant calculated from the $\nu_{o\to 1}$ transition by the formula

$$k_o = (5.9\times 10^{-7})(\nu_{o\to 1})^2\ m_7 \tag{19}$$

where m_7 is the reduced mass associated with the S_{7x} coordinate. m_7 was calculated using Wilson's high frequency approximation[11,23] (Appendix 2). The stretching coordinate $S_5(E')$ and the bending coordinate $S_6(E')$ were taken as the high frequency motions while $S_7(E')$ was the low frequency vibration.

The experimental data[17,18,21,24,25] and the final results are displayed in Tables 2 and 3. Because of the absence of ultraviolet spectra in the literature for the pentafluorides, the $^1A_1' \rightarrow {}^1E'$ ($\Delta\varepsilon_o$) transition was estimated. In the case of AsF_5 and PF_5, $\Delta\varepsilon_o$ was estimated from an SCF[26] calculation. For VF_5, NbF_5, TaF_5, $\Delta\varepsilon_o$ was approximated as the difference between the Hartree energy[19] of a M atomic d orbital and a fluorine 2p orbital.

The interchange barrier was calculated for both the full potential (Eq. 10) and the truncated potential (Eq. 14). The reasonably close agreement for both forms is due to the validity of the inequality, $1 >> 4\ \alpha^2 S_o^2\ (1+\beta S_o)$, allowing truncation of ε_{low} to fourth order (12). For MF_5 molecules we see that $\alpha \approx .2$, $\beta \approx .6$, and $S_o \approx 1$, which sets

$4\alpha^2 S_o^2(1+\beta S_o) \approx .26.$

From the form of the full potential (10) we see that for sufficiently negative values of S_{7x} the quantity inside the square root will become negative, yielding an imaginary potential. This, of course, is physically unreasonable, however this breakdown occurs at a potential energy approximately one hundred times greater than the calculated barrier height. For purposes of calculating barrier heights and equilibrium behavior the potential form (10) is physically well behaved in the regions of interest.

Energy levels were calculated for VF_5 and PF_5 using a forty member harmonic oscillator basis set. The full potential was used for this calculation. The results are found in Table 4. Due to anharmonicity the calculated $\nu_{o\rightarrow 1}$ transition for VF_5 and PF_5 is $\sim 5\ cm^{-1}$ lower than the observed transition (Table 2). One could correct for this by increasing k_o as discussed in Chapter 1, however this small correction would not greatly change the computed barrier height or the inherent anharmonicity of the potential.

C. Discussion: Discussion of Computational Results and Comparison to Previous Work on Axial-Equatorial Interchange

Previous attempts[22,27] to calculate the barrier to interchange in pentafluoride molecules have been based on such crude potential functions that the values obtained can only be considered as order of magnitude estimates. In these instances the potential was approximated by only quadratic terms with the barrier height taken as the value of the quadratic potential at an appropriately chosen C_{4v} intermediate geometry. This approach, at best, can only lead to an upper limit to the true barrier, since it lacks the higher order terms which give the potential the proper anharmonicity to produce a potential maximum at the C_{4v} form. We can get a rough idea of how to correct the previous estimates by considering the barrier calculated from the truncated potential (14) of this work. At the C_{4v} form (i.e. at S_o) the truncated potential yields

$$E_{barrier} = \frac{k_o}{8} S_o^2 \qquad (20)$$

From this we conclude that earlier estimates were about four times too large. Holmes and co-workers[27] found the barrier in AsF_5 to be 3,280 cm^{-1}. Scaling Holmes' value by the correction factor (.25) we obtain 820 cm^{-1} which is in much closer agreement with our figure. The correction factor of one-fourth is only meaningful in cases where the truncated potential is valid. In cases where the full potential is necessary, as in chapter 1, there is no straightforward comparison to the quadratic potential. However, in the future, it might be taken as a rough rule-of-thumb that "inversion" barriers based solely on a quadratic potential are approximately four times too large.

Examination of the barrier heights (Table 3) reveals that, with the exception of VF_5, the pentafluorides have an average interchange barrier of about 1,050 cm^{-1}.

The exceptionally low barrier in VF_5 is due to low lying d orbitals on the vanadium as was discussed earlier (page 44). For these barriers, and the corresponding potentials, we have calculated the inversion splitting in the lowest level (Table 4) and found it to be $\sim 10^{-7}$ cm^{-1} in all cases, including VF_5. This splitting corresponds to an exchange frequency of 10^4 cycles/sec which is in accord with the observation of only one fluorine peak in the nmr spectrum of the studied pentafluorides.[28]

The lack of observable splittings makes the fitting of an arbitrary interchange potential impossible. However, not knowing the actual barrier height, makes it difficult to assess the validity of the derived potential (10). The success of predicting the barriers and energy levels in the MH_3 series, and as we will see in later chapters, a similar ability of this general approach to handle systems more completely characterized than the MF_5 molecules lends some measure of credibility to the results. One way of testing these results is in a Hartree-Fock SCF, or perhaps CI, calculation. The most likely candidate for the computation is PF_5 since it has the fewest number of electrons of the pentafluorides.

D. Theory: Derivation of Equilibrium Potential and Application to Interpretation of MX_5 (D_{3h}) Spectra

In the previous sections we have considered the equatorial-axial interchange path and have demonstrated that it can be appropriately represented as a one dimensional path through a four dimensional space. Our interest centered on computation of the barrier height which is a property of the potential far away from the equilibrium structure. We will now investigate the nature of the potential about the equilibrium region and therefore must consider both axial coordinates (S_{7x},S_{7y}) on equal footing. This does not require a difference in approach as the initial matrix (3) determines the potential in all regions of space. Whereas we previously ignored the coordinates (S_{7y},S_{6y}) we must now include them and resolve (3) for ε_{low}. This complicates matters considerably since the resulting determinant yields a complicated cubic equation for ε. Instead of solving the determinant involving both S_{7x} and S_{7y} we can look now just at the S_{7y} solution and use the fact that the entire potential must exhibit D_{3h} symmetry to deduce a potential involving both S_{7x} and S_{7y}. Setting S_{7x},S_{6x} equal to zero we get a matrix involving just the E'_y coordinates.

$$
\begin{array}{c}
 \\ |{}^1A_1'\rangle \\ |{}^1E_x'\rangle \\ |{}^1E_y'\rangle
\end{array}
\begin{array}{c}
\begin{array}{ccc} |{}^1A_1'\rangle & |{}^1E_x'\rangle & |{}^1E_y'\rangle \end{array} \\
\begin{pmatrix}
-\varepsilon & 0 & aS_{7y}+bS_{6y} \\
0 & \Delta\varepsilon_o-\varepsilon & eS_{7y}+fS_{6y} \\
aS_{7y}+bS_{6y} & eS_{7y}+fS_{6y} & \Delta\varepsilon_o-\varepsilon
\end{pmatrix}
\end{array}
\tag{21}
$$

The approximate potential becomes

$$V = (\tfrac{1}{2})\Delta\varepsilon_o[1-(1 + 4(aS_{7y} + bS_{6y})^2)^{1/2}] + (\tfrac{1}{2})C_7S_{7y}^2 + (\tfrac{1}{2})C_6S_{6y}^2 \tag{22}$$

where we have used the approximation $\Delta\varepsilon_o >> (eS_{7y}+fS_{6y})$ to simplify the potential to that displayed. This is analogous to the procedure used in the previous section (Eqs. 5 and 6). Using the linear coupling approximation (8) between S_{6y} and S_{7y} we get for the final form of the potential

$$V(S_{7y}) = (\tfrac{1}{2})\Delta\varepsilon_o[1-(1 + 4\alpha^2S_{7y}^2)^{1/2}] + (\tfrac{1}{2})K\,S_{7y}^2 \tag{23}$$

where α, K, $\Delta\varepsilon_o$ are the same quantities as in Eq. (10) and have the same numerical values (Tables 2 and 3). There is a noticeable difference between the S_{7y} potential (23) and the S_{7x} potential (10). In the S_{7y} potential there is no term corresponding to the $(1+\beta S_{7x})$ term in the S_{7x} form. The reason for this is clear from a symmetry standpoint. A comparison of the S_{7y} motion to the S_{7x} motion (Fig. 1) shows that the potential in the $S_{7y} > 0$ and $S_{7y} < 0$ directions must be equivalent on the

basis of symmetry. The corresponding symmetry argument does not require $S_{7x} > 0$ and $S_{7x} < 0$ to be equivalent.

In their truncated form the S_{7x} and S_{7y} potentials are

$$V(S_{7x}) = aS_{7x}^2 - bS_{7x}^3 + cS_{7x}^4 \tag{24a}$$

$$V(S_{7y}) = aS_{7y}^2 + cS_{7y}^4 \tag{24b}$$

where a, b are the same in both potentials. The parameter "b" is zero in $V(S_{7y})$ for the just discussed symmetry reasons. What we are seeking is a combined S_{7x}, S_{7y} potential, which at first guess we might take as the sum of Eq. (24a) and Eq. (24b) to give.

$$V(S_{7x}, S_{7y}) = a(S_x^2 + S_y^2) - bS_{7x}^3 + c(S_{7x}^4 + S_{7y}^4) \tag{25}$$

This potential is not acceptable because the cubic and quartic terms are not invariant to all D_{3h} operations. What is needed, and of course, what would have been obtained from an exact solution of Eq. (3), are terms coupling S_{7x} and S_{7y} which make (25) invariant under the D_{3h} point group. Knowing the asymptotic forms in the S_{7x} and S_{7y} directions we can "connect" both potentials and provide the proper symmetry by transforming to polar coordinates (ρ,θ) and modifying the cubic and quartic terms to yield

$$V(\rho,\theta) = a\rho^2 - b\cos(3\theta)\,\rho^3 + c\rho^4 \tag{26}$$

where θ is measured from the axis defined by the $S_{7x} > 0$ direction. In the limits corresponding to the S_{7x} direction ($\theta=0$) or the S_{7y} direction ($\theta = \frac{\pi}{2}$) the polar form (Eq. 26) gives the correct asymptotic behavior (compare to Eqs. 24a, 24b).

$$V(\rho,0) = a\rho^2 - b\rho^3 + c\rho^4 \qquad S_{7x} > 0 \qquad S_{7y} = 0 \tag{26a}$$

$$V(\rho,\tfrac{\pi}{2}) = a\rho^2 \qquad + c\rho^4 \qquad S_{7y} > 0 \qquad S_{7x} = 0 \tag{26b}$$

It is obvious that the polar potential in Eq. (26) is now invariant to D_{3h} operations. Working backward to the full potential we can write a form with D_{3h} symmetry as

$$V(\rho,\theta) = (\tfrac{1}{2})\Delta\varepsilon_o \; [1 - (1+4\alpha^2\rho^2(1+\beta\cos(3\theta)\rho))^{1/2}] + (\tfrac{1}{2})k\,\rho^2 \tag{27}$$

As a first step in determining the eigenvalues of the equilibrium potential (26,27) we can compare contours of constant potential between a purely quadratic potential and the one presented here (Fig. 10). In the quadratic form the contours are circular, because to second order in the coordinates the only form invariant under D_{3h} is a circle. The derived form generates a more physically reasonable contour which also maintains the proper D_{3h} symmetry.

The eigenfunctions of the quadratic potential can be used to evaluate the eigenvalues of the derived potential. The wave functions generated by the quadratic potential are defined in Appendix 3. The basic result of Appendix 3 is that the wave functions of a two dimensional quadratic potential can be expressed in polar coordinates as $\psi = R_n(\rho)e^{\pm im\theta}$.[29] To compute the eigenvalues of the derived potential we form the matrix elements of the "perturbation"

$$V_{pert.} = -\,b\cos(3\theta)\rho^3 + c\rho^4 \tag{28}$$

in the quadratic basis. Because the second term is purely radial it will contribute only to the diagonal elements, due to orthogonality of

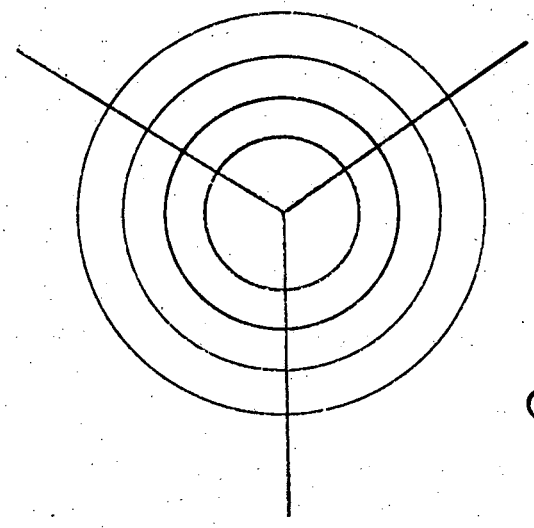

Quadratic Potential

$V = a\rho^2$

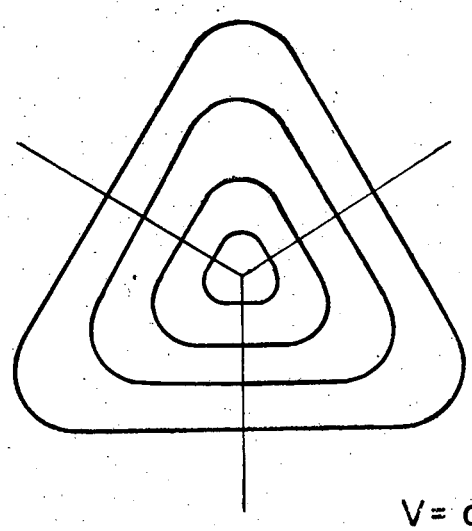

Derived Potential

$V = a\rho^2 - b\cos(3\theta)\rho^3 + c\rho^4$

XBL744-6157

Fig. 10. Contours of constant potential for the quadratic and derived potentials.

the angular functions, $e^{\pm im\theta}$. The angular term can have only certain off diagonal contributions. States with "m" differing by ±3 can couple via the cos(3θ) term (Appendix 3). Using this information we can qualitatively construct a correlation diagram between the quadratic and derived eigenvalues for some of the lower levels (Fig. 11). The first E' level is lowered in energy due to its interaction with the second E' level (second order perturbation theory). The second E' remains approximately at the same energy since its interactions with the first and third E' levels tend to cancel each other. The second A_1' level is lowered through its interaction with its counterpart in the next higher level.

If the perturbation (28) is not too large it will not appreciably scramble the quadratic basis functions. In this limit we can approximate the selection rules for infrared and Raman transitions in PF_5 type molecules by using the quadratic eigenfunctions. For infrared transitions, matrix elements of the form $\langle m|\cos\theta|m'\rangle$, $\langle m|\sin\theta|m'\rangle$ will determine the selection rules. This yields $\Delta m = \pm 1$ for allowed infrared transitions. Determining the selection rules for the allowed Raman transitions is not as clear cut, however the first few allowed transitions will be indicated. These are

$$A_1' \rightarrow E' \tag{29a}$$

$$E' \rightarrow E' \tag{29b}$$

$$A_1' \rightarrow A_1' \tag{29c}$$

where by comparison to Fig. 11 we see that among the lower three levels all possible transitions are Raman allowed.

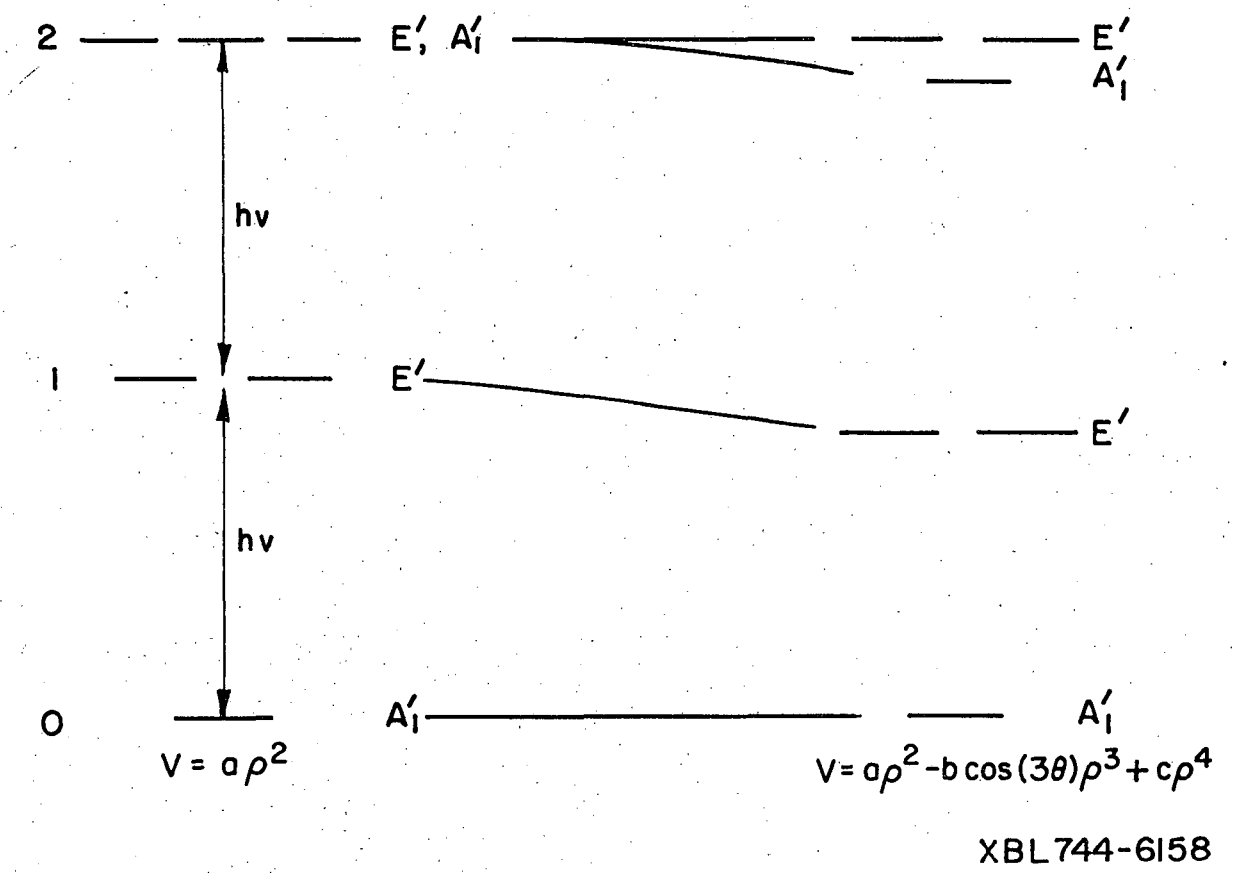

Fig. 11. Correlation diagram for eigenvalues of the quadratic and derived potentials.

For D_{3h} symmetry the highest allowed "true" degeneracy is two (E type level) although for the quadratic form the actual degeneracies can be much larger. These are accidental degeneracies due to the fact that a circle has more than D_{3h} symmetry. When the $\cos(3\theta)$ term is introduced the overall symmetry is lowered to D_{3h} and the degeneracies are lifted. The general effect of the quadratic term ($c\rho^4$) is to cause higher levels to diverge, however the behavior of levels close to the ground state will be governed mainly by the cubic term. The most interesting feature of the eigenvalues of the derived potential is the lowering of the $\nu_{o\to1}$ transition relative to the $\nu_{1\to2}(E'-E')$ transition. This effect is crucial to the interpretation of the spectra and is due to cross terms in S_{7x} and S_{7y} ($\cos(3\theta)$ term) which can only arise from treating the vibrational potential as two dimensional. Witt[30] and co-workers treated the E' vibration as a one dimensional motion to estimate the effects of anharmonicity (cubic term) and therefore concluded that higher levels must converge. Hence they were forced to hypothesize various possible explanations for an unusually intense "anomalous" peak at an energy higher than the main Q branch in the Raman spectra of E" fundamental of PF_5. We see that this feature comes out quite naturally in the our treatment of the E' mode, it is the $\nu_{1\to2}(E'-E')$ transition. The effect of states above those indicated in Fig. 10 is not clear cut. The high degeneracy of the upper states (above 2) will be split in a complicated manner, with some gaining energy, some remaining unaffected, and some being lowered. One might expect that the "average" transition energy would be slightly lowered due to the cubic term ($-b\cos(3\theta)\rho^3$)). The net effect should be a slight increase in intensity to the low energy side of the Q

branch, relative to the high energy side. This is consistent with the observed spectra.[30]

Another factor which should be explored is the relative population of the excited states for such a low energy mode. For PF_5 this is displayed in Table 5. Just on the basis of population the $\nu_{o \to 1}$ Raman transition should be ~ 12% more intense than the $\nu_{1 \to 2}$ transition. This is roughly what is experimentally observed. The higher states, which constitute the remaining 40% of the population, will most likely, not be observed as sharp spectral features. This is due both to the removal of the high degeneracy, and also to the smearing of the remaining 40% over many levels.

In view of the discussion in this section, it should be emphasized that the energy level computation found in Table 4 was done on the interchange potential $V(S_{7x})$, and therefore is not intended to represent the actual vibrational levels. Its purpose was to determine the "inversion" splittings due to tunneling through the C_{4v} barrier, and also to get an estimate of the effect of the anharmonic term $(-bS_{7x}^3)$ on the equilibrium potential (26,27). The effect of the cubic term in the $V(S_{7x})$ potential is roughly 4-5 cm^{-1} in the lower states (Table 4). Its effect on the equilibrium potential should actually be smaller due to averaging over the θ coordinate. The observed splitting of the two Q branches in PF_5 is 3 cm^{-1}, which is reasonable accord with the above reasoning.

To this point we have been considering the equilibrium behavior of "normal" D_{3h} molecules, that is, molecules with a single potential

minimum at the D_{3h} structure. VF_5 does not fall into this category since there is evidence of a slightly distorted equilibrium structure in the lower vibrational states.[20] We have already investigated the reasons for this distortion. Our focus now is on gaining a qualitative picture of the equilibrium potential and its lower vibrational states. Earlier, we saw that the truncated potential (14) yielded a non-D_{3h} minimum of lowest energy for values of the parameter "a" $\lesssim 0$. In this case the truncated form (14) must actually contain higher order terms in S_{7x} because a polynomial to order four can yield at most a total of three distinct potential maxima and potential minima. For VF_5 there are four total minima and maxima between $S_{7x}=0$ and $S_{7x}=S_o$. To correct the truncated potential, terms to at least order five are necessary, and to get a bound potential at large S_{7x} we should go to order six. At this point the truncated potential is actually less convenient to work with than the full potential (10). The immediate problem is to modify the potential to describe the entire equilbrium region. This is achieved identically as for the normal D_{3h} molecules by inclusion of the $\cos(3\theta)$ term. The potential is then identical in form to Eq. (27), but with the understanding that $(\alpha^2\Delta\varepsilon_o-(\frac{1}{2})K)\approx 0$ (12,13) to obtain the distortion. Under these circumstances the potential has three potential minima when the projection of the axial bonds into the equatorial plane is located midway between the three equatorial M-F bonds, three saddle points of higher energy when the projection is along the equatorial M-F bonds, and a potential maximum at the D_{3h} configuration. This can be physically pictured as a hindered pseudorotation between the three minima, which are separated by an angular as well as a "radial" barrier. To gain a qualitative description of the lower vibrational states requires an idea of the depth and location

of these minima. From consideration of the lower limits of resolution of the electric field focusing experiments[20] and electron diffraction measurements[24] on VF_5 we can roughly limit the distortion to the following range

$$1° \leqslant \Delta\beta \leqslant 4° \tag{30}$$

where $\Delta\beta$ is the axial bend as defined previously (Eq. 17). This corresponds to a small distortion, with the potential minima located close to S=0. This would be expected only if $a \approx 0$, because $a \ll 0$ would lead to a relatively distant minimum, For $a \approx 0$ the maxima at D_{3h} and the angular barriers would not be very large.

The experimental spectrum of VF_5 [18] is most unusual. It shows a perfectly normal spectra for a D_{3h} molecule for all the fundamentals except the E' axial bend. The Raman spectra places the E' fundamental at 99 cm^{-1} while infrared measurements indicate a value of 109.5 cm^{-1}. In addition the overtone of the E' mode occurs at 227 cm^{-1} in the Raman spectra, which is too large to explain as simply $2v_{E'}$, ($2\times99 = 198$ cm^{-1}).

In one dimension it is well known that low barriers lead to very anharmonic spacings.[31] Qualitatively, this could be consistent with the abnormally large overtone (227 cm^{-1}) as compared to the observed fundamental (99 cm^{-1}) in the Raman spectra of VF_5. This is most likely a gross simplification because the two dimensional form of the potential as well as the presence of angular barriers will yield a complicated assortment of levels probably able to account for the spectra also. In any case, the main features of the "true" VF_5 potential should include small angular and radial barriers and a slightly displaced minimum.

Table 1. Axial Bend (ν_7) and Equatorial Bend (ν_6) Frequencies

	V_6 (cm^{-1})	V_7 (cm^{-1})
PF_5	533	175
AsF_5	372	130
VF_5	282	109
TaF_5	213	121
NbF_5	226	136

Table 2. Experimental Data for MF_5 Molecules

	$V_7(cm^{-1})$	$r_{M-F}(Å)$	$m_7(amu)$	$k_o\ (\frac{mdyn}{Å})$	$S_o(Å)$	$\Delta\varepsilon_o\ (\frac{mdyn}{Å})$
PF_5	175	1.55	9.49	.171	1.05	3.0
AsF_5	130	1.74	9.92	.099	1.18	3.0
VF_5	109	1.71	9.58	.067	1.16	1.3
NbF_5	136	1.88	10.16	.111	1.28	2.0
TaF_5	121	1.81	10.93	.094	1.23	1.7

Table 3. Final Results for MF_5 Potential Function

	α ($Å^{-1}$)	β ($Å^{-1}$)	$E^{Full}_{Barrier}$ (cm^{-1})	$E^{Trunc}_{Barrier}$ (cm^{-1})
PF_5	.199	.605	1,224	1,197
AsF_5	.175	.406	913	873
VF_5	.180	.600	592	571
NbF_5	.160	.727	1,210	1,142
TaF_5	.168	.688	942	897

Table 4. Computed Energy Levels for VF_5 and PF_5

	PF_5	VF_5
$0_S \rightarrow 0_A$	$\sim 10^{-7}$ cm^{-1}	$\sim 10^{-7}$ cm^{-1}
$0 \rightarrow 1$	169.5	105.2
$1 \rightarrow 2$	164.4	100.9
$2 \rightarrow 3$	158.6	95.9
$3 \rightarrow 4$	153.8	89.8

Table 5. Relative population of V_7 vibrational levels for PF_5 at 298°K assuming 175 cm^{-1} spacings.

Level	Degeneracy	Population
0	1	.32
1	2	.28
2	3	.18
3	4	.10
4	5	.06
5	6	.03
6	7	.01
7	8	.01

IV. RING PUCKERING IN FOUR-MEMBERED, PSEUDO FOUR-MEMBERED, AND FIVE-MEMBERED RINGS

A. Derivation of Puckering Potentials for Four-Membered, Pseudo Four-Membered, and Five-Membered Rings

In this chapter we will explore ring puckering in four-membered, pseudo four-membered, and five-membered rings. The molecules we will pay particular attention to are displayed in Fig. 1. The appropriate ring puckering symmetry coordinates for these types of molecules can be found in Fig. 2. In 4-membered rings the puckering motion occurs in only one dimension (S_{B_1}), while in 5-membered rings there are two degenerate puckering coordinates ($S_{E''_{2a}}$, $S_{E''_{2b}}$). In the pseudo 4-membered rings one of the coordinates is a torsion about a double bond (S_{A_2}) and is expected to occur at much higher energy than the other motion (S_{B_2}). Therefore in pseudo 4-membered rings the puckering can be treated as a one dimensional motion.

The molecules under consideration consist of an entirely σ-bonded framework, with the exception of cyclopentene which contains a π-bond. The electronic structures of such "saturated" (no π bonds) and "slightly" unsaturated (one π bond) rings are diagrammed in Fig. 3. The most general feature of these systems is the existence of many σ-σ^* type transitions at a relatively high energy (9-10 eV).[32] In the case of the slightly unsaturated rings there are a cluster of lower energy π-π^*, σ-π^* transitions,[33,34] however the π^* orbitals are not expected to contribute significantly to the puckering potential. The π^* orbitals are localized primarily about the doubly bonded carbons.

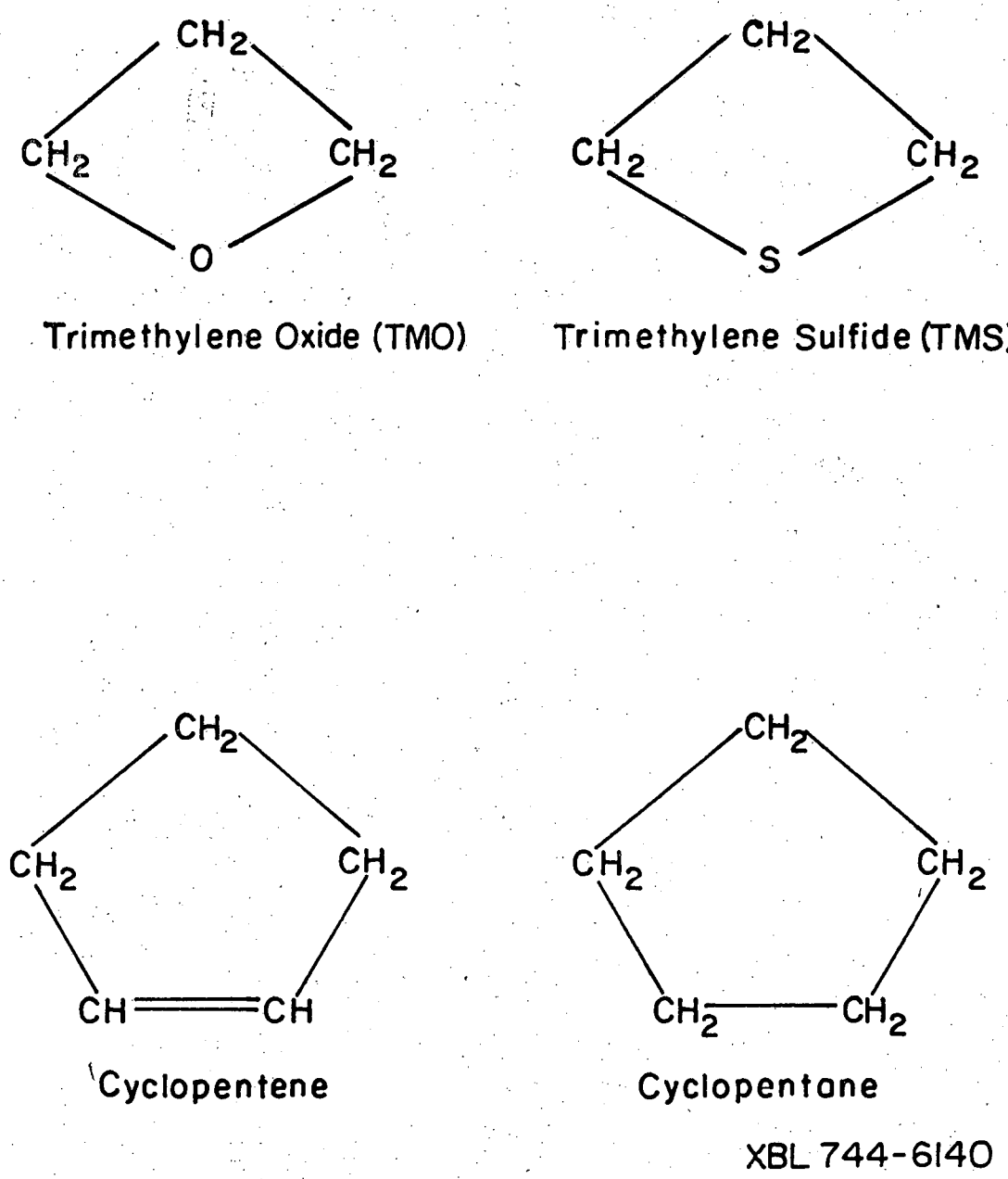

Fig. 1. Examples of four-membered, pseudo four-membered, and five-membered rings.

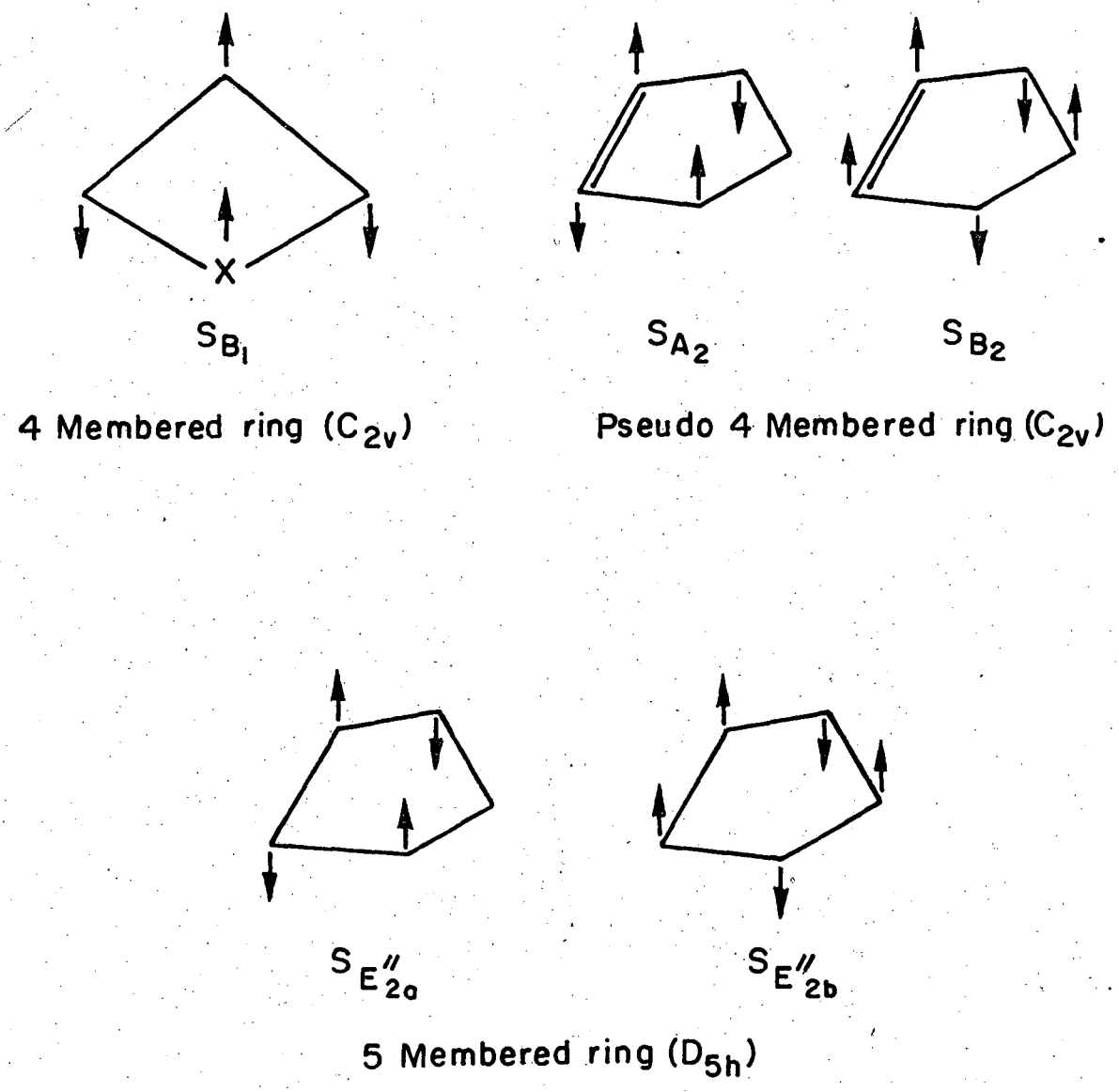

Fig. 2. Ring puckering symmetry coordinates for 4-membered pseudo 4-membered and 5-membered rings.

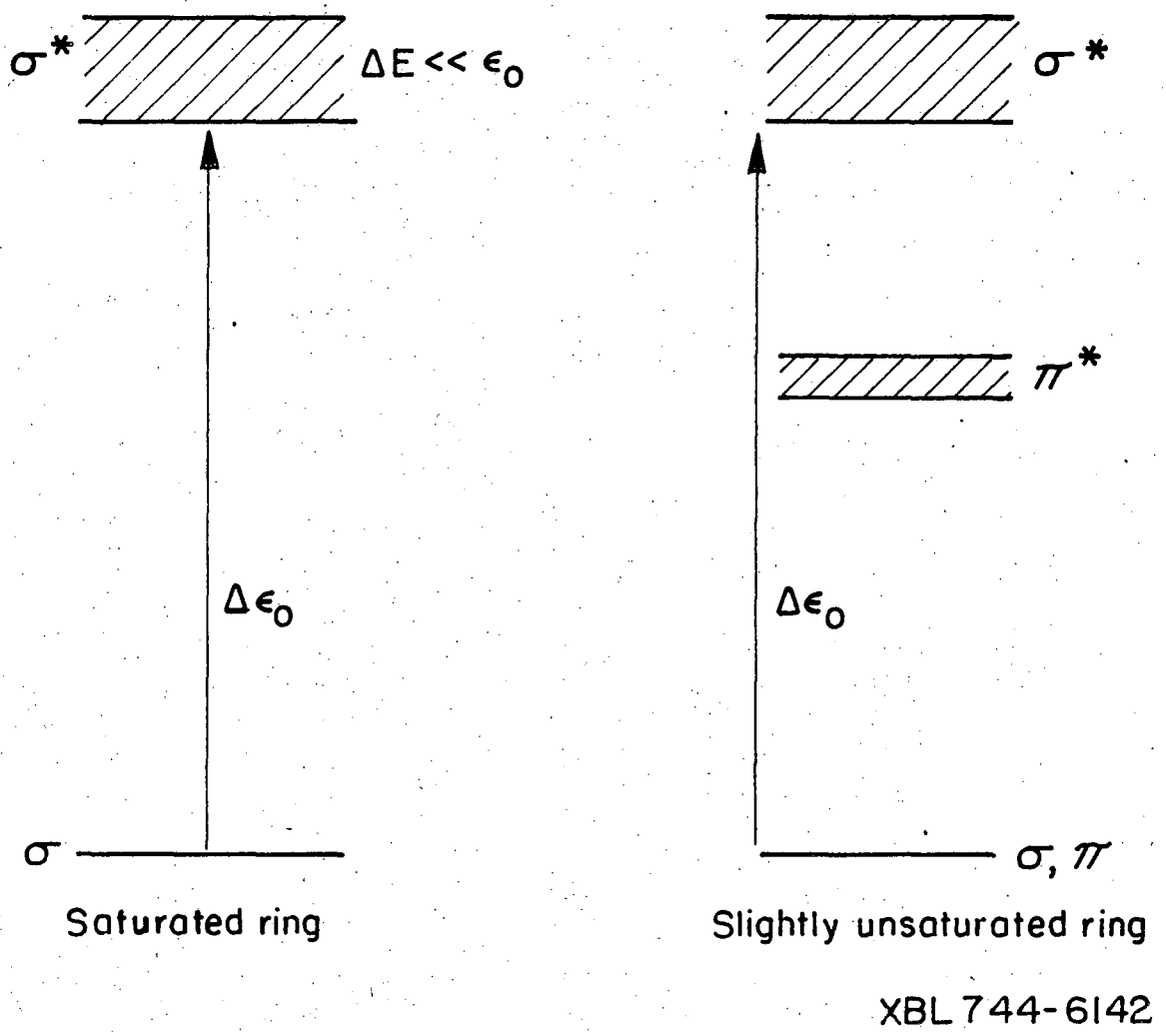

Fig. 3. Schematic diagram of the electronic structure of the excited states of saturated and slightly unsaturated cyclic compounds.

During the puckering motion the doubly bound carbons move as a single unit (Fig. 2) which preserves the local symmetry about these carbons. These factors imply that the π^* orbitals are weakly coupled to the rest of the ring system during the distortion. As a result they don't participate strongly in the puckering process and will be ignored.

We saw in earlier chapters on MX_3, and MX_5 molecules that one particular electronic transition could be identified as coupling strongest to the distortion coordinate(s). In ring systems the situation is not as clear cut. From the electronic structure diagram (Fig. 3) we see that there are many excited electronic states in an energy range (ΔE) small compared to the transition energy ($\Delta\varepsilon_o$). In this cluster there will be many states of the proper symmetry coupled to the ground electronic state via the puckering motion. This complicates matters considerably as the resulting determinant would be of high order, assuming of course that we could identify all the involved excited electronic states in the first place. Fortunately, symmetry considerations permit a simplification of the determinant to a form whose roots can be found analytically.

The construction of the determinant proceeds as in earlier chapters. First we determine the ground electronic state of the various molecules.

$^1A_1$ (C_{2v}) 4-membered ring (TMO, TMS) (1a)

$^1A_1$ (C_{2v}) Pseudo 4-membered ring (cyclopentene) (1b)

$^1A_1'$ (D_{5h}) 5-membered ring (Cyclopentane) (1c)

These all have totally symmetric ground electronic states. This is because there are an even number of electrons in all the systems, with a maximum orbital degeneracies of two (D_{5h}) and one (C_{2v}). Because the degeneracy is one in C_{2v} molecules all the electrons must be paired, hence a singlet state. In the cyclopentane molecule (D_{5h}) we can attribute one basis orbital (sp^3 on carbon, 1s on hydrogen) per valence electron. This implies that of the possible 2n (n is an integer) linear combination of basis orbitals, n molecular orbitals will be filled by 2n electrons. Thus cyclopentane also has a singlet spin in the ground electronic state.

The symmetries of the ground electronic state and the puckering coordinate determines the allowed symmetry of the excited electronic states which can couple to the ground electronic state in the linear matrix element. For the molecules under consideration here the allowed symmetry of the excited electronic states are

$$^1B_1 \quad \text{(TMO, TMS)} \quad C_{2v} \tag{2a}$$

$$^1B_2 \quad \text{(Cyclopentene)} \quad C_{2v} \tag{2b}$$

$$^1E''_2 \quad \text{(Cyclopentane)} \quad D_{5h} \tag{2c}$$

In the one dimensional cases (C_{2v}) the determinant of the linear matrix elements will have the form

$$
\begin{array}{c|cccccc|}
 & |^1A_1\rangle & |^1B_{1,2}(1)\rangle & |^1B_{1,2}(2)\rangle & \cdots & |^1B_{1,2}(n)\rangle \\
|^1A_1\rangle & -\varepsilon & \alpha_1 S_{B_{1,2}} & \alpha_2 S_{B_{1,2}} & \cdots & \alpha_n S_{B_{1,2}} \\
|^1B_{1,2}(1)\rangle & \alpha_1 S_{B_{1,2}} & \Delta\varepsilon_o - \varepsilon & & & \\
|^1B_{1,2}(2)\rangle & \alpha_2 S_{B_{1,2}} & & \Delta\varepsilon_o - \varepsilon & & \bigcirc \\
\vdots & \vdots & \bigcirc & & \ddots & \\
|^1B_{1,2}(n)\rangle & \alpha_n S_{B_{1,2}} & & & & \Delta\varepsilon_o - \varepsilon
\end{array}
\qquad (3)
$$

where

$$\alpha_n = \langle {}^1A_1 \left| \left(\frac{\partial H_v}{\partial S_{B_{1,2}}}\right)_{So} \right| {}^1B_{1,2}(n) \rangle \qquad (4a)$$

$$\Delta\varepsilon_o = \varepsilon_{{}^1B_{1,2}} - \varepsilon_{{}^1A_1} \qquad (4b)$$

where we define

$$\varepsilon_{{}^1A_1} = 0$$

The notation $B_{1,2}$ means we use the B_1 coordinate in the four membered ring case (2a) and the B_2 coordinate in the pseudo four-membered ring case (2b). For simplicity, we will use just the B_1 coordinate in

the remaining equations, because the identical equations result for the B_2 coordinate. In constructing the determinant we have made two assumptions. One is that $\Delta E \ll \Delta\varepsilon_o$ (Fig. 3) which was discussed previously. The second approximation is in neglecting coupling to other modes. In the one dimensional case (C_{2v}) the other modes which can couple to $B_{1,2}$ are determined by the direct product of the excited electronic states. The direct product is $B_{1,2} \times B_{1,2} = A_1$. This tells us that only vibrational modes of A_1 symmetry can couple to the ring puckering mode.

For planar rings an A_1 motion can be a symmetrical stretching of the bonds or an in plane bending motion. As in earlier chapters we do not expect the A_1 coordinates to couple strongly to the distortion mode, hence the A_1 contribution to the determinant (3) is ignored.

The determinant (3) yields the following polynomial equation in ε

$$- \varepsilon(\Delta\varepsilon_o - \varepsilon)^n - (\sum_{K=1}^{n} \alpha_K^2)\ (\Delta\varepsilon_o - \varepsilon)^{n-1}\ S_{B_1}^2 = 0$$

This can be solved exactly to give

$$\varepsilon = \frac{1}{2}\ \Delta\varepsilon_o\ [1 \pm (1 + 4\alpha^2 S_{B_1}^2)^{1/2}] \tag{6}$$

where

$$\alpha^2 = \frac{1}{\Delta\varepsilon_o^{\ 2}} \sum_{K=1}^{n} \alpha_K^{\ 2} \tag{6a}$$

The puckering potential is defined by adding the usual quadratic term to the lower root of Eq. (6) to give

$$V(S_{B_1}) = \frac{1}{2}\ \Delta\varepsilon_o\ [1 - (1+4\alpha^2 S_{B_1}^2)^{1/2}] + \frac{1}{2}\ K\ S_{B_1}^2 \qquad (7)$$

For cyclopentane (D_{5h}) the determinant is

$$\begin{array}{c|ccccccc|}
 & |{}^1A_1'\rangle & |{}^1E''_{2a}(1)\rangle & |{}^1E''_{2b}(1)\rangle & \cdots & |{}^1E''_{2a}(n)\rangle & |{}^1E''_{2b}(n)\rangle \\
|{}^1A_1'\rangle & -\varepsilon & \alpha_1 S_{E''_{2a}} & \alpha_1 S_{E''_{2b}} & \cdots & \alpha_n S_{E''_{2a}} & \alpha_n S_{E''_{2b}} \\
|{}^1E''_{2a}(1)\rangle & \alpha_1 S_{E''_{2a}} & \Delta\varepsilon_o - \varepsilon & & & & \\
|{}^1E''_{2b}(1)\rangle & \alpha_1 S_{E''_{2b}} & & \Delta\varepsilon_o - \varepsilon & & \bigcirc & \\
\vdots & \vdots & \bigcirc & \vdots & \ddots & & \\
|{}^1E''_{2a}(n)\rangle & \alpha_n S_{E''_{2a}} & & & & \Delta\varepsilon_o - \varepsilon & \\
|{}^1E''_{2b}(n)\rangle & \alpha_n S_{E''_{2b}} & & & & & \Delta\varepsilon_o - \varepsilon
\end{array} \qquad (8)$$

where

$$\alpha_n = \langle {}^1A_1' | \left(\frac{\partial H_v}{\partial S_{E''_{2a}}}\right)_{So} | {}^1E''_{2a}\ (n) \rangle = \langle {}^1A_1' | \left(\frac{\partial H_v}{\partial S_{E''_{2b}}}\right)_{So} | {}^1E''_{2b}\ (n) \rangle \tag{9a}$$

$$\Delta\varepsilon_o = \varepsilon_{{}^1E''_2} - \varepsilon_{{}^1A_1'} \tag{9b}$$

where we define

$$\varepsilon_{{}^1A_1'} = 0$$

The same two approximations as used in the one dimensional case have been used for cyclopentane. However we have ignored more coupling terms here due to the two dimensional nature of puckering in 5 member rings. The possible coupling modes are determined by $E''_2 \times E''_2 = A_1' + A_2' + E_1'$. The resulting polynomial equation in ε is

$$-\varepsilon(\Delta\varepsilon_o-\varepsilon)^n - (\sum_{K=1}^{n} \alpha_K^{\ 2})(\Delta\varepsilon_o-\varepsilon)^{n-1}\ (S^2_{E''_{2a}} + S^2_{E''_{2b}}) = 0 \tag{10}$$

This can be solved exactly to yield

$$\varepsilon = \frac{1}{2}\Delta\varepsilon_o\ [1 \pm (1+4\alpha^2(S^2_{E''_{2a}} + S^2_{E''_{2b}}))^{1/2}] \tag{11}$$

with

$$\alpha^2 = \frac{1}{\Delta\varepsilon_o^{\ 2}} \sum_{K=1}^{n} \alpha_K^{\ 2} \tag{11a}$$

The determinant and resulting solution for ε look very similar to the one dimensional case, the difference being the inclusion of another dimension in the puckering motion. Addition of the quadratic terms defines the puckering potential for cyclopentane.

$$V(S_{E''_{2a}}, S_{E''_{2b}}) = \frac{1}{2}\Delta\varepsilon_o[1-(1+4\alpha^2(S^2_{E''_{2a}}+S^2_{E''_{2b}}))^{1/2}] + \frac{1}{2}K\,(S^2_{E''_{2a}}+S^2_{E''_{2b}}) \qquad (12)$$

This form can be expressed conveniently in polar coordinates as

$$V(\rho,\theta) = \frac{1}{2}\Delta\varepsilon_o\,[1-(1+4\alpha^2\rho^2)^{1/2}] + \frac{1}{2}K\,\rho^2 \qquad (13)$$

where we find that there is no angular dependence to the potential. The lack of angular dependence implies a free pseudorotation. This supports experimental observations and earlier theoretical work.[35-40] This aspect will be treated in more detail in the discussion section.

The puckering potentials (7,13) derived in this chapter are identical in form to the inversion potential for MX_3 molecules (Chap. 1, Eq. 15). Therefore the truncated forms and all the equations used to determine the potential parameters will also be the same. For the reader's convenience this information will be summarized. Refer to chapter 1 for details.

The truncated forms of Eq. (7) and Eq. (13) are

$$V_{Trunc}(S_{B_{1,2}}) = -aS^2_{B_{1,2}} + bS^2_{B_{1,2}} \qquad (14)$$

$$V_{Trunc}(\rho,\theta) = -a\rho^2 + b\rho^4 \tag{15}$$

where

$$a = \frac{K_o}{4} \tag{16a}$$

$$b = \frac{K_o}{8S_o^{\ 2}} \tag{16b}$$

S_o is replaced by ρ_o for the D_{5h} potential (15). S_o is the value of the puckering coordinate at the potential minimum. K_o represents the actual curvature at the potential minimum and can initially be approximated by the normal coordinate force constant. Corrections to K_o can be made iteratively as described in the MX_3 chapter.

The equations which determine the parameters α, K, and $\Delta\varepsilon_o$ for the full puckering potentials (7,13) are

$$\frac{\alpha^4}{(1+4\alpha^2 S_o^{\ 2})^{3/2}} = \frac{K_o}{8\ \Delta\varepsilon_o S_o^{\ 2}} \tag{17a}$$

$$K = 2\Delta\varepsilon_o\ \alpha^2\ (1+4\alpha^2 S_o^{\ 2})^{-1/2} \tag{17b}$$

B. Comparison of Derived Theoretically Puckering Potentials to Empirically Derived Puckering Potentials

It is interesting to compare the various potentials empirically determined for ring puckering in 4-membered, pseudo 4-membered, and 5-membered rings with the forms derived in this work. These previous potentials include

$$V_{cm^{-1}} = 12460z^2 + 560140z^4 + 130.2\ \exp(-268.0z^2) \quad \text{(TMO)}^{41} \tag{18a}$$

$$V_{cm^{-1}} = -\ 6738z^2 + 742220z^4 \quad \text{(TMO)}^{42} \tag{18b}$$

$$V_{cm^{-1}} = -\ 23500z^2 + 506000z^4 \quad \text{(TMS)}^{43} \tag{19}$$

$$V_{cm^{-1}} = -\ 33850z^2 + 123400z^4 \quad \text{(Cyclopentene)}^{44} \tag{20}$$

where z(Å) is an appropriately defined puckering coordinate. A comparison of calculated and observed energy levels for these potentials can be found in Table 1, 2 and 3. The most interesting feature of these tables is the excellent agreement between the calculated and observed transitions for such a simple form of the potential. In the TMO work[42] it was found that the two parameter potential (18b), where an inverted parabolic barrier was used, gave an overall more accurate fit to the experiment than the four parameter form Eq. (18a), where the potential barrier was constrained to be gaussian. Similar results were noted by the workers on TMS.[31] This indicates that this simple form must be very close to the true potential. This also demonstrates that there is a "preferred" form for the puckering potential, and

that empirically choosing a different form with more adjustable parameters does not insure an improved or even equivalent fit to experiment. In addition to the molecules discussed in detail here it should be mentioned that the two parameter potential

$$V = -ax^2 + bx^4 \tag{21}$$

has given very accurate results for nearly all 4-membered and pseudo 4-membered ring molecules.[45]

The success of the two parameter form Eq. (21) can be understood in terms of the potentials derived in this chapter. We see that Eq. (21) is nothing more than the truncated form Eq. (14) of the full potential (7). The fact that the truncated form does such a good job implies that the expansion of the full potential (Chap. 1, Eq. (16)) is valid. The criterion for the validity of the expansion was that $1 \gg 4\alpha^2 S_o^{\ 2}$. This criterion can be tested in the molecules considered here. The results are indicated in Table 4. K_o was determined from the corresponding literature potentials (18,19,20) by the relation $K_o = 4a$ Eq. (16a). S_o, the potential minimum, was also calculated from the potentials. $\Delta\varepsilon_o$ was approximated from published spectra on cyclic hydrocarbons,[32] where by observation most cyclic systems had absorptions averaging $\sim 70{,}000\ cm^{-1}$ (1.4 mdyn-Å). α is then solved for by Eq. (17a).

From Table 4 we see that the expansion parameter, $4\alpha^2 S_o^2$, is much smaller for TMO than for TMS and cyclopentene. This indicates that the truncated form of the potential (14) approximates the full potential (7) more accurately for TMO than for TMS and cyclopentene. Consequently the energy levels calculated for TMO using the truncated potential should be closer to the observed levels than for the analogous computations in TMS and cyclopentene (Tables 1,2,3). The agreement between experiment and calculation is substantially better in TMO (Table 1) than in TMS (Table 2) or cyclopentene (Table 3). Because TMS and cyclopentene have almost identical values for the expansion parameter, $4\alpha^2 S_o^2$ (Table 4), we might expect the difference between computed and observed transitions in both cases to be of similar sizes. This is confirmed by comparing Table 2(TMS) with Table 3 (cyclopentene). In the TMS and cyclopentene cases we find that the higher levels, calculated by the truncated potential, occur on the high frequency side of the observed transitions. This indicates that the outer walls of the truncated potential are too steep. The theory derived in the first section is in agreement with this observation. This can be demonstrated by looking at the next higher term (beyond fourth order) in the expansion of the full potential (7). This gives

$$V'(S) = -2\Delta\varepsilon_o \alpha^6 S^6 \tag{22}$$

Because this term is negative, it implies that the full potential (7) will have less steep outer walls than the truncated form (14).

Cyclopentane is different from the other molecules discussed so far in that it has two degenerate puckering coordinates (Fig. 2). This lead to a two dimensional potential (12) which could be conveniently expressed in polar coordinates Eq. (13). In the polar form the potential did not contain any angular dependence, which is analogous to the problem of a rotating-vibrating diatomic molecule constrained to rotate in a plane. Hence, cyclopentane is said to undergo a free pseudorotation.

In previous theoretical investigations on cyclopentane[37] it has been proposed that the absence of an angular term in the potential is primarily a geometrical consequence, because it appeared to be a feature independent of the detailed nature of the assumed intermolecular forces. This work confirms this observation and demonstrates its origin in a straightforward manner.

Angular barriers can arise from two different types of coupling. The first type is the coupling of a degenerate coordinate with other vibrational motions. This is generally a small effect because the coupling term will depend inversely on the force constant of the "other" mode(s). These other modes(s) usually occur at substantially higher energy than the puckering motion, and will have a "large" force constant. The second type of coupling, and the most important, is the coupling of a degenerate pair of coordinates to themselves. We saw an example of this in the MX_5 chapter, where the angular barrier in VF_5 arose from this type of self coupling. In MX_5 (D_{3h}) molecules the possible coupling modes were defined by $E' \times E' = E' + A_1' + A_2'$,

which shows that the E' coordinate can couple to itself. For cyclopentane we found that $E_2'' \times E_2'' = A_2' + A_1' + E_1'$ so that the puckering coordinate E_2'' cannot couple to itself. The only source of an angular term in cyclopentane is from coupling of the first type, which implies a small or even negligible angular barrier(s). Because these arguments are based mainly on group theory concepts, the geometrical basis of pseudorotation in cyclopentane is confirmed.

Another interesting aspect of the cyclopentane potential is the barrier height to planarity. The calculation of the barrier height was done with the full potential (13) rather than the truncated form (15). A look at Table 4 shows that for cyclopentane $4\alpha^2 S_o^2$ is equal to 1.32 which indicates that the expansion of the full potential converges very slowly. With the uncertainty in the location of the potential minimum, ρ_o,[46] calculated from different types of experiments, and the approximations used in pinpointing $\Delta\varepsilon_o$ the calculated range of the potential barrier to planarity is 2,300-2,600 cm^{-1}. Pitzer and Donath[35] estimated the barrier at 1,680 cm^{-1}, by taking into account c-c-c bond angle strain, torsional forces, and nonbonded interactions. Allinger and co-workers[39] found the barrier to be 2,220 cm^{-1}, using a semiclassical approach. Finally, Hoyland[38] placed the barrier at 2,820 cm^{-1} using an SCF model.

Table 1. Comparison of calculated and observed transitions in TMO. From the work of Borgers et al.[42]

$$V_{cm}-1 = -6738z^2 + 742220z^4 \quad \text{(See 18b)}$$

Transition	Calculated (cm^{-1})	Observed (cm^{-1})
0-1	53.4	53.4
1-2	89.9	89.9
2-3	104.8	104.7
3-4	118.2	118.1
4-5	129.2	128.8
5-6	138.7	138.9
6-7	147.1	147.3
7-8	154.7	155.0
8-9	161.6	161.6
9-10	168.0	168.2
10-11	174.0	174.9

Table 2. Comparison of calculated and observed transitions in TMS. From the work of Borgers and Strauss.[43]

$$V_{cm}-1 = -23500z^2 + 506000z^4 \quad \text{(See 19)}$$

Transition	Calculated (cm^{-1})	Observed (cm^{-1})
0-1	.27	.27
1-2	139.8	138.3
3-4	86.1	85.7
4-5	63.2	62.7
5-6	85.0	84.3
7-8	100.8	99.7
8-9	107.9	107.6
9-10	114.3	114.0
10-11	120.2	118.3

Table 3. Comparison of calculated and observed transitions in cyclopentene. From the work of Laane and Lord.[44]

$$V_{cm}-1 = -33850z^2 + 123400z^4 \quad \text{(See 20)}$$

Transition	Calculated (cm^{-1})	Observed (cm^{-1})
0-1	.79	.91
1-2	126.6	127.1
2-3	23.6	25.2
3-4	81.7	83.1
4-5	76.2	76.6
5-6	91.7	92.0
6-7	100.1	99.8
7-8	108.2	107.5
8-9	115.3	113.3
9-10	121.8	119.4
10-11	127.8	126.1

Table 4. Experimental[36,42-44] and derived parameters for some cyclic compounds.

	K_o ($\frac{mdyn}{Å}$)	S_o (Å)	Mass (amu)	$\Delta\varepsilon_o$ (mdyn-Å)	α ($\frac{1}{Å}$)	$4\alpha^2 S_o^2$
TMO	.54	.067	97.2	1.4	1.9	.065
TMS	1.78	.152	104.7	1.4	1.8	.30
Cyclopentene	2.71	.117	155.1	1.4	2.2	.27
Cyclopentane	1.43	.48	28.1	1.4	1.2	1.32

V. PSEUDOROTATION IN IF_7 AND ReF_7

A. Derivation of Pseudorotation Potentials for IF_7 and ReF_7

In this chapter we will consider distortions of a MX_7 molecule from a D_{5h} structure. The molecules which will be specifically studied are IF_7 and ReF_7. The symmetry coordinates for a MX_7 (D_{5h}) molecule are drawn in Fig. 1. The distortion which will be discussed is one along the E_2'' symmetry coordinates (S_{11a}, S_{11b}). This is equivalent to the puckering of a 5-member (D_{5h}) ring, which was discussed in detail for cyclopentane in the previous chapter. However for MX_7 molecules there is an additional feature, the coupling of the axial bend $S_7(E_1')$ to the puckering motion. For cyclopentane we found that the possible modes which could couple to the puckering were defined by $E_2'' \times E_2'' = E_1' + A_1' + A_2'$. In a MX_7 molecule there are no A_2' modes, three E_1' modes, and two A_1' modes (Fig. 1). For reasons to be discussed later, we will couple only the axial bend $S_7(E_1')$ to the distortion coordinates $S_{11}(E_2'')$.

As in MX_3 and MX_5 molecules the distortion in the MX_7 case can be considered to arise from a coupling of the ground electronic state to a certain electronic state via the distortion coordinates, S_{11a}, S_{11b}. The electronic structures of both IF_7,[47] and ReF_7 are diagrammed in Figs. 2 and 3. We see that both IF_7 and ReF_7 have a totally symmetric ground electronic state $^1A_1'$. The only allowed symmetry of the excited electronic state that couples to the $^1A_1'$ ground electronic via the E_2'' distortion coordinate must be $^1E_2''$. In both

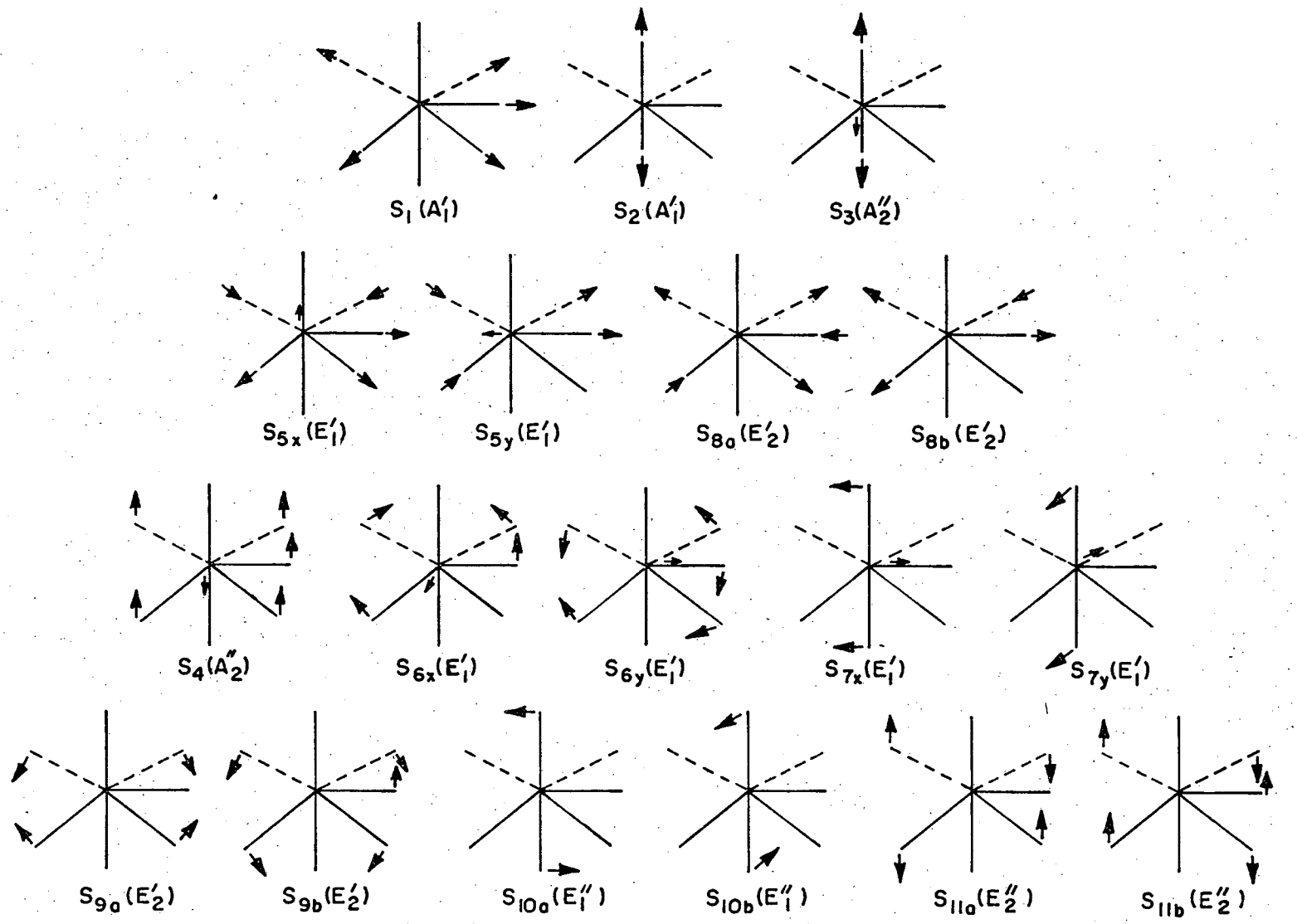

Fig. 1. Symmetry coordinates for a $MX_7(D_{5h})$ molecule.

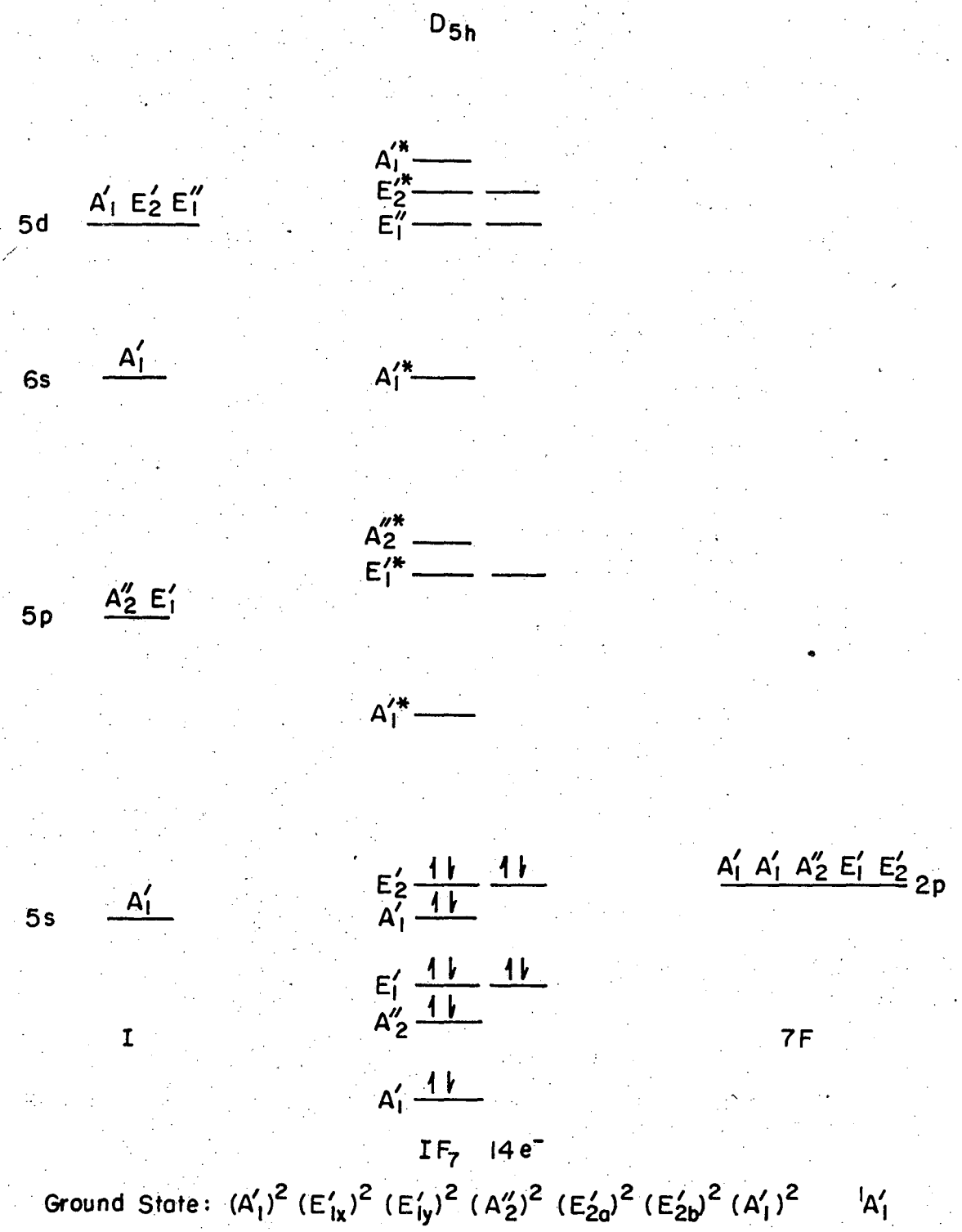

Ground State: $(A'_1)^2\,(E'_{1x})^2\,(E'_{1y})^2\,(A''_2)^2\,(E'_{2a})^2\,(E'_{2b})^2\,(A'_1)^2 \qquad {}^1A'_1$

XBL 744-6137

Fig. 2. Molecular orbital diagram for IF_7.

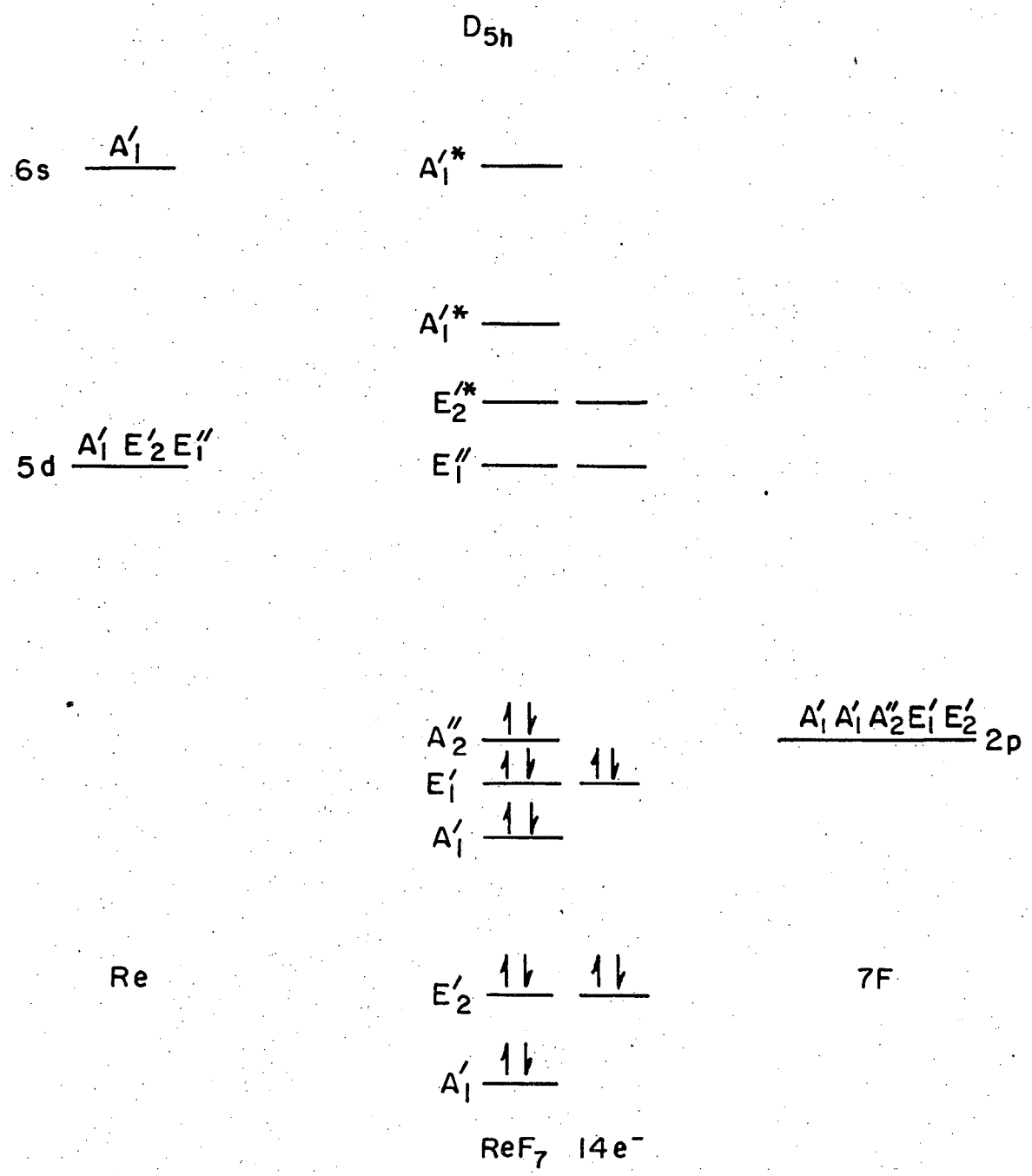

Ground State: $(A_1')^2\ (E_{2a}')^2\ (E_{2b}')^2\ (A_1')^2\ (E_{1x}')^2\ (E_{1y}')^2\ (A_2'')^2\ \ ^1A_1'$

XBL744-6138

Fig. 3. Molecular orbital diagram for ReF_7.

IF_7 and ReF_7 there will be many transitions leading to $^1E_2''$ excited states, however to pick the one that contributes most to the distortion process we can use the same guidelines as in the MX_5 chapter. These were (i) the molecular orbital from which the electron is excited should be localized on the atoms involved in the distortion,,(ii) the excited molecular orbital into which the electron goes should be one that can best help stabilize the distorted geometry. These factors indicate that the distortion process is facilitated by a charge transfer process in which charge is transferred from an orbital localized on the ligand atoms to an excited molecular orbital localized on the central atom. This transfer of charge should have the effect of relieving some of the repulsive forces due to the proximity of the five equatorial atoms. With these considerations the most reasonable choice of transitions is from the E_1' (F_{2p}) orbital to the E_1'' (5 dxz,yz) orbitals localized on the central atoms (Re, I). The symmetries of the excited states formed by this transition will be $E_1' \times E_1'' = E_2'' + A_1'' + A_2''$ which contains the species of interest, E_2''.

We are now in a position to construct the matrix of the linear term in the electronic basis $|^1A_1\rangle$, $|^1E_{2a}''\rangle$, $|^1E_{2b}''\rangle$. The matrix can be written as

$$
\begin{array}{c}
 \\ |^1A_1'\rangle \\ |^1E_{2a}''\rangle \\ |^1E_{2b}''\rangle
\end{array}
\begin{array}{c}
\begin{array}{ccc} |^1A_1'\rangle & |^1E_{2a}''\rangle & |^1E_{2b}''\rangle \end{array} \\
\begin{pmatrix}
-\varepsilon & & C_{11}S_{11b} \\
C_{11}S_{11a} & C_{7y}S_{7y} + \Delta\varepsilon_o - \varepsilon & C_{7x}\,S_{7x} \\
C_{11}S_{11b} & C_{7x}S_{7x} & -C_{7y}S_{7y} + \Delta\varepsilon_o - \varepsilon
\end{pmatrix}
\end{array}
\qquad (1)
$$

where

$$C_{11} = \langle {}^1A_1' \mid \left(\frac{\partial H_v}{\partial S_{11a}}\right)_{S_o} \mid {}^1E_{2a}'' \rangle = \langle {}^1A_1' \mid \left(\frac{\partial H_v}{\partial S_{11b}}\right)_{S_o} \mid {}^1E_{2b}'' \rangle \qquad (2a)$$

$$C_{7y} = \langle {}^1E_{2a}'' \mid \left(\frac{\partial H_v}{\partial S_{7y}}\right)_{S_o} \mid {}^1E_{2a}'' \rangle = -\langle {}^1E_{2b}'' \mid \left(\frac{\partial H_v}{\partial S_{7y}}\right)_{S_o} \mid {}^1E_{2b}'' \rangle \qquad (2b)$$

$$C_{7x} = \langle {}^1E_{2a}'' \mid \left(\frac{\partial H_v}{\partial S_{7x}}\right)_{S_o} \mid {}^1E_{2b}'' \rangle \qquad (2c)$$

$$\Delta\varepsilon_o = \varepsilon_{{}^1E_2''} - \varepsilon_{{}^1A_1'}$$

where we define $\varepsilon_{{}^1A_1'} = 0$

For simplicity we can work with the determinant of the matrix (1) in the form

$$
\begin{array}{c}
 \\ |^1A_1'\rangle \\ |^1E_{2a}''\rangle \\ |^1E_{2b}''\rangle
\end{array}
\begin{array}{c}
\begin{array}{ccc} |^1A_1'\rangle & |^1E_{2a}''\rangle & |^1E_{2b}''\rangle \end{array} \\
\begin{vmatrix}
-\varepsilon & A_1 & A_2 \\
A_1 & B_1 + \Delta\varepsilon_o - \varepsilon & B_2 \\
A_2 & B_2 & -B_1 + \Delta\varepsilon_o - \varepsilon
\end{vmatrix}
\end{array}
\qquad (3)
$$

where

$$A_1 = C_{11} S_{11a} \tag{4a}$$

$$A_2 = C_{11} S_{11b} \tag{4b}$$

$$B_1 = C_{7y} S_{7y} \tag{4c}$$

$$B_2 = C_{7x} S_{7x} \tag{4d}$$

The resulting polynomial equation in ε is

$$-\varepsilon[(\Delta\varepsilon_o-\varepsilon)^2 - (B_1^2 + B_2^2)] + 2A_1A_2B_2 - (A_1^2+A_2^2)(\Delta\varepsilon_o-\varepsilon) + B_1(A_1^2-A_2^2) = 0 \tag{5}$$

With the assumption that $\Delta\varepsilon_o \gg \varepsilon$, B_1, B_2, which should be valid for small distortions, the cubic equation (5) can be simplified to a second order equation in ε.

$$-\varepsilon(\Delta\varepsilon_o-\varepsilon) + \frac{2A_1A_2B_2}{\Delta\varepsilon_o} + \frac{B_1(A_1^2-A_2^2)}{\Delta\varepsilon_o} - (A_1^2 + A_2^2) = 0 \tag{6}$$

This equation shows explicity the coupling of the puckering motion (A_1,A_2) to the axial bend (B_1, B_2). In the limit that the coupling constants C_{7x} and C_{7y} are zero, the second and third terms in Eq. (6) would vanish and we would be left with essentially the same equation as in the cyclopentane molecule. The roots of Eq. (6) are

$$\varepsilon = \frac{1}{2}\Delta\varepsilon_o\ [1\pm(1+\frac{4}{\Delta\varepsilon_o^2}\{(A_1^2+A_2^2) - \frac{2A_1A_2B_2}{\Delta\varepsilon_o} + \frac{B_1(A_2^2-A_1^2)}{\Delta\varepsilon_o}\})^{1/2}] \tag{7}$$

This can be recast into the original coordinates (4) to yield

$$\varepsilon = \frac{1}{2}\Delta\varepsilon_o[1\pm(1+4\alpha^2\{(S_{11a}^2+S_{11b}^2) - 2\beta_x S_{11a}S_{11b}S_{7x} + \beta_y S_{7y}(S_{11b}^2-S_{11a}^2)\})^{1/2}] \tag{8}$$

where

$$\alpha = \frac{C_{11}}{\Delta\varepsilon_o} \tag{9a}$$

$$\beta_x = \frac{C_{7x}}{\Delta\varepsilon_o} \tag{9b}$$

$$\beta_y = \frac{C_{7y}}{\Delta\varepsilon_o} \tag{9c}$$

The full distortion potential, including axial coupling, is defined by adding the appropriate quadratic terms to the lower root of Eq. (8).

$$\begin{aligned} V(S_{7x},S_{7y},S_{11a},S_{11b}) = \frac{1}{2}\Delta\varepsilon_o[1-(1+4\alpha^2\{(S_{11a}^2+S_{11b}^2)-2\beta_x S_{11a}S_{11b}S_{7x} \\ +\beta_y S_{7y}(S_{11b}^2-S_{11a}^2)\})^{1/2}] + \frac{1}{2}K_7(S_{7x}^2 + S_{7y}^2) \\ + \frac{1}{2}K_{11}\ (S_{11a}^2 + S_{11b}^2) \end{aligned} \tag{10}$$

The leading terms of an expansion of Eq. (10) which couple the E_2'' and E_1'' modes are of the form

$$V_{couple} = -\Delta\varepsilon_o\alpha^2[\beta_y S_{7y}(S_{11b}^2 - S_{11a}^2) - 2\beta_x S_{11a} S_{11b} S_{7x}] \qquad (11)$$

We can solve for the E_1' motion in terms of the E_2'' mode by requiring the E_1' coordinates to follow the E_2'' motion in such a way as to minimize the potential energy Eq. (10). This can be accomplished by taking $\partial V/\partial S_{E_1'} = 0$ and solving the resulting equation for E_1' in terms of E_2''. The equivalent approximation was made in the MX_5 chapter (Eqs. 8,9) to reduce a two dimensional potential to a one dimensional potential.

$$\frac{\partial V}{\partial S_{7x}} \approx \frac{\partial V_{couple}}{\partial S_{7x}} + K_7 S_{7x} = 2\Delta\varepsilon_o\alpha^2\beta_{7x} S_{11a} S_{11b} + K_7\, S_{7x} = 0 \qquad (12)$$

$$S_{7x} = -\frac{2\Delta\varepsilon_o\alpha^2\beta_x}{K_7}\, S_{11a}\, S_{11b}$$

The same approximation applied to S_{7y} gives

$$S_{7y} = \frac{\Delta\varepsilon_o\alpha^2\beta_y}{K_7}\,(S_{11b}^2 - S_{11a}^2) \qquad (13)$$

These equations for S_{7y}, S_{7x} can be substituted back into V_{couple} in Eq. (11).

$$V_{couple} = -\frac{\Delta\varepsilon_o^2\,\alpha^4}{K_7}\,[\beta_y^2\,(S_{11b}^2 - S_{11a}^2)^2 + 4\beta_x^2\,S_{11a}^2\,S_{11b}^2] \tag{14}$$

In this form (14) there is an angular dependence to the potential in the form of the cross terms in S_{11a} and S_{11b}. If we assume that $\beta_y \approx \beta_x$, Eq. (14) takes on a particularly simple form.

$$V_{couple} = -\frac{\Delta\varepsilon_o^2\,\alpha^4\beta^2}{K_7}\,(S_{11b}^2 + S_{11a}^2)^2 \tag{15}$$

There is no angular dependence to Eq. (15) if polar coordinates are introduced. For simplicity, and also because it seems physically plausible that $\beta_{7y} \approx \beta_{7x}$, we will use form Eq. (15) for V_{couple} in the remainder of this chapter.

In this approximation (15) the full potential (10) reduces to just a function of the E_2'' coordinates.

$$V(S_{11a};S_{11b}) = \frac{1}{2}\,\Delta\varepsilon_o[1-(1+4\alpha^2[(S_{11a}^2+S_{11b}^2) + \delta^2(S_{11a}^2+S_{11b}^2)^2])^{1/2}]$$

$$+ \frac{1}{2}\,K_{11}\,(S_{11a}^2 + S_{11b}^2) \tag{16}$$

where

$$\delta^2 = \frac{\Delta\varepsilon_o\beta^2\alpha^2}{2K_7} \tag{17}$$

In polar coordinates (ρ,θ) the full potential in Eq. (16) becomes

$$V(\rho,\theta) = \frac{1}{2}\,\Delta\varepsilon_o\,[1-(1+4\alpha^2\rho^2(1+\delta^2\rho^2))^{1/2}] + \frac{1}{2}\,K_{11}\,\rho^2 \tag{18}$$

The truncated form of Eq. (18) will look like

$$V_{Trunc}(\rho,\theta) = -\,a\rho^2 + b\rho^4 \tag{19}$$

where a,b are adjustable parameters.

In order to get quantitative values for the three parameters of the full potential in Eq. (18), α, δ, K_{11}, we must find three linearly independent relationships among them. Using the two derivative conditions (1) first derivative of the potential is zero at $\rho=0$ (potential maximum) and at $\rho=\rho_o$ (equilibrium geometry), and (2) the second derivative equals the curvature k_o ($\approx$ force constant) at the equilibrium position ρ_o, we can get two relationships. These are

$$\frac{\alpha^4(1+2\delta^2\rho_o^2)^2}{[1+4\alpha^2\rho_o^2(1+\delta^2\rho_o^2)]^{3/2}} - \frac{4\alpha^2\delta^2}{[1+4\alpha^2\rho_o^2(1+\delta^2\rho_o^2)]^{1/2}} = \frac{k_o}{8\Delta\varepsilon_o\rho_o^{\,2}} \tag{20a}$$

$$K_{11} = \frac{2\Delta\varepsilon_o\alpha^2(1+2\delta^2\rho_o^2)}{[1+4\alpha^2\rho_o^2(1+\delta^2\rho_o^2)]^{1/2}} \tag{20b}$$

You might recall that in the MX_5 chapter there were also three parameters, and using conditions on the derivatives we were able to quantitatively define all three (Chap. 2, Eq. (15a,b,c)). In the MX_5 case the origin of the third relationship was that the third derivative of the potential be zero at the potential maximum. This insured that the symmetry was of the double minimum variety. However, the lack of a cubic term in the MX_7 potential means the third derivative is always identically zero regardless of the values of the three parameters. Hence, we must look elsewhere for another relation.

We can find this third equation in the form of the coupling relationships in Eqs. (12,13) in conjunction with the definition of δ in Eq. (17). In the approximation $\beta_x \approx \beta_y$ in Eq. (15) it turns out that the magnitude of the axial bend $|S_7|$ is constant and can be related to the puckering coordinate ρ as

$$|S_7| = \alpha\delta \left(\frac{2\Delta\varepsilon_o}{K_7}\right)^{1/2} \rho_o^{\,2} \tag{21}$$

where we now have the three Eqs. (20a, 20b, 21) to solve for α, δ, K_{11}. In Eq. (21) $|S_7|$ and ρ_o are determined by electron diffraction measurements,[48,49] and K_7 is simply the force constant of the axial bend.

B. Definition of Coordinate System and Estimate of Some Potential Parameters

The symmetry coordinates for the axial bend (S_7) and the equatorial puckering mode (S_{11}) are defined by[50]

$$S_{7x} = \frac{r_{M-F(ax)}}{\sqrt{5}} [(\Delta\beta_{26}+\Delta\beta_{27}-\Delta\beta_{56}-\Delta\beta_{57})\sin 72° + (\Delta\beta_{36}+\Delta\beta_{37}-\Delta\beta_{46}-\Delta\beta_{47})\sin 144°] \tag{22a}$$

$$S_{7y} = \frac{r_{M-F(ax)}}{\sqrt{5}} [(\Delta\beta_{16}+\Delta\beta_{17}) + (\Delta\beta_{26}+\Delta\beta_{27}+\Delta\beta_{56}+\Delta\beta_{57})\cos 72° + (\Delta\beta_{36} + \Delta\beta_{37} + \Delta\beta_{46} + \Delta\beta_{47}) \cos 144°] \tag{22b}$$

$$S_{11a} = \frac{r_{M-F(eq)}}{\sqrt{5}} [(\Delta\beta_{26}-\Delta\beta_{27} - \Delta\beta_{56}+\Delta\beta_{57}) \sin 144° - (\Delta\beta_{36} - \Delta\beta_{37} - \Delta\beta_{46} + \Delta\beta_{47}) \sin 72°] \tag{23a}$$

$$S_{11b} = \frac{r_{M-F(eq)}}{\sqrt{5}} [(\Delta\beta_{16}-\Delta\beta_{17}) + (\Delta\beta_{26}-\Delta\beta_{27}+\Delta\beta_{56}-\Delta\beta_{57})\cos 144 + (\Delta\beta_{36}-\Delta\beta_{37} + \Delta\beta_{46}-\Delta\beta_{47}) \cos 72°] \tag{23b}$$

where r_{M-F} is the M-F bond distance, and $\Delta\beta_{ij}$ is the change in angle between the equatorial fluorines (1,2,3,4,5) and the axial fluorines (6,7). For the axial coordinates in Eqs. (22a, 22b) the terms $\Delta\beta_{16}$, $\Delta\beta_{17}$

also represent the angular displacement from the linear axial configuration, since the motion in S_{7y} is directed towards one of the equatorial atoms (Fig. 1). For the puckering motion (23a, 23b) $\Delta\beta_{ij}$ also represents the angle of a M-F_{eq} bond with a hypothetical planar arrangement of the five equatorial atoms. This fact allows us to convert easily from the coordinate system used in the electron diffraction work[48,49] to the symmetry coordinates in Eqs. (22,23). The electron diffraction coordinates were,

$$\alpha_i = \alpha^o \cos 2\left(\frac{\pi}{5} i + \phi\right) \qquad i = 1, \ldots, 5 \tag{24}$$

where α_i is the angle the i'th fluorine makes with the hypothetical planar ring. The parameter, ϕ, is the phase of the distortion, in the sense of the relative amounts of S_{11a} and S_{11b}. That is, ϕ=0 corresponds to a distortion just along S_{11b}, while ϕ=45° corresponds to just S_{11a}, and intermediate phases, $0° \leqslant \phi \leqslant 45°$, represent some linear combination of S_{11a} and S_{11b}.[48] If we now take ϕ=0 we have in effect defined S_{11b} because the α_i are identical to the $\Delta\beta_{ij}$. With S_{11b} quantitatively fixed, so is the equilibrium geometry, ρ_o. Because

$$\rho_o = S_{11a}^2 + S_{11b}^2$$

it (ρ_o) is independent of the relative phase (ϕ) of S_{11a} and S_{11b}, therefore the choice ϕ=0 is for convenience. For ϕ=0 we have S_{11a}=0 which leaves $\rho_o = |S_{11b}|$.

The conversion of the diffraction parameter (β) for the axial bend to the symmetry coordinate in Eq. (22) is also straightforward. The parameter β represents the magnitude of the axial bend, where β is the $M\text{-}F_{(ax)}$ bond angle relative to a linear arrangement of the axial fluorines. We can identify β directly with $\Delta\beta_{16}$ and $\Delta\beta_{17}$ in S_{7y}. In the preceding section we saw that the magnitude of the axial bend $|S_7|$ was constant (21), thus the absolute value of S_{7y}, which is fixed by β, also represents $|S_7|$.

The mass (m_{11}) associated with the puckering mode (S_{11}) can be taken as the inverse of the corresponding G-matrix element.[50]

$$m_{11} = \frac{m_F}{2} \tag{25}$$

where m_F is the mass of a fluorine atom. Wilson's high frequency approximation[11] is not needed for the puckering motion because there is only one mode of E_2'' symmetry for a MX_7 (D_{5h}) molecule (Fig. 1). Hence, there are no cross terms in the G-matrix. Defining the axial bend mass (m_7) is more involved, because there are three E_1' motions (Fig. 1). For simplicity, and also because the axial motion is not our primary interest, the mass (m_7) will be approximated by its diagonal component in the G-matrix,[50]

$$m_7 \approx \frac{2m_F m_M}{5m_M + 10m_F} \tag{26}$$

where m_M is the mass of the central atom (M).

The force constants associated with the puckering mode (k_o) and axial bend (k_7) were calculated by the equation

$$K = (5.9\times10^{-7})(V_{0\to1})^2 m \tag{27}$$

where, with m (amu) and $V_{0\to1}$ (cm^{-1}), K will be in mdyn/Å (Chap. 1, Eq. (33)).

Since the E_2'' mode is inactive[51-53] in both the Raman and infrared, a suitable guess must be made for $V_{0\to1}^{E_2''}$ of the puckering motion before k_o can be calculated via Eq. (27). A good approximation to the E_2'' motion in MX_7 (D_{5h}) molecules is the T_{2u} mode of octahedral MX_6 molecules. A visual comparison of the T_{2u} mode (Fig. 4) with the S_{11a} coordinate (Fig. 1) shows that these two motions are almost identical. Therefore the T_{2u} fundamentals of ReF_6 and TeF_6[54] (IF_6 does not exist) should be reasonable guesses for the E_2'' fundamentals of ReF_7 and IF_7. We will take $V_{0\to1}^{E_2''}$ (ReF_7) = 150 cm^{-1} and $V_{0\to1}^{E_2''}$ (IF_7) = 200 cm^{-1} (Table 1). An independent check of this approach is provided, in that the T_{1u} bend for MX_6 molecules (Fig. 4) is similar to the A_2'' (S_4) mode (Fig. 1) in MF_7 molecules. For ReF_6 $V_{T_{1u}}$ = 257 cm^{-1} and in TeF_6 $V_{T_{1u}}$ = 325 cm^{-1}. For ReF_7[17] $V_{A_2''}$ = 299 cm^{-1} and in IF_7[17] $V_{A_2''}$ = 365 cm^{-1}. We see that $V_{T_{1u}}^{MX_6} < V_{A_2''}^{MX_7}$. This is physically reasonable in that MX_7 molecules contain an extra equatorial fluorine which should lead to a slightly steeper potential for the umbrella type motion due to increased F-F repulsion. The extra

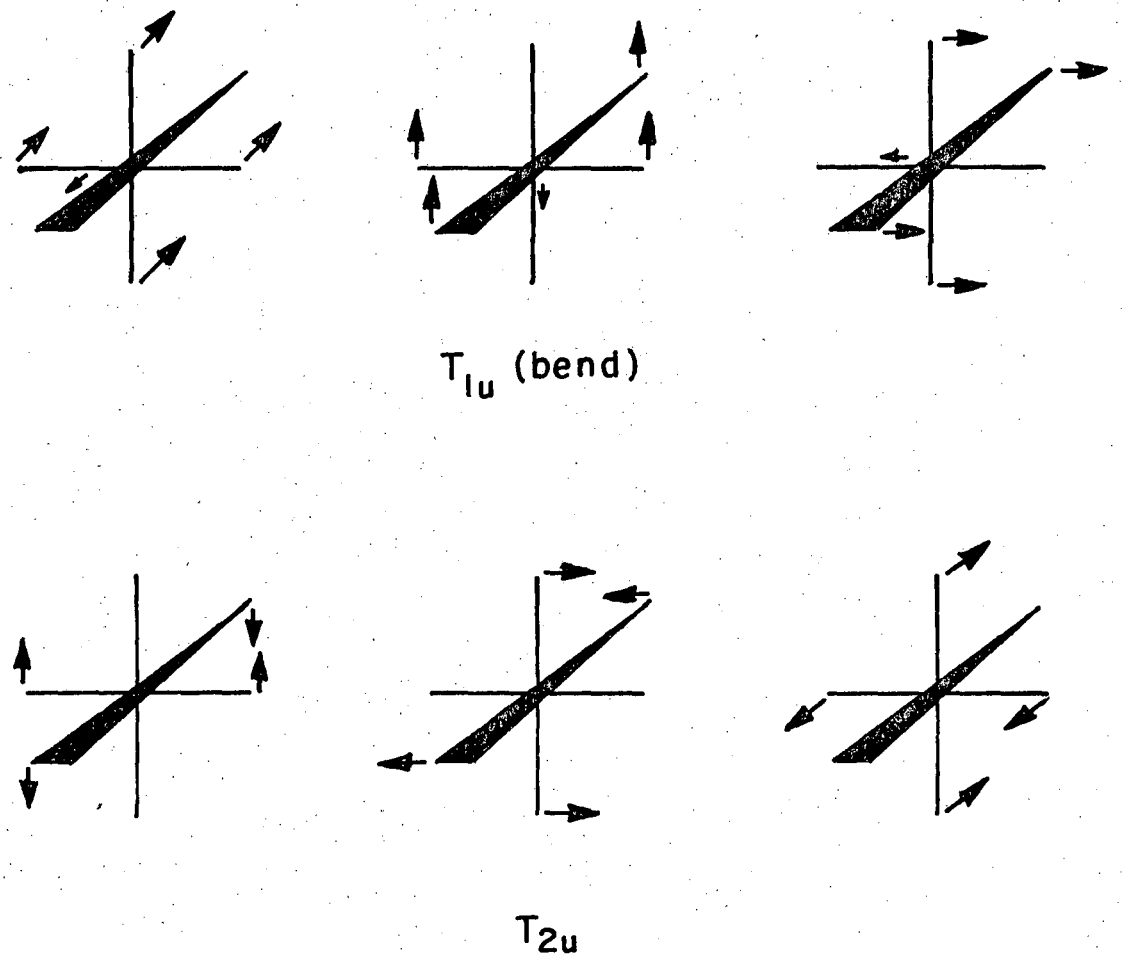

XBL744-6139

Fig. 4. T_{1u}(bend) and T_{2u} symmetry coordinates for an octahedral molecule.

equatorial fluorine should not be as big a factor in the T_{2u}, E_2'' motions, due to the symmetry of the modes. The corresponding comparison between the T_{2u}, E_2'' motions should be better than the A_2'', T_{1u} comparison.

The electronic transition energy $\Delta\varepsilon_o$ ($^1A_1' \rightarrow {}^1E_2''$) was approximated in both IF_7 and ReF_7 due to a lack of published ultraviolet spectra. In the case of ReF_7, $\Delta\varepsilon_o$ was crudely estimated as the difference[19] in energy between a F(2p) orbital and a Re(5d) orbital (Fig. 3), which places $\Delta\varepsilon_o \approx 65{,}000\ cm^{-1}$ (1.3 mdyn/Å). Because the 5d orbitals of I are virtual orbitals (not occupied in the I electronic ground state), it is more difficult to estimate $\Delta\varepsilon_o$ than for ReF_7. However the 5d's on I will be substantially higher in energy than those of Re, so $\Delta\varepsilon_o$ is arbitrarily placed at $\Delta\varepsilon_o \approx 100{,}000\ cm^{-1}$ (2 mdyn/Å).

With $\Delta\varepsilon_o$, k_o, k_7, ρ_o, and $|S_7|$ now quantitatively defined it is possible to find quantitative puckering potentials for IF_7 and ReF_7 using the relations (20a, 20b, 21). The final results are found in Table 2.

C. Discussion of Other Work on IF_7 and ReF_7

The most direct evidence for distortions in IF_7 and ReF_7 is from electron diffraction measurements.[48,49] It was concluded from an analysis of the radial distribution curves for both molecules that only a distortion along the E_2'' (S_{11}) coordinates coupled in a particular way to the axial bend E_1' (S_7) could account most precisely for the experimental data. The suggested coupling was of the form

$$(E_2'')^2 \; (E_1')_{axial} \tag{28}$$

which is identical to the coupling we have derived in the first section (11). One limitation of the diffraction experiments is that they could not supply direct evidence for a dynamic model (pseudo-rotation). The diffraction work could only determine the magnitude of the puckering and axial distortion.

Electric field deflection experiments are complimentary to the diffraction work, in that they can distinguish between a static deformation and a pseudo-rotating model, assuming that there is some sort of dipole moment. If the dipole moment is static then its magnitude and orientation in the molecular frame will be essentially temperature independent. On the other hand, if the dipole moment is fixed in magnitude but changing orientation in the molecular frame (psuedorotating) its behavior will be strongly temperature dependent. Both IF_7 and ReF_7 show a strong temperature dependence in the field deflection work.[55] Furthermore, ReF_7 shows a stronger effect than IF_7, which is in agreement with the larger axial distortion in ReF_7, hence a larger dipole moment. The phenomenon of electric field deflection is discussed in detail in the last chapter. The sketchy outline presented here is only to point out that there is strong evidence for a pseudorotating model in IF_7 and ReF_7. From the form of the full potential (18) (no angular dependence) we have derived a pseudorotating model for both IF_7 and ReF_7.

Our assignment of the fundamental frequencies in IF_7 and ReF_7 can be found in Table 3. A comparison of various assignments[51-53] for IF_7 and ReF_7 shows that there is strong disagreement over the assignment of the E_1' axial bend (V_2), the A_2'' umbrella motion (V_4), the E_1' equatorial stretch (V_8), and the E_1'' axial bend (V_{10}). Claasen and co-workers[53] assigned $V_7 = 257\ cm^{-1}$ and $V_4 = 365\ cm^{-1}$ in IF_7, while Eysel and co-workers[52] assigned $V_7 = 363\ cm^{-1}$ and $V_4 = 257\ cm^{-1}$. Eysel based his assignment on a comparison of the band contours of these modes with those expected for a static D_{5h} structure. This is dangerous because the axial bend (V_2) is strongly coupled to the psuedorotating mode (E_2'') which could drastically change the nature of the expected band contours. Further evidence against Eysel's assignment is the comparison of $V_4(A_2'')$ for MX_7 molecules to $V_{T_{1u}}$ (bend) of MX_6 molecules, where for TeF_6 $V_{T1u} = 325\ cm^{-1}$. If, as Eysel proposes, $V_4 = 257\ cm^{-1}$ then $V_{T_{1u}}^{MX_6} > V_{A_2''}^{MX_7}$ which is contrary to what was rationalized in the previous section. For these reasons we accept Claasen's assignment of V_4 and V_7 in IF_7.

For IF_7 Claasen places the E_1' equatorial stretch at $V_8 = 352\ cm^{-1}$ and the E_1'' axial bend at $V_{10} = 510\ cm^{-1}$, while Eysel places $V_8 = 510\ cm^{-1}$ and $V_{10} = 310\ cm^{-1}$. Claasen's unusual assignment of a stretching mode having a much lower frequency than a bending mode was motivated by an improved fit to the combination bands. This assignment is physically unreasonable, because we saw earlier that V_7 which is also an axial bend occurs at $257\ cm^{-1}$. Thus V_{10}, also an axial bend, should occur at a similar frequency. The problem of assigning combination and overtone

bands will in some part be complicated by the pseudorotation mode. For these reasons Eysel's assignment of V_{10} and V_{10} is accepted here. Claasen's assignment of V_9 and V_{10} in ReF_7 has been changed to be consistent with the IF_7 assignment.

In addition to the problem of assigning the fundamentals for IF_7 and ReF_7, there is a striking difference in the appearance of the IF_7 and ReF_7 spectra. Claasen noted that[53] "(1) two bond stretching, infrared-active fundamentals are found for IF_7, where as only one is observed for ReF_7, (2) two intense and highly polarized Raman bands are observed for IF_7 and only one for ReF_7, (3) the infrared fundamentals of ReF_7 have half-intensity widths roughly twice as great as those of IF_7." We will comment on the first and third observations, as Claasen has already proposed a reasonable explanation for the second observation.

An $MX_7(D_{5h})$ molecule has 18 degrees of vibrational freedom which fall under the symmetry species $2A_1' + 2A_2'' + 3E_1' + 2E_2' + E_1'' + E_2''$ (Fig. 1). The species A_1', E_1'', E_2' are Raman active, while A_2'', E_1' are infrared active and E_2'' is inactive in both Raman and infrared. The possible modes which can couple to the E_2'' distortion were defined by $E_2'' \times E_2'' = E_1' + A_1' + A_2'$. Although we treated the axial bend (E_1') coupling in detail, we would find the same general features for E_2'' coupling with the remaining E_1' modes and the A_1' modes (there is no A_2' mode). The leading coupling term for these other cases would be of the form

$$V_{couple} = \frac{\Delta}{K} (E_2'')^2 (\Gamma) \qquad (29)$$

where Γ is an E_1' or A_1' coordinate, K is the force constant of the Γ mode, and Δ is a product of linear matrix elements Eq. (11). The two A_1' modes in MX_7 molecules are symmetrical stretches (Fig. 1) which occur at a relatively high energy, thus K is large. The net effect would be a small coupling term (29), which means the A_1' motions would be relatively unaffected by small or even moderate E_2'' distortions. There are two E_1' bending modes and one E_1' stretch. Because the E_1' bend occurs at relatively low energy (small K) the coupling will be stronger than in the A_1' case. The effect of coupling a degenerate E_1' mode to the E_2'' distortion will be two-fold (1) the E_1' frequency will shift as a function of the E_2'' coordinates (2) the doubly degenerate E_1' mode will be split by the coupling. Even though the coupling to the E_1' stretch will be weaker than the E_1' bend, the removal of the degeneracy will enhance the broadening effect of the coupling. Because the A_2'' stretch and E_1' stretch occur at comparable frequencies in the infrared for IF_7, it is concieveable that the larger E_2'' distortion in the ReF_7 case would sufficiently broaden the E_1' stretch to, in effect, mask the A_2'' stretch. In summary, the theory derived here predicts that the infrared fundamentals will be perturbed much more by the E_2'' motion than the Raman bands. Also, the effect in ReF_7 will be larger than in IF_7.

It was mentioned at the beginning of this chapter that only coupling of the axial bend to the E_2'' pucker would be considered. The reason for this is now clear, because the axial bend occurs at much lower energy than the remaining E_1' modes, and the two A_1' stretches

(Table 3). Hence, coupling to the axial bend will predominate over the other couplings.

At the present time there are no published values for the barriers to planarity in IF_7 and ReF_7. The estimates here place the IF_7 barrier at 1481 cm^{-1} and the ReF_7 barrier at 2236 cm^{-1}. The error of these values will be on the order of the error in estimating $\Delta\varepsilon_o$. Since there are no available ultraviolet spectra for IF_7 or ReF_7 there is no way to determine the error in $\Delta\varepsilon_o$. However, it is unlikely that the approximate $\Delta\varepsilon_o$'s are beyond a ± 30% (2-3 eV) range of their true values.

Table 1. Fundamental frequencies for the $T_{1u(bend)}$ and T_{2u} modes of the octahedral molecules TeF_6 and ReF_6.

	$T_{1u(bend)}$ (cm^{-1})	T_{2u} (cm^{-1})
TeF_6	325	197
ReF_6	257	147

Table 2. Experimental and potential parameters for IF_7 and ReF_7.

Parameter	IF_7	ReF_7
$r_{M-F(eq)}$ (Å)	1.86	1.86
$r_{M-F(ax)}$ (Å)	1.79	1.79
$\nu_{11}^{E''_2}$ (cm^{-1})	200	150
m_{11} (amu)	9.5	9.5
k_o ($\frac{mdyn}{Å}$)	.224	.126
$\nu_7^{E'_1}$ (cm^{-1})	257	217
m_7 (amu)	6.3	6.3
k_7 ($\frac{mdyn}{Å}$)	.245	.175
ρ_o (Å)	.544	.630
$\Delta\varepsilon_o$ (mdyn-Å)	2	1.3
$\lvert S_7 \rvert$ (Å)	.230	.375
α ($\frac{1}{Å}$)	.757	.867
δ ($\frac{1}{Å}$)	.254	.283
k_{11} ($\frac{mdyn}{Å}$)	1.83	1.39
Barrier to Planarity (cm^{-1})	1481	2236

Table 3. Assignment of Fundamental Frequencies for IF_7 and ReF_7.

Fundamental	Symmetry	IF_7 (cm^{-1})	ReF_7 (cm^{-1})
V_1	A_1'	676	736
V_2	A_1'	635	645
V_3	A_2''	670	703
V_4	A_2''	365	299
V_5	E_1'	746	703
V_6	E_1'	425	353
V_7	E_1'	257	217
V_8	E_2'	510	597
V_9	E_2'	352	489
V_{10}	E_1''	310	352
V_{11}	E_2''	(200)[a]	(150)[a]

[a]These are guesses based on TeF_6, ReF_6 (see calculation section).

VI. PSEUDOROTATION IN XENON HEXAFLUORIDE (XeF_6)

A. Theory: Derivation of the Pseudorotational Potential Function (XeF_6)

The coordinate system which will be used in this chapter to describe the internal motions of XeF_6 are the symmetry coordinates of an octahedral (O_h) MX_6 molecule. These are pictured in Fig. 1. From the symmetry we see that distortions of an MX_6 molecule from an octahedral geometry can take place along pathways in a twelve dimensional space. Our focus in this chapter will be primarily on distortions arising from T_{1u} displacements (mostly $S_4(T_{1u}$ bend)), which are strongly coupled to the $T_{2g}(S_5)$ mode. Other possible couplings will also be considered in detail.

The electronic structure of XeF_6 is diagrammed in Fig. 2. From the molecular orbital diagram (Fig. 2) we might expect that the first excited electronic state (T_{1u}) is relatively close to the ground electronic state ($^1A_{1g}$), while the other excited electronic states are of considerably higher energy than the T_{1u} state. There are actually two T_{1u} states, a singlet $^1T_{1u}$ state and a triplet $^3T_{1u}$ state, however orthogonality of the triplet spin on $^3T_{1u}$ with the singlet spin on $^1A_{1g}$ precludes coupling between these states. Spin-orbit effects can mix $^1T_{1u}$ and $^3T_{1u}$ to modify this argument, which will be discussed in a later section. In this section only coupling of the $^1T_{1u}$ state with the $^1A_{1g}$ ground state via T_{1u} distortions will be considered.

The possible modes which can couple to a T_{1u} distortion are defined by $T_{1u} \times T_{1u} = A_{1g} + E_g + T_{1g} + T_{2g}$. From Fig. 1 we find that the species A_{1g}, E_g, and T_{2g} correspond to actual symmetry coordinates while T_{1g} does not. In addition we note that $T_{2u}(S_6)$ displacements do not couple to the T_{1u} distortions. Of the modes that couple, the $T_{2g}(S_5)$

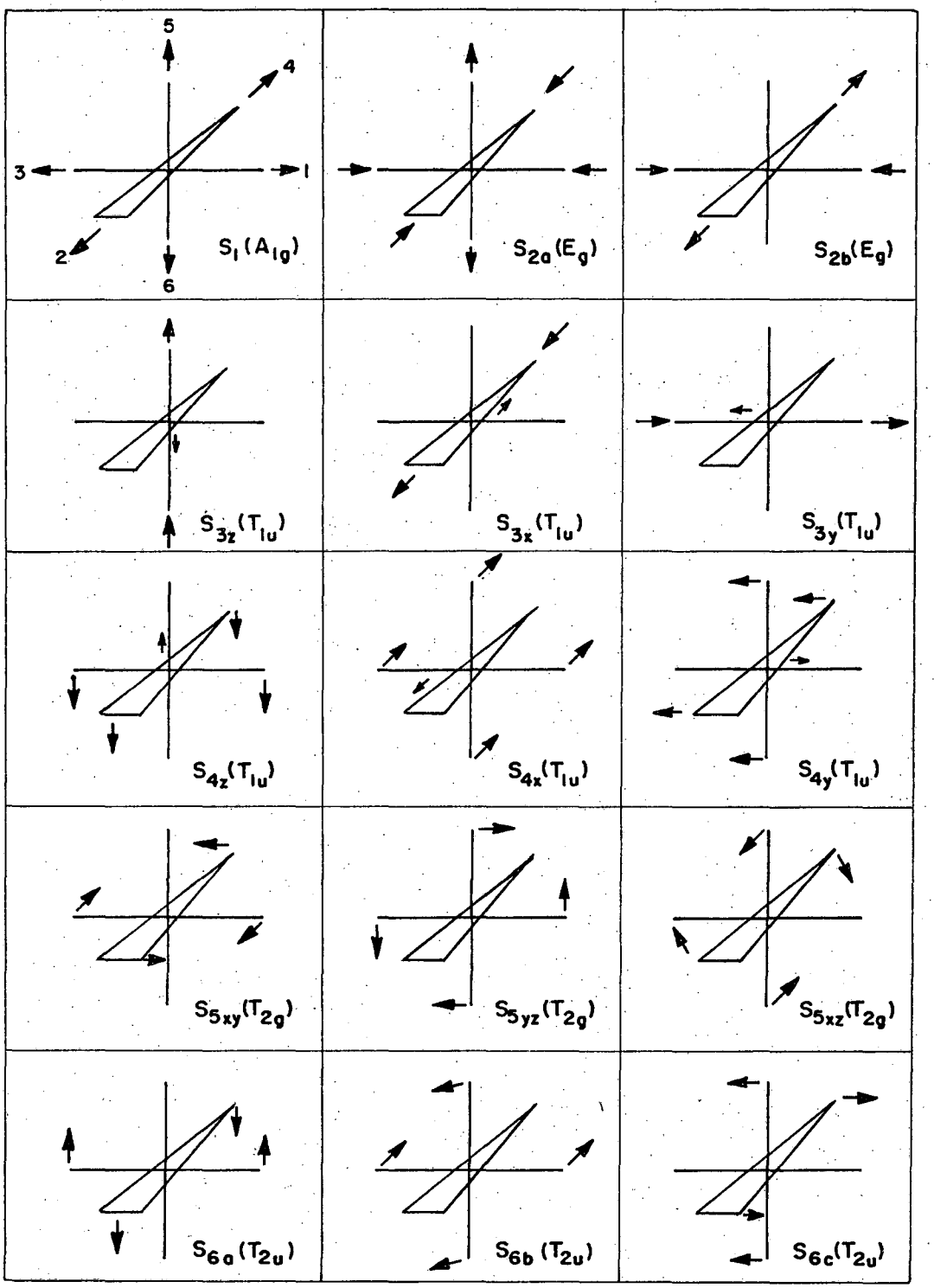

XBL744-6125

Fig. 1. Symmetry coordinates for an octahedral $MX_6(O_h)$ molecule.

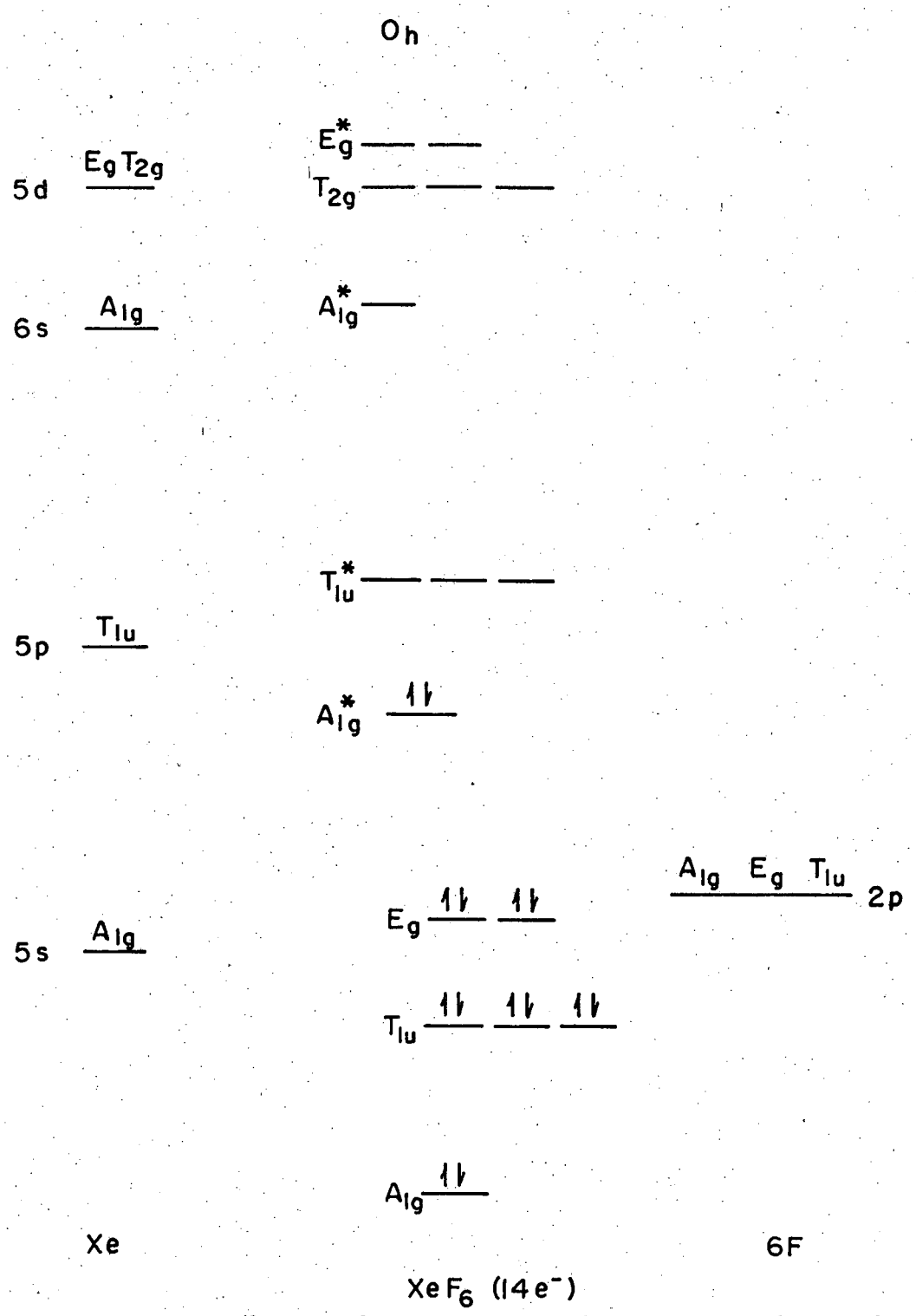

XeF_6 (14 e^-)

Ground State: $(A_{1g})^2\ (T_{1u_x})^2\ (T_{1u_y})^2\ (T_{1u_z})^2\ (E_{g_a})^2\ (E_{g_b})^2\ (A^*_{1g})^2\quad {}^1A_{1g}$

1st Excited State: $(A_{1g})^2\ (T_{1u_x})^2 (T_{1u_y})^2 (T_{1u_z})^2 (E_{g_a})^2 (E_{g_b})^2 (A^*_{1g})$

$(T^*_{1u})\ {}^1T_{1u}\quad {}^3T_{1u}$

XBL 744-6126

Fig. 2. Molecular orbital diagram of $XeF_6(O_n)$.

motion should be of lowest energy since it is a bending mode, while $A_{1g}(S_1)$ and $E_g(S_2)$ are stretching modes. This implies that the T_{2g} force constant is considerably smaller than that of E_g or A_{1g}, hence its coupling to the T_{1u} motion will be strongest. Essentially for the same reasoning as in all the previous chapters the coupling of the symmetrical stretch, A_{1g}, to the distortion mode (T_{1u}) will be ignored.

The matrix of the linear terms in the $T_{1u}(S_3,S_4)$, $E_g(S_2)$ and $T_{2g}(S_5)$ coordinates arising from an expansion of the vibronic hamiltonian in symmetry coordinates can be evaluated in the electronic basis $|^1T_{1u_x}\rangle$, $|^1T_{1u_y}\rangle$, $|^1T_{1u_z}\rangle$.[1]

$$
\begin{array}{c}
 \\ |^1A_{1g}\rangle \\ |^1T_{1u_x}\rangle \\ |^1T_{1u_y}\rangle \\ |^1T_{1u_z}\rangle
\end{array}
\begin{array}{c}
\begin{array}{cccc} |^1A_{1g}\rangle & |^1T_{1u_x}\rangle & |^1T_{1u_y}\rangle & |^1T_{1u_z}\rangle \end{array} \\
\begin{pmatrix}
-\varepsilon & c_3S_{3x}+c_4S_{4x} & c_3S_{3y}+c_4S_{4y} & c_3S_{3z}+c_4S_{4z} \\
c_3S_{3x}+c_4S_{4x} & \Delta\varepsilon_o+\frac{c_2}{\sqrt{2}}(-3S_{2b}+\sqrt{3}S_{2a})-\varepsilon & c_5S_{5xy} & c_5S_{5xz} \\
c_3S_{3y}+c_4S_{4y} & c_5S_{5xy} & \Delta\varepsilon_o+\frac{c_2}{\sqrt{2}}(3S_{2b}+\sqrt{3}S_{2a})-\varepsilon & c_5S_{5yz} \\
c_3S_{3z}+c_4S_{4z} & c_5S_{5xz} & c_5S_{5yz} & \Delta\varepsilon_o-\frac{2\sqrt{3}}{\sqrt{2}}c_2S_{2a}-\varepsilon
\end{pmatrix}
\end{array}
\qquad (1)
$$

where

$$c_3 = \langle {}^1T_{u_x}|\left(\frac{\partial H_v}{\partial S_{3x}}\right)_{S_o}|^1A_{1g}\rangle = \langle {}^1T_{1u_y}|\left(\frac{\partial H_v}{\partial S_{3y}}\right)_{S_o}|^1A_{1g}\rangle = \langle {}^1T_{1u_z}|\left(\frac{\partial H_v}{\partial S_{3z}}\right)_{S_o}|^1A_{1g}\rangle \qquad (2a)$$

$$c_4 = \langle {}^1T_{1u_x} | (\frac{\partial H_v}{\partial S_{4x}})_{S_o} | {}^1A_{1g} \rangle \quad \text{(same definition for } {}^1T_{1u_y}, {}^1T_{1u_z}) \tag{2b}$$

$$c_2 = \langle {}^1T_{1u_x} | (\frac{\partial H_v}{\partial S_{2a}})_{S_o} | {}^1T_{1u_x} \rangle = \langle {}^1T_{1u_x} | (\frac{\partial H_v}{\partial S_{2b}})_{S_o} | {}^1T_{1u_x} \rangle \quad \text{(same definition for } {}^1T_{1u_y}, {}^1T_{1u_z}) \tag{2c}$$

$$c_5 = \langle {}^1T_{1u_x} | (\frac{\partial H_v}{\partial S_{5xy}})_{S_o} | {}^1T_{1u_y} \rangle = \langle {}^1T_{1u_x} | (\frac{\partial H_v}{\partial S_{5xz}})_{S_o} | {}^1T_{1u_z} \rangle =$$

$$\langle {}^1T_{1u_y} | (\frac{\partial H_v}{\partial S_{5yz}})_{S_o} | {}^1T_{1u_z} \rangle \tag{2d}$$

$$\Delta\varepsilon_o = \varepsilon_{{}^1T_{1u}} - \varepsilon_{{}^1A_{1g}} \qquad \text{where we define } \varepsilon_{{}^1A_{1g}} = 0 \tag{2e}$$

For simplicity we can work with the determinant of Eq. (1) in the form

$$\begin{array}{c|cccc|}
 & |{}^1A_{1g}\rangle & |{}^1T_{1u_x}\rangle & |{}^1T_{1u_y}\rangle & |{}^1T_{1u_z}\rangle \\
|{}^1A_{1g}\rangle & -\varepsilon & A_1 & A_2 & A_3 \\
|{}^1T_{1u_x}\rangle & A_1 & \Delta\varepsilon_o+C_1-\varepsilon & B_1 & B_2 \\
|{}^1T_{1u_y}\rangle & A_2 & B_1 & \Delta\varepsilon_o+C_2-\varepsilon & B_3 \\
|{}^1T_{1u_z}\rangle & A_3 & B_2 & B_3 & \Delta\varepsilon_o+C_3-\varepsilon
\end{array} \tag{3}$$

where

$$A_1 = c_3 S_{3x} + c_4 S_{4x} \tag{4a}$$

$$A_2 = c_3 S_{3y} + c_4 S_{4y} \tag{4b}$$

$$A_3 = c_3 S_{3z} + c_4 S_{4z} \tag{4c}$$

$$B_1 = c_5 S_{5xy} \tag{4d}$$

$$B_2 = c_5 S_{5xz} \tag{4e}$$

$$B_3 = c_5 S_{5yz} \tag{4f}$$

$$C_1 = \frac{c_2}{\sqrt{2}} \left(-3S_{2b} + \sqrt{3}\, S_{2a}\right) \tag{4g}$$

$$C_2 = \frac{c_2}{\sqrt{2}} \left(3S_{2b} + \sqrt{3}\, S_{2a}\right) \tag{4h}$$

$$C_3 = -\frac{2\sqrt{3}}{\sqrt{2}}\, c_2\, S_{2a} \tag{4i}$$

The resulting polynomial equation in ε from the determinant (3) is

$$-\varepsilon[(\Delta\varepsilon_o-\varepsilon)^3 + (C_1+C_2+C_3)(\Delta\varepsilon_o-\varepsilon)^2 + (C_1C_2 + C_2C_3 + C_1C_3$$

$$-B_1^2-B_2^2-B_3^2)(\Delta\varepsilon_o-\varepsilon) + (C_1C_2C_3 + 2B_1B_2B_3 - B_1^2C_3$$

$$- B_2^2C_2^2 - B_3^2C_1)] \quad - (\Delta\varepsilon_o-\varepsilon)^2(A_1^2 + A_2^2 + A_3^2)$$

$$+ (\Delta\varepsilon_o-\varepsilon)(2A_1A_3B_2 + 2A_1A_2B_1 + 2A_2A_3B_3 - A_1^2(C_2+C_3)$$

$$- A_2^2(C_1 + C_3) - A_3^2(C_1 + C_2)) + (-2A_1A_2B_2B_3$$

$$-2A_1A_3B_1B_3 - 2A_2A_3B_1B_2 + A_1^2B_3^2 + A_2^2B_2^2 + A_3^2B_1^2$$

$$+ 2A_1A_2B_1C_3 + 2A_1A_3B_2C_2 + 2A_2A_3B_3C_1 - A_1^2C_2C_3$$

$$- A_2^2C_1C_3 - A_3^2C_1C_2) = 0 \qquad (5)$$

The quartic equation in ε (5) can be reduced to one of order two by recognizing that $\Delta\varepsilon_o >> \varepsilon$ for small or even moderate displacements. This approximation is reasonable because $\Delta\varepsilon_o$ represents an electronic transition which typically falls in the energy range of 10^4-10^5 cm^{-1}, while ε is basically the energy associated with distorting the octahedral configuration which will be on the order of vibrational energies 10^2-10^3 cm^{-1}. Dividing through by $(\Delta\varepsilon_o-\varepsilon)^2 \approx \Delta\varepsilon_o^2$ in Eq. (5) we have

$$-\varepsilon\left[(\Delta\varepsilon_o-\varepsilon) + (C_1+C_2+C_3) + \frac{(C_1C_2+C_1C_3+C_2C_3-B_1^2-B_2^2-B_3^2)}{\Delta\varepsilon_o}\right.$$

$$\left. + \frac{(C_1C_2C_3+2B_1B_2B_3-B_1^2C_3-B_2^2C_2^2-B_3^2C_1)}{\Delta\varepsilon_o^2}\right]$$

$$-(A_1^2+A_2^2+A_3^2) + \Big(2A_1A_3B_2+2A_1A_2B_1+2A_2A_3B_3-A_1^2(C_2+C_3)$$

$$- A_2^2(C_1+C_3)-A_3^2(C_1+C_2)\ /\Delta\varepsilon_o + (-2A_1A_2B_2B_3 - 2A_1A_3B_1B_3$$

$$- 2A_2A_3B_1B_2 + A_1^2B_3^2 + A_2^2B_2^2 + A_3^2B_1^2 + 2A_1A_3B_2C_2 + 2A_2A_3B_3C_1$$

$$+ 2A_1A_2B_1C_3 - A_1^2C_2C_3 - A_2^2C_1C_3 - A_3^2C_1C_2\Big)/\Delta\varepsilon_o^2 = 0 \qquad (6)$$

where Eq. (6) is now of order two and can be solved exactly. Before solving for the roots of Eq. (6) we can rewrite it in a simpler form

$$-\varepsilon\left[(\Delta\varepsilon_o-\varepsilon) + U + \frac{V}{\Delta\varepsilon_o} + \frac{W}{\Delta\varepsilon_o^2}\right] - X + \frac{Y}{\Delta\varepsilon_o} + \frac{Z}{\Delta\varepsilon_o^2} \qquad (7)$$

where

$$U = (C_1+C_2+C_3) \qquad (8a)$$

$$V = (C_1C_2+C_1C_3+C_2C_3-B_1^2-B_2^2-B_3^2) \qquad (8b)$$

$$V = (C_1C_2C_3+2B_1B_2B_3-B_1^2C_3-B_2^2C_2^2-B_3^2C_1) \qquad (8c)$$

$$X = (A_1^2+A_2^2+A_3^2) \qquad (8d)$$

$$Y = (2A_1A_3B_2+2A_1A_2B_1+2A_2A_3B_3-A_1^2(C_2+C_3)-A_2^2(C_1+C_3)-A_3^2(C_1+C_2)) \tag{8e}$$

$$Z = (-2A_1A_2B_2B_3-2A_1A_3B_1B_3-2A_2A_3B_1B_2+A_1^2B_3^2+A_2^2B_2^2 \tag{8f}$$

$$+ A_3^2B_1^2 + 2A_1A_2B_1C_3 + 2A_1A_3B_2C_2 + 2A_2A_3B_3C_1$$

$$- A_1^2C_2C_3 - A_2^2C_1C_3 - A_3^2C_1C_2)$$

The roots of Eq. (7) are

$$\varepsilon = (\tfrac{1}{2})\left[(\Delta\varepsilon_o+U+\frac{V}{\Delta\varepsilon_o}+\frac{W}{\Delta\varepsilon_o^2}) \pm (\Delta\varepsilon_o+U+\frac{V}{\Delta\varepsilon_o}+\frac{W}{\Delta\varepsilon_o^2})\left(1+\frac{4(X-\frac{Y}{\Delta\varepsilon_o}-\frac{Z}{\Delta\varepsilon_o^2})}{(\Delta\varepsilon_o+U+\frac{V}{\Delta\varepsilon_o}+\frac{W}{\Delta\varepsilon_o^2})^2}\right)^{1/2}\right] \tag{9}$$

We can expand the lower root of Eq. (9) to yield

$$\varepsilon_{low} \approx \frac{-(X-\frac{Y}{\Delta\varepsilon_o}-\frac{Z}{\Delta\varepsilon_o^2})}{(\Delta\varepsilon_o+U+\frac{V}{\Delta\varepsilon_o}+\frac{W}{\Delta\varepsilon_o^2})} + \frac{(X-\frac{Y}{\Delta\varepsilon_o}-\frac{Z}{\Delta\varepsilon_o^2})^2}{(\Delta\varepsilon_o+U+\frac{V}{\Delta\varepsilon_o}+\frac{W}{\Delta\varepsilon_o^2})^3} + \cdots \tag{10}$$

With the approximation

$$\frac{1}{(\Delta\varepsilon_o+U+\frac{V}{\Delta\varepsilon_o}+\frac{W}{\Delta\varepsilon_o^2})} \approx \frac{1}{\Delta\varepsilon_o}(1-\frac{U}{\Delta\varepsilon_o}-\frac{V}{\Delta\varepsilon_o^2}-\frac{W}{\Delta\varepsilon_o^3}+\cdots) \tag{11}$$

and keeping only terms of order three or less in $\Delta\varepsilon_o$ Eq. (10) becomes

$$\varepsilon_{low} = -\frac{X}{\Delta\varepsilon_o}+\frac{UX+Y}{\Delta\varepsilon_o^2}+\frac{X^2+Z+VX-UY}{\Delta\varepsilon_o^3} \tag{12}$$

We can translate ε_{low} back into the A, B, C coordinates using the definitions in Eqs. (8).

$$\varepsilon_{low} = -\frac{(A_1^2+A_2^2+A_3^2)}{\Delta\varepsilon_o} + (A_1^2+A_2^2+A_3^2)(C_1+C_2+C_3) \tag{13}$$

$$+ (2A_1A_3B_2 + 2A_1A_2B_1 + 2A_2A_3B_3 - A_1^2(C_2+C_3) - A_2^2(C_1+C_3)$$

$$- A_3^2(C_1+C_2)\,)/\Delta\varepsilon_o^2$$

$$+ \frac{(A_1^2+A_2^2+A_3^2)}{\Delta\varepsilon_o^3} + \frac{(C_1C_2+C_1C_3+C_2C_3-B_1^2-B_2^2-B_3^2)(A_1^2+A_2^2+A_3^2)}{\Delta\varepsilon_o^3}$$

$$+(-2A_1A_2B_2B_3 - 2A_1A_3B_1B_3 - 2A_2A_3B_1B_2 + A_1^2B_3^2 + A_2^2B_2^2$$

$$+ A_3^2B_1^2 + 2A_1A_2B_1C_3 + 2A_1A_3B_2C_2 + 2A_2A_3B_3C_1$$

$$- A_1^2C_2C_3 - A_2^2C_1C_3 - A_3^2C_1C_2)/\Delta\varepsilon_o^3$$

$$-(C_1+C_2+C_3)(2A_1A_3B_2 + 2A_1A_3B_2 + 2A_2A_3B_3 - A_1^2(C_2+C_3)$$

$$- A_2^2(C_1+C_3) - A_3^2(C_1+C_2)\,)/\Delta\varepsilon_o^3$$

To form the complete distortion potential the quadratic terms for the E_g, T_{2g}, $T_{1u(bend)}$, and $T_{1u(stretch)}$ must be added to ε_{low} (13). For simplicity we will look at each vibrational mode individually, including its coupling terms to the T_{1u} motion. To translate ε_{low} (12) into the original set of symmetry coordinates use the transformation Eqs. (4a-4i).

The potential for the A_{1g} stretch (S_1) is

$$V_{A_{1g}}(S_1) = \frac{1}{2} k_1 S_1^2 \tag{14}$$

where k_1 is the $A_{1g}(S_1)$ force constant. The A_{1g}-T_{1u} coupling was ignored in deriving ε_{low}(13) which is why the A_{1g} potential (14) has a simple form.

The potential for the E_g stretch (S_2) can be written as

$$V_{E_g}(S_{2a},S_{2b},S_{4x},S_{4y},S_{4z}) = \frac{1}{2} K_2(S_{2a}^2 + S_{2b}^2) \tag{15}$$

$$+ \frac{\sqrt{3}\, c_2 c_4^2}{\sqrt{2}\, \Delta\varepsilon_o^2} S_{2a}(S_{4x}^2 + S_{4y}^2 - 2S_{4z}^2)$$

$$+ \frac{3\, c_2 c_4^2}{\sqrt{2}\, \Delta\varepsilon_o^2} S_{2b}\, (S_{4y}^2 - S_{4x}^2)$$

where only the leading terms coupling $E_g(S_2)$ to the T_{1u} bend (S_4) have been included from ε_{low} (13). The $E_g(S_2)$ force constant is K_2.

The potential for the T_{1u} stretch (S_3) is

$$V_{T_{1u}\,\text{stretch}}(S_{3x},S_{3y},S_{3z},S_{4x},S_{4y},S_{4z}) = (\tfrac{1}{2})k_3(S_{3x}^2 + S_{3y}^2 + S_{3z}^2)$$

$$- \frac{2\, c_3 c_4}{\Delta\varepsilon_o} (S_{3x}S_{4x} + S_{3y}S_{4y} + S_{3z}S_{4z}) \tag{16}$$

where, as for the E_g mode, only the leading terms coupling the T_{1u} stretch to the T_{1u} bend are indicated. K_3 is the T_{1u} stretch force constant.

For the $T_{2g}(S_5)$ potential we have

$$V_{T_{2g}}(S_{5xy},S_{5xz},S_{5yz},S_{4x},S_{4y},S_{4z}) = \frac{1}{2} k_5 \ (S_{5xy}^2 + S_{5xz}^2 + S_{5yz}^2)$$
$$+ \frac{2c_4^2 c_5}{\Delta\varepsilon_o^2} \ (S_{4x}S_{4y}S_{5xy} + S_{4x}S_{5xy} + S_{4x}S_{4z}S_{5xa} + S_{4y}S_{4z}S_{5yz}) \tag{17}$$

where k_5 is the $T_{2g}(S_5)$ force constant. Only the leading terms coupling the T_{2g}-T_{1u} bends are included in $V_{T_{2g}}$.

The $T_{2u}(S_6)$ potential is

$$V_{T_{2u}}(S_{6a},S_{6b},S_{6c}) = \frac{1}{2} k_6 (S_{6a}^2 + S_{6b}^2 + S_{6c}^2) \tag{18}$$

where k_6 is the $T_{2u}(S_6)$ force constant. We found earlier that there are no T_{1u}-T_{2u} coupling terms. This is only true to the approximation that only the $^1T_{1u}$ excited electronic state is involved in coupling to the $^1A_{1g}$ ground state. To include T_{2u}, T_{1u} coupling would involve including additional excited states into the matrix of the linear terms (1). We rationalized earlier that higher electronic states are of considerably less importance than the first electronic state, $^1T_{1u}$, insofar as T_{1u} motions are concerned.

The T_{1u} bend (S_4) potential is obtained by including all leading terms coupled to the $T_{1u}(S_4)$ motion, as defined in the other potentials.

$$V_{T_{1u}\,\text{bend}}(S_{4x},S_{4y},S_{4z},T_{1u}(\text{stretch}),E_g,T_{2g}) = \frac{1}{2} k_4 (S_{4x}^2 + S_{4y}^2 + S_{4z}^2)$$
$$- \frac{c_4^2}{\Delta\varepsilon_o} (S_{4x}^2 + S_{4y}^2 + S_{4z}^2) + \frac{c_4^4}{\Delta\varepsilon_o^3} (S_{4x}^2 + S_{4y}^2 + S_{4z}^2)^2 + V_{E_g} + V_{T_{2g}} + V_{T_{1u}\,\text{stretch}} \tag{19}$$

The T_{1u} bend potential (19) is effectively an eleven dimensional potential due to its coupling to the E_g, T_{2g} and T_{1u}(stretch). We can reduce this to a three dimensional potential just in the T_{1u} bend (S_4) coordinates in the same manner as the dimensionality of the MX_5 and MX_7 potentials were reduced. This process involved taking the first derivative of the coupled potential with respect to the one of the coupling coordinates and then solving for the coupling coordinate in terms of the distortion mode coordinates.

Applying this procedure to the T_{1u}-E_g coupling we have

$$\frac{\partial V_{T_{1u}\ \mathrm{bend}}}{\partial S_{2a}} = \frac{\partial V_{Eg}}{\partial S_{2a}} = \sqrt{\frac{3}{2}}\ \frac{c_2 c_4^2}{\Delta\varepsilon_o^2}\ (S_{4x}^2 + S_{3y}^2 - 2S_{4z}^2) + k_2 S_{2a} = 0$$

$$S_{2a} = -\sqrt{\frac{3}{2}}\ \frac{c_2 c_4^2}{k_2 \Delta\varepsilon_o^2}\ (S_{4x}^2 + S_{4y}^2 - 2S_{4z}^2) \tag{20}$$

Similarly, S_{2b} becomes

$$S_{2b} = -\frac{3}{\sqrt{2}}\ \frac{c_2 c_4^2}{k_2 \Delta\varepsilon_o^2}\ (S_{4y}^2 - S_{4x}^2) \tag{21}$$

Substitution of Eqs. (20,21) back into V_{E_g} (15) gives the "average" effect of the E_g mode on the $T_{1u}(S_4)$ motion.

$$V_{E_g}(T_{1u}) = \frac{-3c_2^2 c_4^4}{k_2 \Delta\varepsilon_o^4}\ [(S_{4x}^2 + S_{4y}^2 + S_{4z}^2) - 3(S_{4x}^2 S_{4y}^2 + S_{4x}^2 S_{4z}^2 + S_{4y}^2 S_{4z}^2)] \tag{22}$$

For the T_{1u}(stretch) - T_{1u}(bend) we find

$$S_{3x} = \frac{2c_3c_4}{k_3\Delta\varepsilon_o} S_{4x} \tag{23a}$$

$$S_{3y} = \frac{2c_3c_4}{k_3\Delta\varepsilon_o} S_{4y} \tag{23b}$$

$$S_{3z} = \frac{2c_3c_4}{k_3\Delta\varepsilon_o} S_{4z} \tag{23c}$$

The effect of the T_{1u} stretch on the T_{1u} bend is determined by substituting Eqs. (23) back into $V_{T_{1u}\ \text{stretch}}$ (16).

$$V_{T_{1u}\ \text{stretch}}(T_{1u}\ \text{bend}) = \frac{2c_3^2c_4^2}{k_3\Delta\varepsilon_o^2} (S_{4x}^2 + S_{4y}^2 + S_{4z}^2) \tag{24}$$

The T_{1u}(bend) - T_{2g} coupling gives

$$S_{5xy} = \frac{-2c_4^2c_5}{k_5\Delta\varepsilon_o^2} S_{4x}S_{4y} \tag{25a}$$

$$S_{5xz} = \frac{-2c_4^2c_5}{k_5\Delta\varepsilon_o^2} S_{4x}S_{4z} \tag{25b}$$

$$S_{5yz} = \frac{-2c_4^2c_5}{k_5\Delta\varepsilon_o^2} S_{4y}S_{4z} \tag{25c}$$

Substitution of Eqs. (25) into $V_{T_{2g}}$ (17) yields

$$V_{T_{2g}}(T_{1u}) = \frac{-2c_4^4c_5^2}{k_5\Delta\varepsilon_o^4}\left(S_{4x}^2S_{4y}^2 + S_{4x}^2S_{4z}^2 + S_{4y}^2S_{4z}^2\right) \tag{26}$$

Using the "effective" coupling potentials (22,24,26) we can write the T_{1u} potential (19) just in terms of the $T_{1u}(S_4)$ coordinates.

$$\begin{aligned} V_{T_{1u}}(S_{4x},S_{4y},S_{4z}) = &\left(-\frac{c_4^2}{\Delta\varepsilon_o} + \frac{k_4}{2} + \frac{2c_3^2c_4^2}{k_3\Delta\varepsilon_o^2}\right)\left(S_{4x}^2 + S_{4y}^2 + S_{4z}^2\right) \\ &+ \left(\frac{c_4^4}{\Delta\varepsilon_o^3} - \frac{3c_2^2c_4^4}{k_2\Delta\varepsilon_o^4}\right)\left(S_{4x}^2 + S_{4y}^2 + S_{4z}^2\right) \\ &+ \left(\frac{9c_2^2c_4^4}{k_2\Delta\varepsilon_o^4} - \frac{2c_4^4c_5^2}{k_5\Delta\varepsilon_o^4}\right)\left(S_{4x}^2S_{4y}^2 + S_{4x}^2S_{4z}^2 + S_{4y}^2S_{4z}^2\right) \end{aligned} \tag{27}$$

The T_{1u} potential (27) can be compactly written as

$$\begin{aligned} V_{T_{1u}}(S_4) = &-a(S_{4x}^2 + S_{4y}^2 + S_{4z}^2) + b(S_{4x}^2 + S_{4y}^2 + S_{4z}^2)^2 \\ &- c(S_{4x}^2S_{4y}^2 + S_{4x}^2S_{4z}^2 + S_{4y}^2S_{4z}^2) \end{aligned} \tag{28}$$

The particular choice of sign for a, b, and c will become clear in later sections. The parameters a, b, and c are defined by

$$a = \frac{c_4^2}{\Delta\varepsilon_o} - \frac{k_4}{2} - \frac{2c_3^2c_4^2}{k_3\Delta\varepsilon_o^2} \tag{29a}$$

$$b = \frac{c_4^4}{\Delta\varepsilon^3} - \frac{3c_2^2c_4^4}{k_2\Delta\varepsilon_o^4} \tag{29b}$$

$$c = \frac{2c_4^4c_5^2}{k_5\Delta\varepsilon_o^4} - \frac{9c_2^2c_4^4}{k_2\Delta\varepsilon_o^4} \tag{29c}$$

The first two terms in the T_{1u} potential (28) have spherical symmetry, while the third term has octahedral symmetry. In spherical coordinates (R, θ, φ) the T_{1u} potential (28) is

$$V_{T_{1u}}(R,\theta,\phi) = -aR^2 + bR^4 - cR^4\,[\sin^4\theta(\frac{\sin^2 2\phi}{4} - 1) + \sin^2\theta] \tag{30}$$

where

$$S_{4x} = R\sin\theta\cos\phi \tag{31a}$$

$$S_{4y} = R\sin\theta\sin\phi \tag{31b}$$

$$S_{4z} = R\cos\phi \tag{31c}$$

The third term in the potential (30), the octahedral field term, introduces an angular dependence to the potential. This angular dependence causes the potential to have a minimum centered on the faces of the octahedron, a saddle point centered on the edges, and a maximum at the corners. A simple explanation of this behavior is that the mixing of s and p orbitals on the central Xe atom (Fig. 2) caused by the T_{1u} distortion gives a directional preference to the "lone" pair of electrons

(A_{1g}^{*}). When the lone pair "pops" out centered on a face of the octahedron formed by the fluorine ligands its repulsive interaction with the ligands is minimized, hence the potential is a minimum (Fig. 3). When the lone pair pops out directly in line with one of the fluorine atoms its repulsive interaction is largest, hence the potential is a maximum. When the lone pair pops out centered on an edge of the octahedran it is closer to the ligands than in the face centered situation and farther than in the corner case, which makes the potential a saddle point here.

We can view the potential (30) at these three types of locations on the octahedron.

$$V_{C_{3v}} = -a\ R^2 + b\ R^4 - 0.333\ c\ R^4 \tag{32a}$$

$$V_{C_{2v}} = -a\ R^2 + b\ R^4 - 0.250\ c\ R^4 \tag{32b}$$

$$V_{C_{4v}} = -a\ R^2 + b\ R^4 \tag{32c}$$

This demonstrates that the potential (3) is softest in the C_{3v} direction (32a), steepest in the C_{4v} direction (32b), and intermediate in the C_{2v} direction (32b). In the limit that the angular barrier vanishes (c=0), the potential becomes spherically symmetric and identical in form to that of a rotating-vibrating diatomic molecule.

The form of the potential (28,30) which has been discussed so far is what we have called the truncated form in previous chapters. This is because this form (28,30) resulted from an expansion (10)

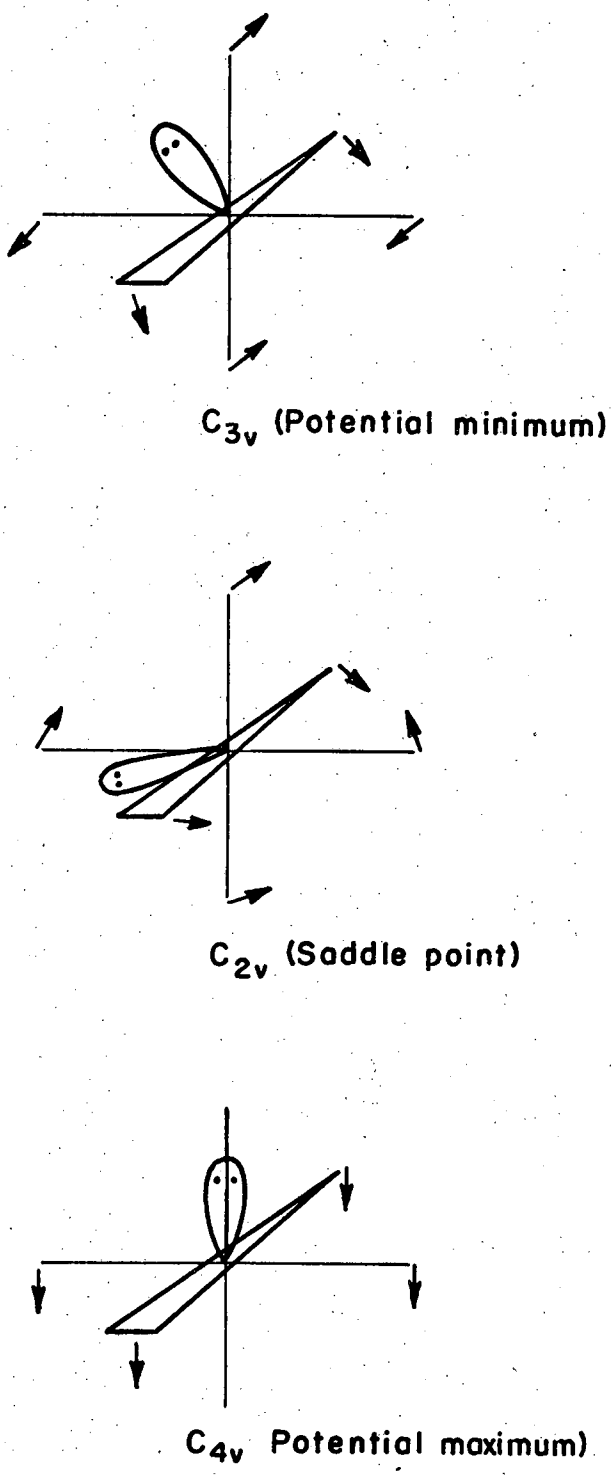

Fig. 3. Possible distortions caused by directional preference of the lone pair.

of the exact solution (9). Due to the more complicated nature of the XeF_6 potential than those studied in earlier chapters it is desirable to work with a simplified form (28,30). However, as in previous cases, we must worry about the validity of truncating the exact potential to just fourth order. The question of validity will be handled in a later section, although a reasonable approximation to the exact solution is presented below.

$$V_{T_{1u}}(R,\theta,\phi) = \frac{1}{2}\Delta\varepsilon_o\,[1 - (1 + 4\alpha^2 R^2)^{1/2}] + \frac{1}{2}k\,R^2$$

$$- cR^4[\sin^4\theta(\frac{\sin^2 2\phi}{4} - 1) + \sin^2\theta]$$

where α, k, and c are adjustable parameters, and $\Delta\varepsilon_o$ is still the $^1A_{1g} \rightarrow {}^1T_{1u}$ electronic transition energy.

B. Calculations

The symmetry coordinates[56] (Fig. 1) for the $T_{1u}(S_4)$ mode and those modes which couple to it are defined by

$$S_{2a} = \frac{1}{\sqrt{12}} (2\Delta r_5 + 2\Delta r_6 - \Delta r_1 - \Delta r_2 - \Delta r_3 - \Delta r_4) \tag{33a}$$

$$S_{2b} = \frac{1}{2} (- \Delta r_1 - \Delta r_3 + \Delta r_2 + \Delta r_4) \tag{33b}$$

$$S_{3x} = \frac{1}{\sqrt{2}} (\Delta r_2 - \Delta r_4) \tag{33c}$$

$$S_{3y} = \frac{1}{\sqrt{2}} (\Delta r_1 - \Delta r_3) \tag{33d}$$

$$S_{3z} = \frac{1}{\sqrt{2}} (\Delta r_5 - \Delta r_6) \tag{33e}$$

$$S_{4x} = \frac{r}{\sqrt{8}} (\Delta\alpha_{12}+\Delta\alpha_{23}+\Delta\alpha_{25}+\Delta\alpha_{26}-\Delta\alpha_{14}-\Delta\alpha_{34}-\Delta\alpha_{46}-\Delta\alpha_{45}) \tag{33f}$$

$$S_{4y} = \frac{r}{\sqrt{8}} (\Delta\alpha_{12}+\Delta\alpha_{14}+\Delta\alpha_{15}+\Delta\alpha_{16}-\Delta\alpha_{23}-\Delta\alpha_{35}-\Delta\alpha_{34}-\Delta\alpha_{36}) \tag{33g}$$

$$S_{4z} = \frac{r}{\sqrt{8}} (\Delta\alpha_{15}+\Delta\alpha_{35}+\Delta\alpha_{25}+\Delta\alpha_{45}-\Delta\alpha_{36}-\Delta\alpha_{16}-\Delta\alpha_{26}-\Delta\alpha_{46}) \tag{33h}$$

$$S_{5xy} = \frac{r}{2} (-\Delta\alpha_{12}-\Delta\alpha_{34}+\Delta\alpha_{14}+\Delta\alpha_{23}) \tag{33i}$$

$$S_{5xz} = \frac{r}{2} (-\Delta\alpha_{25}-\Delta\alpha_{46}+\Delta\alpha_{26}+\Delta\alpha_{45}) \tag{33j}$$

$$S_{5yz} = \frac{r}{2}\,(-\Delta\alpha_{36}-\Delta\alpha_{15}+\Delta\alpha_{35}+\Delta\alpha_{16}) \qquad (33k)$$

where r is the Xe-F bond distance, Δr_i is the change in bond length of the i'th fluorine, and $\Delta\alpha_{ij}$ is the change in angle between fluorines i and j. The numbering scheme for the fluorines is indicated on $S_2(A_{1g})$ in Fig. 1.

The mass (m_4) associated with the $T_{1u}(S_4)$ distortion was determined by Wilson's high frequency approximation.[11,56] (See Appendix IV). The low frequency motion was taken as the T_{1u} bend and the high frequency motion as the T_{1u} stretch. No attempt was made to determine the dependence of the mass on either the magnitude of the distortion, or the coupling to other modes, particularly T_{2g}. For XeF_6 the effective $T_{1u}(S_4)$ mass in m_4 = 6.56 amu.

C. Discussion of the Previous Experimental Work and Refinement of the Potential Function

The XeF_6 discussion section is divided into six separate parts: (1) Electron diffraction of XeF_6, (2) Infrared and Raman spectra of XeF_6, (3) Ultraviolet spectrum of XeF_6, (4) Thermodynamics of XeF_6, (5) Electric field deflection of XeF_6, and (6) comparison to other theoretical approaches. Each of the first five subsections includes a discussion of previous experimental work and its interpretation in terms of the T_{1u} potential (30) derived in this work.

1. Electron Diffraction

A comparison of the experimental radial distribution curve (20°C)[57] with that of a hypothetical octahedral XeF_6 configuration of the same bond length is found in Fig. 4. The experimental curve is characterized by an Xe-F bond length peak at 1.895 Å, an adjacent F-F peak at 2.51 Å, and a "long" F-F peak at 3.76 Å. If XeF_6 were octahedral the adjacent F-F peak would occur at $\sqrt{2}\ r_{Xe-F}$ (2.68 Å) and the long F-F peak at $2r_{Xe-F}$ (3.79 Å). The most noticeable difference between the octahedral configuration and the experimental curve is the skewing of the experimental adjacent F-F peak considerably to the left of its octahedral counterpart.

Hedberg[57] and Bartell[58,59] have done extensive single structure calculations in an attempt to understand the XeF_6 radial distribution curve. Through these calculations they have reached the same basic conclusions, which are (1) a single C_{2v}, or C_{3v}, or C_s configuration

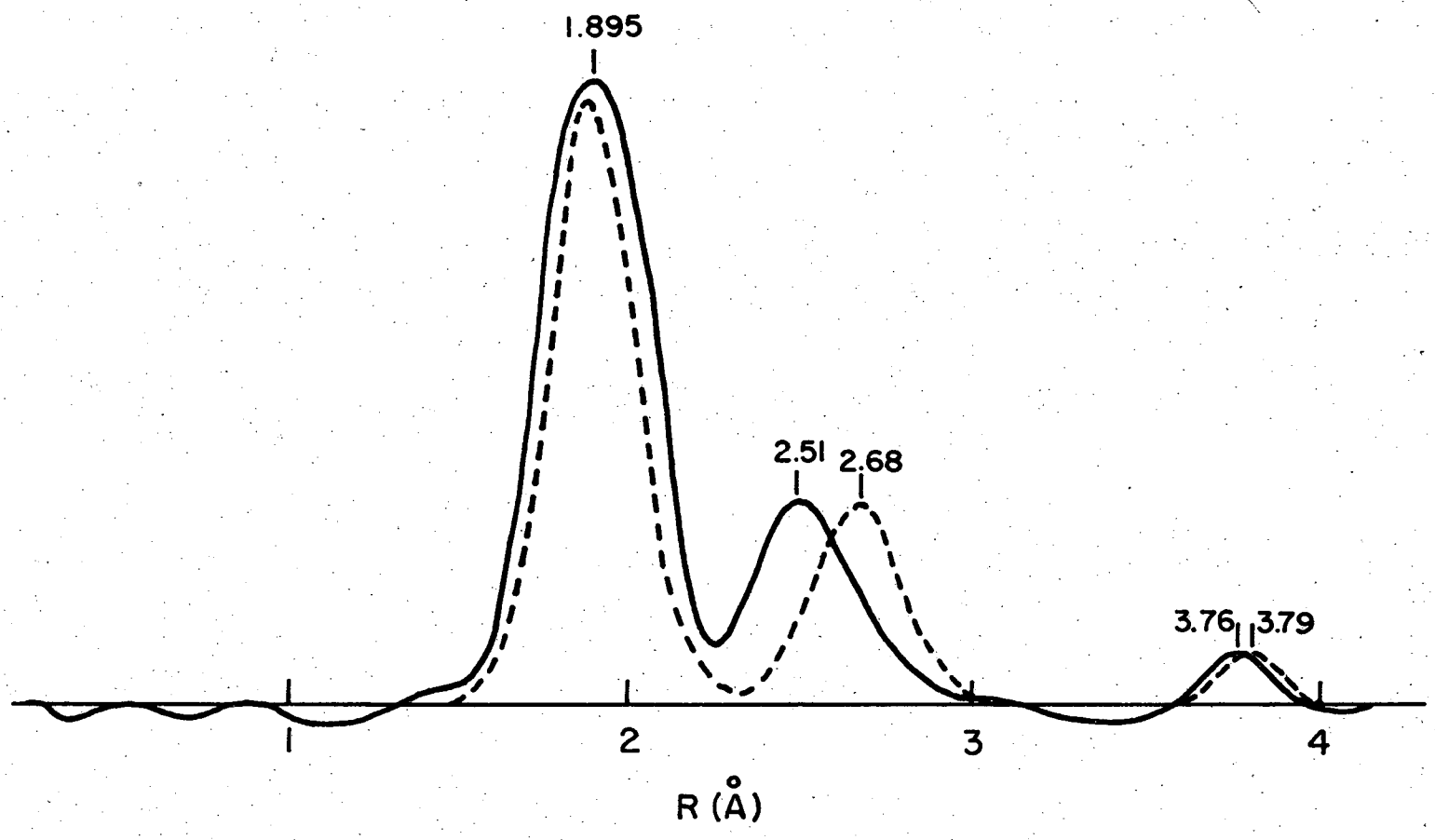

XBL 744-6128

Fig. 4. Comparison of experimental radial distrubition curve for XeF_6 (solid line) with a hypothetical octahedral XeF_6 configuration (dashed line).

can fit the experimental distribution reasonably well, (2) only a coupling of the T_{1u} (bend) with the T_{2g} mode can adequately fit the shortened adjacent F-F distribution, (3) the single, static model calculations require unusually large nonbonded vibrational amplitudes to fit the experimental data.

The situation in XeF_6 is similiar to that in IF_7 and ReF_7. That is, the electron diffraction experiments only yields direct information about the magnitude of the distortion. Evidence for pseudorotation is indirectly provided, in the sense that several models (C_s, C_{2v}, C_{3v}) give adequate fits to the data, and the nonbonded amplitudes are unusually large. The maximum information we might hope to extract from the electron diffraction work is (1) an estimate of where the radial potential minimum is located (R_o), (2) a quantitative description of the T_{1u} (bend)-T_{2g} coupling.

To extract this information we chose to work with the best static C_{3v} model.[57] The reason for making this choice is that the potential minimum is most likely at the C_{3v} configuration, hence the C_{3v} structure should be weighted heaviest of all possible structures. By symmetry a C_{3v} structure can have two kinds of bond lengths, three types of adjacent F-F distances, and only one type of long F-F distance. The multiplicities, and values for these distances are listed in Table 1. Notice the large nonbonded vibrational amplitudes (.1-.3 Å). In TeF_6,[59] a normal octahedral molecule, the nonbonded F-F amplitude is approximately ~.06 Å. The parameters ANG4, and ANG5 are angular variables which can be directly related to the T_{1u} (bend) and T_{2g} symmetry coordinates.

In the C_{3v} geometry the T_{1u} (33 f-h) and T_{2g} (33 i-k) symmetry coordinates simplify to

$$S_{4x} = S_{4y} = S_{4z} = \sqrt{8}\ r\ ANG4 \tag{34a}$$

$$S_{5xy} = S_{5xz} = S_{5yz} = 2r\ ANG5 \tag{34b}$$

The radial coordinate, R(31), becomes

$$R = \sqrt{S_{4x}^2 + S_{4y}^2 + S_{4z}^2} = |2\sqrt{6}\ r\ ANG4| \tag{35}$$

Using the experimental values for the C_{3v} model (Table 1) we find that $S_{4_{x,y,z}} = .502$ Å, $S_{5_{xy,xz,yz}} = .482$ Å, and R_o (radial minimum) = .870 Å. We can use this information to derive both the value of the T_{1u}-T_{2g} coupling parameter, and a relation among the potential parameters a,b,c (30). Using the C_{3v} potential, $V_{C_{3v}}$ (32a), we take the first derivative to define the C_{3v} potential minimum (R_o).

$$\frac{\partial V_{C_{3v}}}{\partial R} = -2aR + 4\,(b - .333c)R^3 = 0 \tag{36}$$

$$R = 0 \quad \text{at} \quad O_h \text{ configuration}$$

$$R_o^{\ 2} = \frac{a}{2(b-.333c)} \quad \text{at} \quad C_{3v} \text{ minimum}$$

Knowledge of the value of R_o(.87 Å) requires that a, b, and c are related by

$$a = 2(.87)^2 (b-.333c) \tag{37}$$

If two additional independent relations among a, b, and c can be found by analysis of other experimental data of XeF_6 the potential (30) can be quantitatively defined.

In the theory section of this chapter we found $T_{1u}(S_4)$ and $T_{2g}(S_5)$ were coupled (25) in the following manner

$$S_{5xy} = - C_{T_{2g}} S_{4x} S_{4y} \tag{38a}$$

$$S_{5xz} = - C_{T_{2g}} S_{4x} S_{4z} \tag{38b}$$

$$S_{5yz} = - C_{T_{2g}} S_{4y} S_{4z} \tag{38c}$$

where

$$C_{T_{2g}} = \frac{2c_4^2 \, c_5}{k_5 \Delta\varepsilon_o^{\,2}} \tag{39}$$

The diffraction work requires that $C_{T_{2g}}$ be positive[59] in order to get the $T_{1u} - T_{2g}$ coupling which best fits the experimental radial distribution. This implies that the linear matrix element, c_5, must be positive. With values for S_4 (.502 Å) and S_5 (.482 Å), the coupling constant, $C_{T_{2g}}$, can be computed from Eq. (38) to be $C_{T_{2g}} = 1.91$ (1/Å).

This compares favorably with Bartell's analysis[59] of the coupling constant, in which the range of $C_{T_{2g}}$ was determined as

$$1\ (\tfrac{1}{\text{Å}}) \leqslant C_{T_{2g}} \leqslant 2\ (\tfrac{1}{\text{Å}}).$$

Because two different bond lengths were refined for the C_{3v} model we can extract the value of the T_{1u} (bend) - T_{1u} (stretch) coupling constant. The T_{1u} (S_3) stretch symmetry coordinates (33 c-e) can be written in the C_{3v} form as

$$S_{3x} = \sqrt{2}\ \Delta r \tag{40a}$$

$$S_{3y} = \sqrt{2}\ \Delta r \tag{40b}$$

$$S_{3z} = \sqrt{2}\ \Delta r \tag{40c}$$

where Δr is the change in the Xe-F bond length. The form of the T_{2u}(bend) - T_{1u}(stretch) coupling is (23)

$$S_{3x} = C_{T_{1u}}\ S_{4x} \tag{41a}$$

$$S_{3y} = C_{T_{1u}}\ S_{4y} \tag{41b}$$

$$S_{3z} = C_{T_{1u}}\ S_{4z} \tag{41c}$$

where

$$C_{T_{1u}} = \frac{2\ c_3 c_4}{k_3 \Delta\varepsilon_o} \tag{42}$$

The experimental C_{3v} model requires that $C_{T_{1u}}$ is positive. This is physically reasonable because it is in agreement with the intuitive argument that bonds nearest the lone pair increase slightly to help minimize repulsive interactions. From Table 1, Δr is placed at $\Delta r = .046$ Å relative to the average r_{Xe-F} of 1.895 Å. The T_{1u}(stretch) coordinate, S_3, is determined to be $S_{3x,y,z} = .065$ Å, which places $C_{T_{1u}}$ at $C_{T_{1u}} = .13$. It is interesting to note that the T_{1u}(bend) - T_{2g} coupling is stronger than the T_{1u}(bend) - T_{1u}(stretch) coupling by an order of magnitude. This is in line with earlier speculation on the relative strengths of the various couplings, where it is primarily the size of the coupling mode's force constant that determines the strength of the coupling. Obviously, k_3, the T_{1u} stretch force constant must be larger than k_5, the T_{2g} bend force constant.

The parameters calculated so far have been based on the best static C_{3v} model. It would be worthwhile to recalculate these parameters using the best static C_{2v}, C_s or C_{4v} model to see if similar results are obtained. We can eliminate the C_{4v} model from consideration as it seems incapable of fitting the experimental data nearly as well as the other symmetries. There is a basic problem with the C_{2v} and C_s geometries, in that their symmetries are sufficiently low as to permit so many independently adjustable geometric parameters that a unique best static model cannot be defined. Instead there are a variety of C_{2v} and C_s structures which fit the experimental data equally well. The net result is that we are forced to look elsewhere

(spectroscopy, thermodynamics) to assess the accuracy of the potential parameters based on the best static C_{3v} structure.

We have approached the discussion of the XeF_6 diffraction results so far from a static structure viewpoint. We have explored, in collaboration with Professor Hedberg's group at Oregon State University, the possibility of fitting a dynamic (i.e. pseudorotation) XeF_6 model to the experimental diffraction results. The experimental radial distribution curve of XeF_6 can be thought of as a weighted superposition of radial distribution curves corresponding to the "instantaneous" XeF_6 structures which are swept out during the pseudorotation. This can be expressed mathematically as[59]

$$F(r) = \frac{\int_0^{2\pi}\int_0^{\pi}\int_0^{\infty} e^{-V_{T_{1u}}(R,\theta,\phi)/kT} f_{R,\theta,\phi}(r)\, R^2 \sin^2\theta \, dR d\theta d\theta}{\int_0^{2\pi}\int_0^{\pi}\int_0^{\infty} e^{-V_{T_{1u}}(R,\theta,\phi)/kT} R^2 \sin^2\theta dR d\theta d\phi}$$

where the observed radial distribution curve, F(r), is the superposition of the instantaneous radial distribution curves, $f_{R,\theta,\phi}(r)$, weighted by the negative exponential of the pseudorotation potential, $V_{T_{1u}}(R,\theta,\phi)$(30). Each instantaneous structure represented by $f_{R,\theta,\phi}(r)$ is restricted to have normal nonbonded vibrational amplitudes, in contrast to the single static model approach where the refined nonbonded amplitudes were enormous in order to adequately fit the experimental radial distribution curve. In the dynamic treatment the breadth of the nonbonded portion of the radial distribution curve comes from the

superposition of different distance distributions for different geometries, and not from abnormally large nonbonded vibrational amplitudes. In principle, one could adjust the parameters of the potential, $V_{T_{1u}}(R,\theta,\phi)$, until the best agreement between F(r) and the experimental radial distribution curve is obtained. In practice, due to programming and computing limitations, the superposition of an infinite number of structures is reduced to a finite sum over a representative sampling of possible structures.

$$F(r) \approx \frac{\sum_i e^{-V(R_i,\theta_i,\phi_i)/kT} f_{R_i,\theta_i,\phi}(r)}{\sum_i e^{-V(R_i,\theta_i,\phi_i)/kT}}$$

There is some ambiguity in the selection of a limited number of finite structures from an infinite number of possibilities. We can use physical insight to make this selection as meaningful as possible. There are only four different types of symmetries generated by our pseudorotational model. These symmetries are C_{3v}, C_{2v}, C_{4v} and C_s. If we glance back at Fig. 3 we can see how the directional preference of the lone pair of electrons selects these various geometries. C_s geometries will occur whenever the lone pair is not oriented in any of the special directions pictured in Fig. 3. If we let the lone pair "rattle" slightly, about each of the special positions (Fig. 3), it will sweep out the C_s structures in the neighborhood of each special position.

This corresponds to slightly increasing the nonbonded vibrational amplitudes for the structures defined by the special positions (i.e. C_{2v}, C_{3v}, C_{4v}). We can see that if we sum just over the C_{2v}, C_{3v}, and C_{4v} geometries, and slightly increase the nonbonded amplitudes of these structures, we have approximated the effect of including the infinite number of C_s structures in the superposition. We must be careful not to increase the nonbonded vibrational amplitudes too much or we will have essentially regressed back to the static model approach. It should be mentioned that we have also considered approximations to F(r) which have included C_s structures intermediate between the highly symmetric C_{2v}, C_{3v} and C_{4v} forms in evaluating the weighted sum.

Although the work on the dynamic model has not yet been completed several general features have emerged. These are (1) the dynamic approach does not uniquely determine the potential function, although it does limit the relative sizes of the potential parameters in order to guarantee distortions of the proper magnitude, (2) structures of near C_{4v} and C_{4v} symmetry do not contribute significantly to the radial distribution curve, and (3) it seems that the dynamic model, with normal nonbonded vibrational amplitudes for the instantaneous structures, is capable of an equivalent or possibly better fit to the experimental data than can be obtained through the single static model approach. While the dynamic model approach in itself will not lead to a unique potential it can be used to test potentials refined by other means (spectroscopic, thermodynamic).

2. Infrared and Raman spectra of XeF_6

If XeF_6 were octahedral, its fifteen vibrational degrees of freedom would belong to the species $A_{1g} + E_g + 2T_{1u} + T_{2g} + T_{2u}$. The species A_{1g}, E_g, T_{2g} are Raman active, T_{1u} is infrared active, and T_{2u} is inactive (Table 2). The infrared spectrum would show two bands, a T_{1u} stretch, and a T_{1u} bend, while the Raman would show three bands, a polarized A_{1g} stretch, a depolarized E_g stretch, and a depolarized T_{2g} bend. The experimental XeF_6 Raman and infrared spectra[60,61] are reproduced in Figs. 5-9. The stretching region in the infrared spectra (Fig. 5,6) indicate three, possibly four bands. In the Raman, the stretching region (Fig. 8,9) is composed of at least three, probably four or more, bands. This alone definitely rules out an octahedral structure for XeF_6. It is useful, however, to consider distorting a $MX_6(O_h)$ structure and correlating the new set of fundamentals with those of a hypothetical octahedral configuration (Fig. 10). It is seen that the general effect of lowering the symmetry from O_h is to increase the number of fundamentals by splitting the degenerate T and E type bands. In addition, the number of observed infrared and Raman transitions increases, with some absorptions now being coincident (Table 2). Because of the breadth of the absorptions in the room temperature Raman and infrared XeF_6 spectra (Fig. 5,8) it is impossible to give a strong preference to any one of the four possible geometries (C_{3v}, C_{2v}, C_{4v}, C_s). This is indirect evidence supporting the indeterminancy of the XeF_6 structure at moderate temperatures (~ 300°K), which implies a free pseudorotation. However,

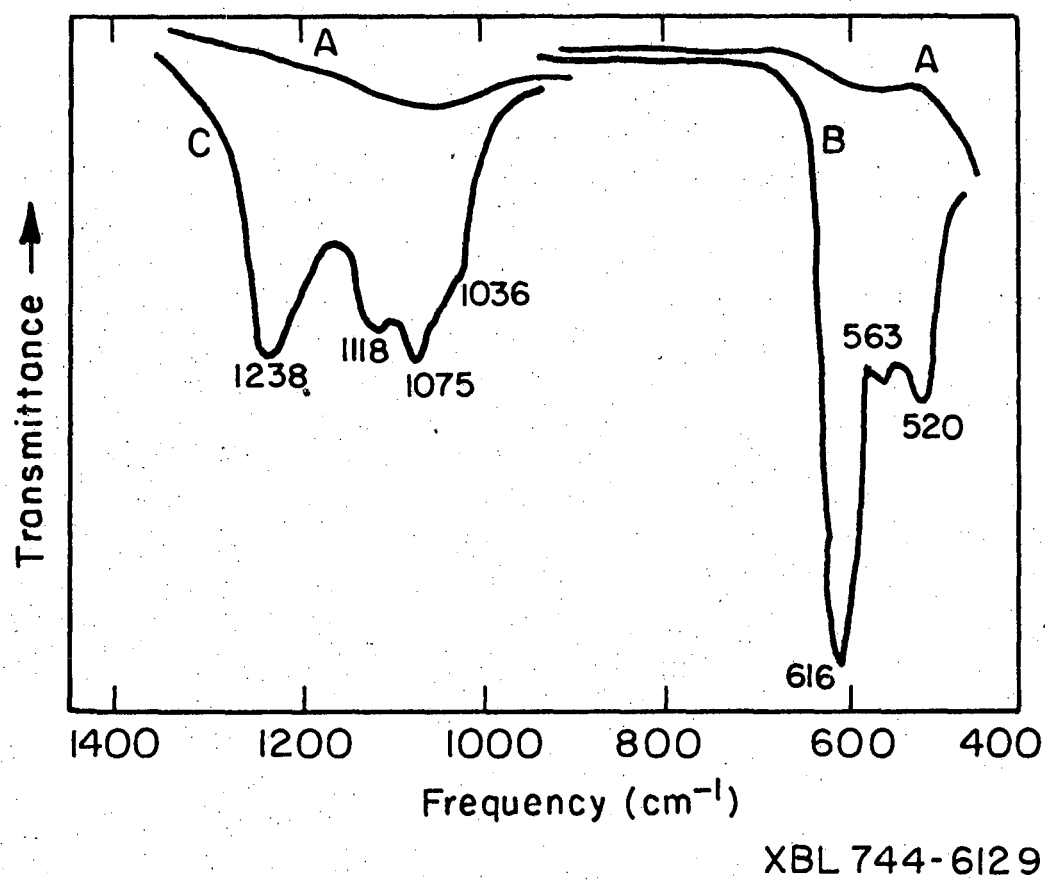

Fig. 5. Infrared spectrum of gaseous XeF_6 at room temperature: A, background; B, 10-cm cell, vapor pressure at -10°; C, 60-cm path cell, vapor pressure at 10°. From the work by Claassen, Goodman and Kim.[60]

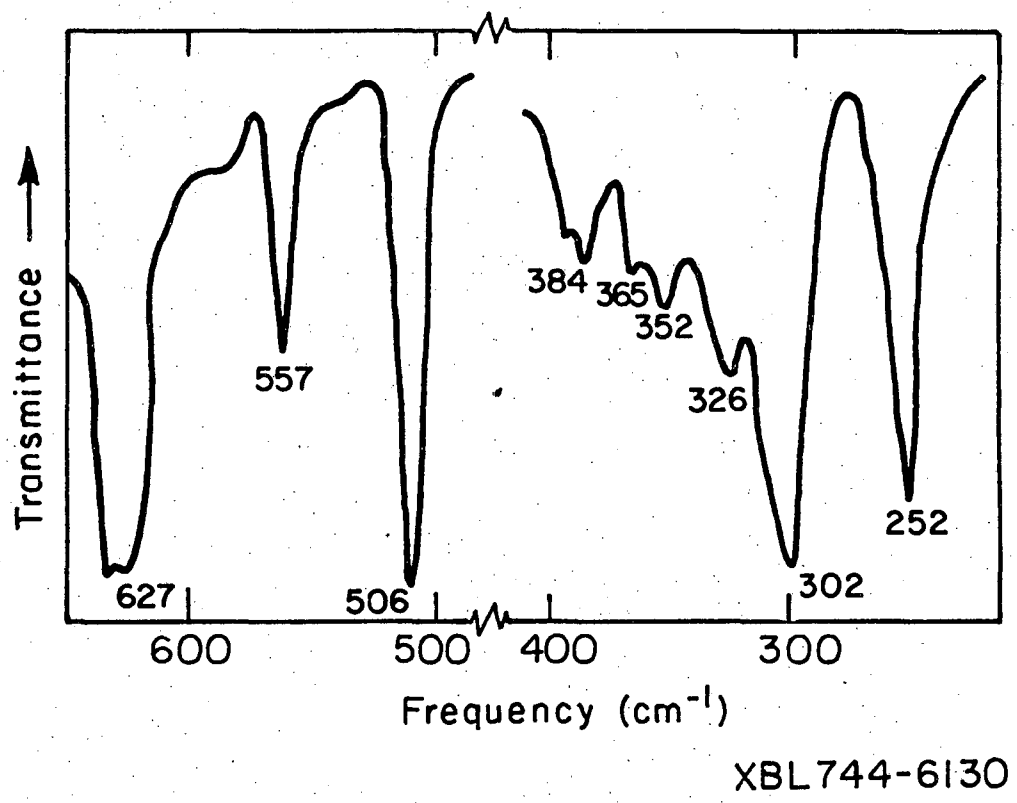

Fig. 6. Matrix-isolation infrared spectrum of XeF_6 in argon at ~7°K. From the work by Claassen, Goodman and Kim.[60]

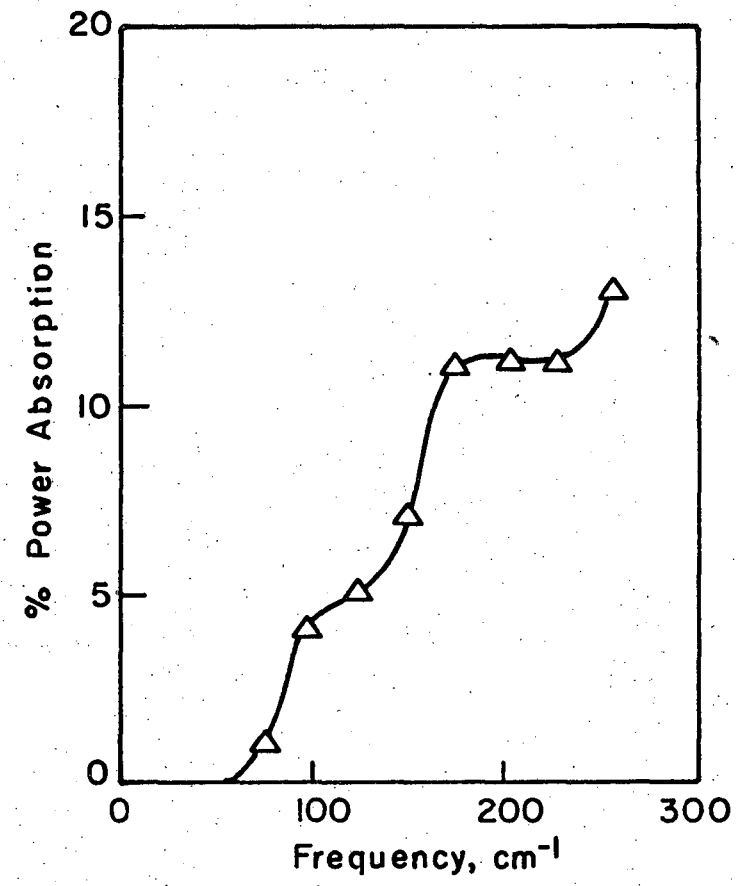

XBL 744-6131

Fig. 7. Far-Infrared spectrum of XeF_6 at room temperature. From the work by Claassen by Claassen, Kim and Pearson.[61]

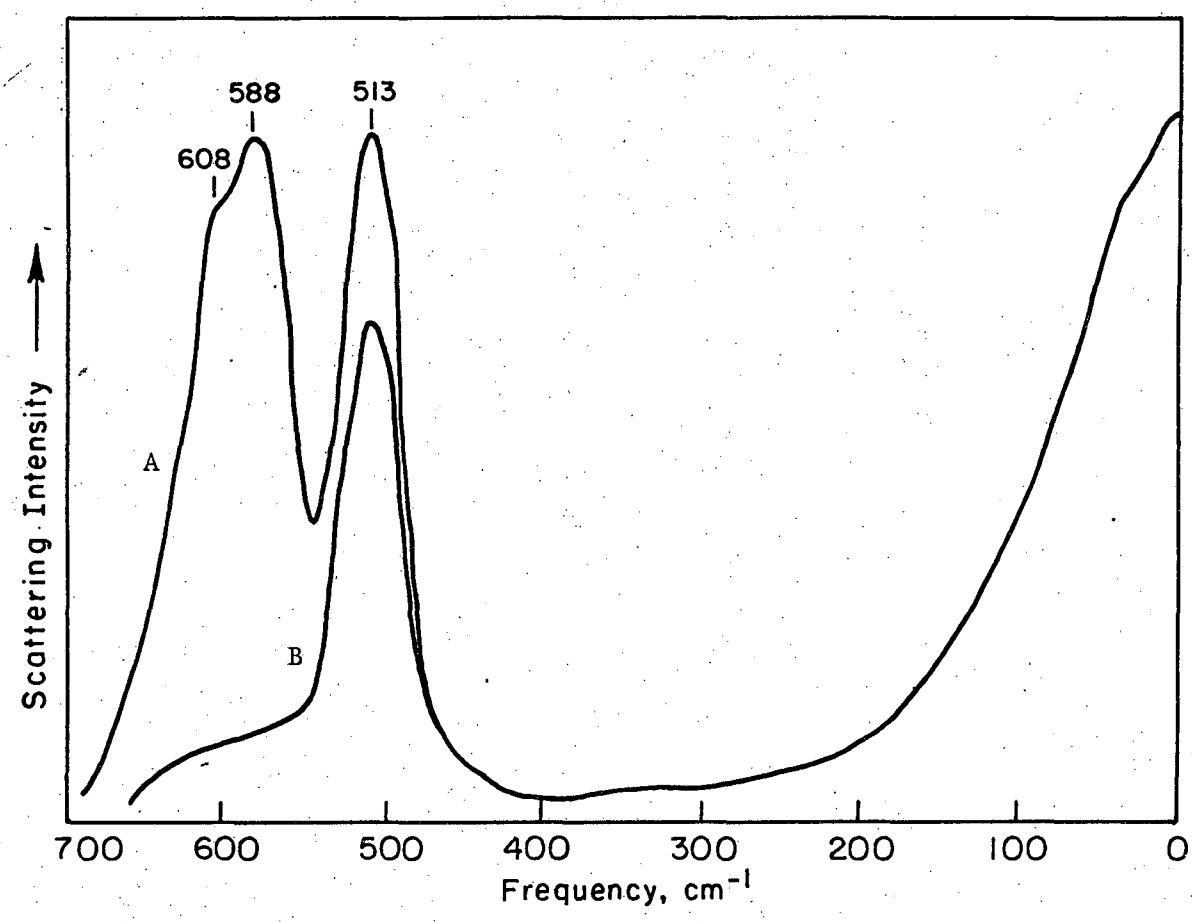

XBL744-6132

Fig. 8. Raman spectrum of XeF_6 vapor at one atmosphere pressure and 85°C. 6471 A° excitation. A, incident polarization perpendicular; B, incident polarization parallel. From the work of Claassen, Goodman and Kim.[60]

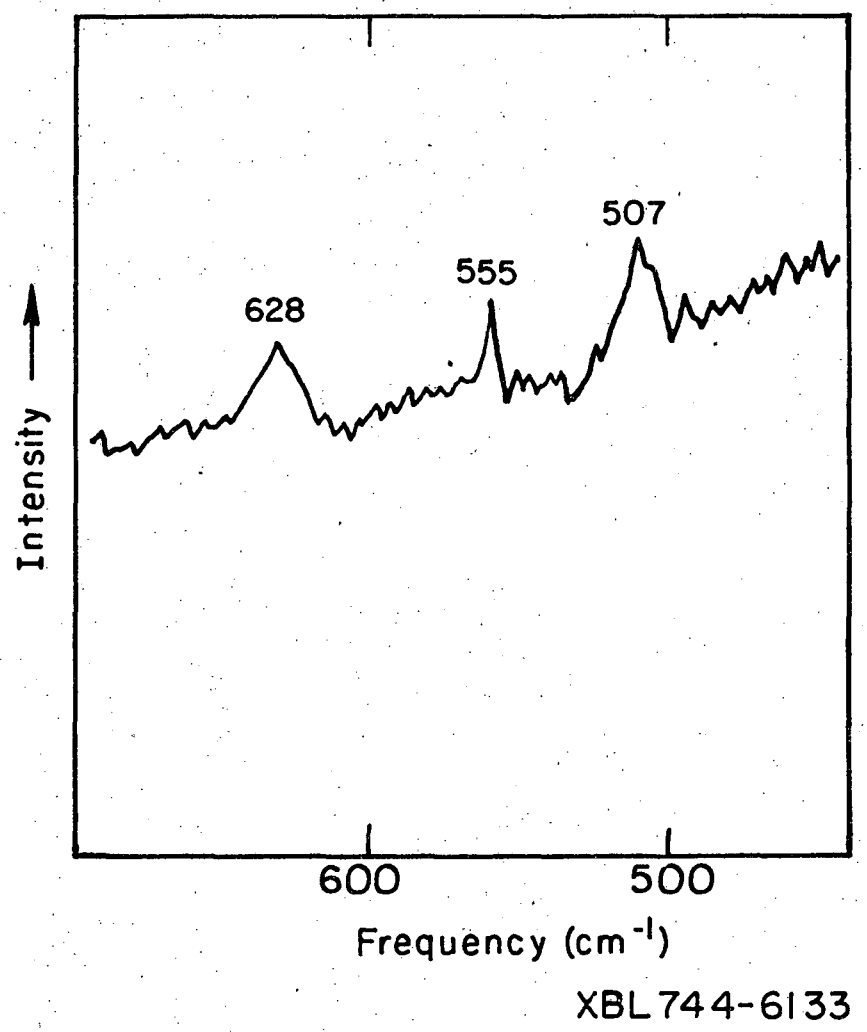

Fig. 9. Matrix-isolation Raman spectrum of XeF_6 in argon at ~7°K. From the work of Claassen, Goodman and Kim.[60]

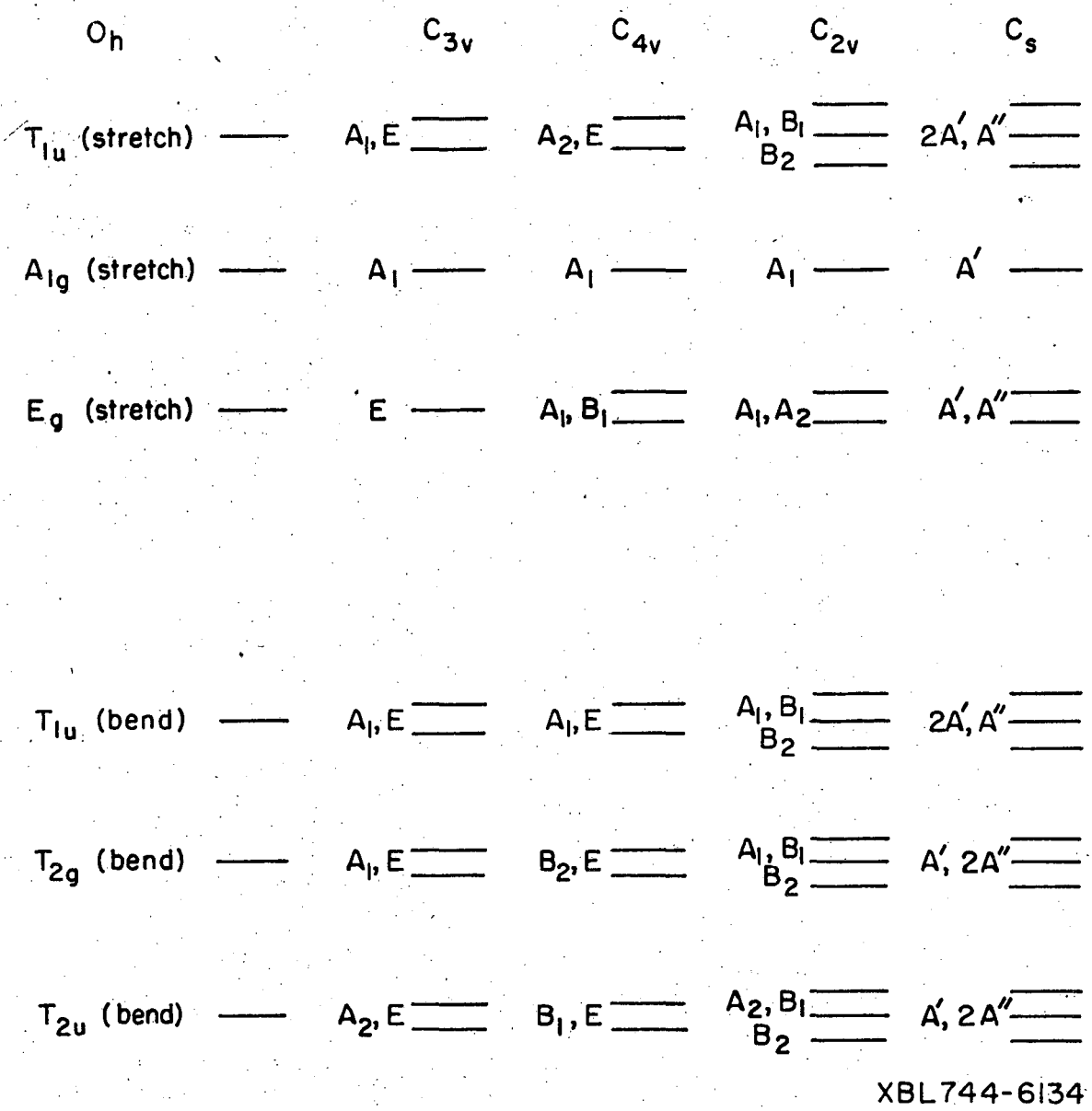

Fig. 10. Correlation diagram for the vibrational modes of a MX_6 molecule of varying symmetry.

at low temperatures (4-7°K) the Raman and infrared spectra sharpen considerably (Fig. 6,9). In the low temperature infrared spectrum (Fig. 6) one can count four bands in the stretching region at 506 cm^{-1}, 557 cm^{-1}, 624 cm^{-1}, 630 cm^{-1}. The band at 627 cm^{-1} (Fig. 6) is really composed of a 624 cm^{-1} and 630 cm^{-1} band, which is clearer in other spectra.[60] The low temperature Raman work (Fig. 9) clearly shows three distinct absorptions at 628 cm^{-1}, 555 cm^{-1}, and 507 cm^{-1}. Furthermore, it is known from the room temperature Raman spectrum (Fig. 8) that the region above ~ 600 cm^{-1} is strongly polarized while the region below 600 cm^{-1} has depolarized components. There is only one geometry that is consistent with the low temperature data, C_{3v}. This is intuitively satisfying because it supports the idea that the potential has a C_{3v} minimum, in which in may be trapped at low temperature. C_s can be ruled out because it would display too many bands in both the Raman and infrared (Fig. 10, Table 2). C_{2v} and C_{4v} would yield too many Raman bands. The assignment of the C_{3v} stretching modes in the low temperature spectra is, A_1 (from T_{1u} stretch) = 630 cm^{-1}, A_1(from A_{1g} stretch) = 624 cm^{-1}, E(from T_{1u} stretch) = 557 cm^{-1}, and E (E_g) = 506 cm^{-1}. The assignment of the two A_1 stretches is based on the strong polarization in the Raman above 600 cm^{-1} (Fig. 8). Furthermore, it is reasonable that these two A_1 bands are close, because the A_{1g} and T_{1u} (stretch) absorptions for normal MX_6 (O_h) molecules are very close for those with bond lengths comparable to XeF_6 (~ 1.9 Å).

The $E(E_g)$ mode is assigned to the more intense Raman band (506 cm^{-1}) because one would not expect the $E(T_{1u})$ motion to gain a great deal of intensity in the Raman for small, or even moderate C_{3v} distortions of XeF_6. The $E(T_{1u})$ mode is a split component of the parent T_{1u} state in the octahedral configuration, which is Raman inactive.

We can get a rough idea of where the C_{3v} bending motions should occur in the low temperature XeF_6 spectrum (Fig. 6) by comparison with normal hexafluorides of similiar bond length. Because the bending frequences should be strongly correlated to bond length we can bound XeF_6(1.9 Å) on the high frequency side by TeF_6(1.86 Å) and on the low frequency side by PuF_6 (1.97 Å). The T_{1u} (bend), T_{2g} and T_{2u} frequencies[54] for PuF_6 and TeF_6 are found in Table 2. Assuming a roughly linear correlation of frequency with bond length the "unperturbed" $XeF_6(O_h)$ frequencies should occur at, T_{1u}(bend) = 289 cm^{-1}, T_{2g} = 280 cm^{-1}, and T_{2u} = 189 cm^{-1}. In Fig. 10, we find that the T_{1u}(bend) will split into an A_1 and E component in C_{3v} symmetry. Both components have infrared activity (Table 2). The A_1 component of the T_{1u}(bend) represents the radial (R) motion in the C_{3v} potential (32b) while the E component can be thought of as a low frequency "rattle," which is essentially the pseudorotation mode. We might expect the A_1 band to be coupled strongly to the E rattle, since they have their origin in the same parent T_{1u} mode. This would lead to an absorption with several components on the high frequency side of the main transition. This is exactly what is observed in the low temperature infrared spectra (Fig. 6) for the 302 cm^{-1} peak. The T_{2g} fundamental yields an A_1 and E component in C_{3v} symmetry, with both modes having infrared activity.

A single, sharp peak is observed at 252 cm^{-1} (Fig. 6), which is in the general area of the predicted T_{2g} type absorption (280 cm^{-1}). Because the measurement did not extend below 200 cm^{-1}, it is possible that the other component lies below 200 cm^{-1}. It is also possible that the other component is buried somewhere in the 302 cm^{-1} band. The problem of assigning the A_1, and E components of the T_{2g} mode will be discussed in more detail in a later part of this section. The T_{2u} band splits into an inactive A_2 mode and on infrared active E fundamental. We would not expect to see the $E(T_{2u})$ mode in the low temperature infrared because it probably occurs below 200 cm^{-1}. This is partially confirmed by a room temperature far infrared XeF_6 spectrum (Fig. 7). Although the exact location of the band is difficult to pinpoint, it probably lies in the range 150-200 cm^{-1}. The width of this band is undoubtedly related to coupling with the pseudorotation mode.

Because we have a detailed theoretical description of the coupling of various modes to the T_{1u} motion, it is possible to extract quantitative information about various coupling terms by relating them to the observed spectroscopic splitting of the degenerate modes (T_{1u} stretch, T_{2g}). The quantum mechanical Hamiltonian for the T_{2g} potential (17), $H_{T_{2g}}$, coupled to the $T_{1u}(S_4)$ motion has the form

$$H_{T_{2g}} = -\frac{\hbar^2}{2m_5}\left(\frac{\partial^2}{\partial S_{5xy}^2} + \frac{\partial^2}{\partial S_{5xz}^2} + \frac{\partial^2}{\partial S_{5yz}^2}\right) + \frac{1}{2}k_5\,(S_{5xy}^2 + S_{5xz}^2 + S_{5yz}^2)$$

$$+ \frac{2c_4^2\,c_5}{\Delta\varepsilon_o^2}\,(S_{4x}S_{4y}S_{5xy} + S_{4x}S_{4z}S_{5xz} + S_{4y}S_{4z}S_{5yz}) \qquad (43)$$

where m_5 is the mass associated with the T_{2g} motion. For a C_{3v} geometry we know that $S_{4x} = S_{4y} = S_{4z}$ which allows (43) to be simplified to

$$H_{T_{2g}} = -\frac{\hbar^2}{2m_5}\left(\frac{\partial^2}{\partial S_{5xy}^2} + \frac{\partial^2}{\partial S_{5xz}^2} + \frac{\partial^2}{\partial S_{5yz}^2}\right) + \frac{1}{2}k_5(S_{5xy}^2 + S_{5xz}^2 + S_{5yz}^2)$$
$$+ \frac{2c_4^2\, c_5\, s_4^2}{\Delta\varepsilon_o^2}(S_{5xy} + S_{5xz} + S_{5yz}) \tag{44}$$

The presence of the linear S_5 terms causes the $V_{T_{2g}}$ potential minimum to be displaced from $S_5 = 0$ (25). If one expands about the potential minimum (S_{5min})

$$U_{5xy} = S_{5xy} - S_{5xy\,min} \tag{45a}$$

$$U_{5xz} = S_{5xz} - S_{5xz\,min} \tag{45b}$$

$$U_{5yz} = S_{5yz} - S_{5yz\,min} \tag{45c}$$

the Hamiltonian, $H_{T_{2g}}$ (44), is transformed to

$$H_{T_{2g}} = \frac{-\hbar^2}{2m_5}\left(\frac{\partial^2}{\partial U_{5xy}^2} + \frac{\partial^2}{\partial U_{5xz}^2} + \frac{\partial^2}{\partial U_{5yz}^2}\right) + \frac{1}{2}k_5(U_{5xy}^2 + U_{5xz}^2 + U_{5yz}^2) \tag{46}$$

where it is seen that in the transformed Hamiltonian (46), the quadratic force constant, k_5, is left unchanged. It should be pointed

out that in this treatment of the $T_{2g} - T_{1u}$ coupling, the T_{1u} motion is considered to be much slower than the T_{2g} motion, so that the S_4 coordinates are treated as constants. This is equivalent to the Born-Oppenheimer separation of nuclear and electronic motion.

One notices that the Hamiltonian (46) is separable into three independent, equivalent parts, and as such cannot explain the lifting of the triple degeneracy of the T_{2g} mode as the molecule distorts to a C_{3v} structure. The type of coupling capable of removing this degeneracy must include cross terms in the S_5 coordinates. You will remember that only the leading terms coupling T_{2g} to the T_{1u}(bend) were considered in the $V_{T_{2g}}$ potential (17). This now necessitates looking for higher order coupling terms in ε_{low} (13). One might expect the following terms (13) to be of use

$$H'_{T_{2g}} = -\frac{2}{\Delta\varepsilon_o^3}(A_1A_2B_2B_3 + A_1A_3B_1B_3 + A_2A_3B_1B_2) \tag{47}$$

where $H'_{T_{2g}}$ is considered as a perturbation on the $H_{T_{2g}}$ Hamiltonian (46). Translation of $H'_{T_{2g}}$ from the A_1B coordinates into the transformed T_{2g} coordinates, U_5, yields

$$\begin{aligned} H'_{T_{2g}} = -\frac{2c_4^2\, c_5^2\, S_4^2}{\Delta\varepsilon_o^3} \Big(& U_{5xy}U_{5xz} + U_{5xy}U_{5yz} + U_{5xy}U_{5xz} \\ & + S_{5xymin}U_{5xz} + S_{5xzmin}U_{5xy} + S_{5xymin}U_{5yz} \\ & + S_{5yzmin}U_{5xy} + S_{5xymin}U_{5xz} + S_{5xzmin}U_{5xy} \\ & + S_{5xymin}S_{5xzmin} + S_{5xymin}S_{5yzmin} + S_{5xymin}S_{5xzmin}\Big) \end{aligned} \tag{48}$$

The perturbation, $H'_{T_{2g}}$ (48), can be evaluated in the basis set defined by the solutions to the unperturbed Hamiltonian, $H_{T_{2g}}$ (46). The solutions to $H_{T_{2g}}$ (46) are of the form

$$\psi = \psi_{n_{5xy}} \psi_{n_{5yz}} \psi_{n_{5xz}} \tag{49}$$

where ψ_n is just the familiar harmonic oscillator wave function.

$$\psi_{n_{5xy}} = Ne^{-(\beta/2)\, U_{5xy}^2} H_{n_{5xy}}(U_{5xy}) \tag{50}$$

$\psi_{n_{5xz}}$, $\psi_{n_{5yz}}$ are similarly defined. We will only consider terms in $H'_{T_{2g}}$ of form $U_{5xy}U_{5xz}$, etc. This is because they connect the three degenerate components of the first excited states (n=1) to each other, and therefore will have a larger effect on these states than terms like $S_{5xy_{min}} U_{5xz}$ which connect states differing by one ($\Delta n = \pm 1$) vibrational quanta. The terms of type $S_{5xy_{min}} S_{5xz_{min}}$ can be ignored as they are constants, and will only serve to redefine the zero of energy. We are now considering the perturbation as

$$H'_{T_{2g}} = \frac{2c_4^2\, c_5^2\, S_4^2}{\Delta\varepsilon_o^{\,3}} \left(U_{5xy}U_{5xz} + U_{5xy}U_{5yz} + U_{5xy}U_{5xz}\right) \tag{51}$$

The determinant of $H'_{T_{2g}}$ in the $|n_{5xy}, n_{5xz}, n_{5yz}\rangle$ basis is

$$
\begin{array}{c|cccc|}
 & |001\rangle & |010\rangle & |100\rangle & |000\rangle \\
|001\rangle & V^{o}_{T_{2g}} - \varepsilon & a & a & 0 \\
|010\rangle & a & V^{o}_{T_{2g}} - \varepsilon & a & 0 \\
|100\rangle & a & a & V^{o}_{T_{2g}} - \varepsilon & 0 \\
|000\rangle & 0 & 0 & 0 & -\varepsilon
\end{array}
$$

where

$$a = -\frac{2c_4^2\, c_5^2\, S_4^2}{\Delta\varepsilon_o^{\,3}} \langle 001|U_{5yz}U_{5xz}|010\rangle \quad \text{etc.} \tag{53a}$$

$$\langle 001\,|U_{5xy}U_{5xz}|\,010\rangle = \frac{h}{4\pi^2 m_5 V^{o}_{T_{2g}}} \tag{53b}$$

and $V^{o}_{T_{2g}}$ is the unperturbed T_{2g} frequency. Equations (53a, 53b) define the following relation between the linear matrix elements c_4, and c_5 (2).

$$c_4^2\, c_5^2 = \frac{|a|V^{o}_{T_{2g}}\, m_5\, 2\pi^2\, \Delta\varepsilon_o^{\,3}}{h\, S_4^2} \tag{54}$$

Once $|a|$, $V^{o}_{T_{2g}}$, m_5, and $\Delta\varepsilon_o$ are determined then Eq. (54) will be quantitatively defined.

The solutions to the polynomial resulting from the determinant (52) are

$$\varepsilon = 0 \quad \text{ground state} \tag{55a}$$

$$\varepsilon = V^{o}_{T_{2g}} - a,\ V^{o}_{T_{2g}} - a,\ V^{o}_{T_{2g}} + 2a \quad \text{first excited states} \tag{55b}$$

The first excited state is split into a doublet (E) and a singlet (A_1), which was expected on the basis of the correlation diagram (Fig. 10). The assignment of the split T_{2g} mode can be made as

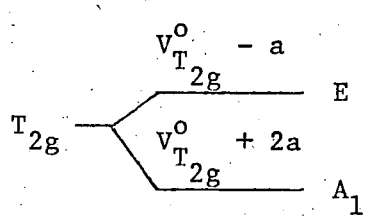

(56)

where $V^{o}_{T_{2g}} + 2a$ is lower than $V^{o}_{T_{2g}} - a$ because "a" (53a) is negative. There is still the ambiguity of whether the 252 cm^{-1} peak (Fig. 6) is the A_1 or E component. We can make a reasonable guess based on the earlier prediction that $T_{2g} \approx 280\ cm^{-1}$, where the PuF_6 and TeF_6 T_{2g} frequencies were used as lower and upper bounds respectively. Thus, $A_1 = 252\ cm^{-1}$ and the E component is probably masked by the 302 cm^{-1} peak (Fig. 6). If we assume the E (T_{2g}) is approximately E = 342 cm^{-1} than the splitting between A_1 and E is $3|a| = 90\ cm^{-1}$, or $|a| = 30\ cm^{-1}$. This places the "unperturbed" T_{2g} frequency at $V^{o}_{T_{2g}} = 312\ cm^{-1}$.

The mass (m_5) associated with the T_{2g} motion can be determined from its G-matrix[12] element (G_5) by

$$m_5 = \frac{m_F}{4} \tag{57}$$

where m_F is the mass of fluorine atom. The mass, m_5, equals 4.75 amu.

The electronic transition energy, $\Delta\varepsilon_o$ ($^1A_{1g} \rightarrow {}^1T_{1u}$), has not yet been determined; however, for the purpose of calculating $c_4^2\ c_5^2$ (54), we can use the value $\Delta\varepsilon_o$ = .87 (mdyn-Å), whose origin will be discussed in the XeF_6 ultraviolet spectrum section. We now have values for all the parameters needed to define $c_4^2\ c_5^2$ (54).

$$c_4^2\ c_5^2 = .0351\ \text{mdyn}^4 \tag{58}$$

The importance of deriving this relation between c_4 and c_5, is that once either quantity is determined, the value of the other is fixed by Eq. (58). Knowledge of c_4 and c_5 gives us an independent check of the $T_{1u} - T_{2g}$ coupling constant, which was calculated from electron diffraction data (39). This check is independent because the relation between c_4, and c_5 (58) was derived strictly from a spectroscopic point of view.

The analysis of the $T_{1u(bend)} - T_{1u(stretch)}$ interaction, which splits the degeneracy of the $T_{1u(stretch)}$ in the C_{3v} configuration, is quite similar to the analysis just presented in detail for the T_{1u}-T_{2g} interaction. Because of the similarities only a sketchy outline is presented for the $T_{1u} - T_{1u}$ case.

The terms responsible for splitting the T_{1u} stretch are (13)

$$H'_{T_{1u}} = \frac{8c_3^2\, c_4^2\, S_4^2}{\Delta\varepsilon_o^{\,3}} \left(S_{3x}S_{3y} + S_{3x}S_{3z} + S_{3y}S_{3z}\right) \tag{59}$$

This leads to the following eigenvalues

$$\varepsilon = 0 \qquad \text{ground state} \tag{60a}$$

$$\varepsilon = V^o_{T_{1u}} - b,\ V^o_{T_{1u}} - b,\ V^o_{T_{1u}} + 2b \qquad \text{first excited states} \tag{60b}$$

where

$$b = \frac{8\, c_3^2\, c_4^2\, S_4^2}{\Delta\varepsilon_o^{\,3}} \langle 001 | S_{3x}\, S_{3y} | 010 \rangle \quad \text{etc.} \tag{61}$$

Because "b" is positive the split $T_{1u(\text{stretch})}$ components are assigned as

$$T_{1u(\text{stretch})} \begin{cases} V^o_{T_{1u}} + 2b & A_1\ (630\ \text{cm}^{-1}) \\ V^o_{T_{1u}} - b & E\ (557\ \text{cm}^{-1}) \end{cases} \tag{62}$$

This assignment is the same as our earlier guess which was based mainly on the polarization of the Raman bands. We find that $b = 24.3\ \text{cm}^{-1}$ and the unperturbed T_{1u}(stretch) frequency is $V^o_{T_{1u}} = 581\ \text{cm}^{-1}$. We can use Eq. (61) to define a relation between c_3, and c_4.

$$c_3^2\, c_4^2 = .0529 \text{ mdyn}^4 \tag{63}$$

As in the T_{2g} case, if either c_3 or c_4 is found the other is fixed by (63). Knowledge of c_3 and c_4 would allow an independent check on the T_{1u}(bend) - T_{1u}(stretch) coupling constant, $C_{T_{1u}}$ (42), determined by the electron diffraction work.

The T_{1u}(bend) linear matrix element, c_4, can be estimated in the following manner. The second derivative of the C_{3v} potential (32a) yields

$$\left(\frac{\partial^2 V_{C_{3v}}}{\partial R^2}\right)_{R_o} = -\,2a + 12\,(b - .333c)\,R_o^2 = K_{C_{3v}} \tag{64}$$

where $K_{C_{3v}}$ is the curvature at the radial minimum, R_o. The second derivative relationship can be combined with the first derivative Eq. (36) to give

$$a = \frac{K_{C_{3v}}}{4} \tag{65a}$$

$$(b - .333c) = \frac{K_{C_{3v}}}{8\,R_o^{\,2}} \tag{65b}$$

In the XeF_6 theory section the parameter "a" was defined as (29a)

$$a = \frac{c_4^2}{\Delta\varepsilon_o} - \frac{k_4}{2} - \frac{2\,c_3^{\,2} c_4^{\,2}}{k_3 \Delta\varepsilon_o^{\,2}} \tag{66}$$

With Eqs. (63,65a,66) we can solve for c_4.

$$c_4^2 = \Delta\varepsilon_o \left(\frac{K_{C_{3v}}}{4} + \frac{k_4}{2} + \frac{2(.0529)}{k_3 \, \Delta\varepsilon_o^{\,2}} \right) \tag{67}$$

The value of $K_{C_{3v}}$ can be approximated as the force constant for the radial motion.

$$K_{C_{3v}} = (5.9\times10^{-7})(V_{A_1(T_{1u}\text{bend})})^2 m_4 \tag{68}$$

where for

$$V_{A_1(T_{1u}\text{bend})} = 302 \text{ cm}^{-1}, \; m_4 = 6.56 \text{ amu},$$

$$K_{C_{3v}} = .349 \left(\frac{\text{mdyn}}{\text{Å}}\right) .$$

The parameter, k_4, can be interpretted as the T_{1u}(bend) force constant for a hypothetical octahedral XeF_6 molecule, in which there is no mixing of the $s(A_{1g}^*)$ and $p(T_{1u})$ orbitals on the Xe atom due to the T_{1u} motion. This corresponds to the limit that $\Delta\varepsilon_o(^1A_{1g} \rightarrow {}^1T_{1u})$ becomes infinite. We can approximate k_4 from the unperturbed T_{1u} bend frequency found by comparison of XeF_6 to PuF_6 and TeF_6. With $V_{T_{1u}(\text{bend})} = 284 \text{ cm}^{-1}$, k_4 equals .314 (mdyn/Å). The linear matrix element, c_4, is computed (67) to be

$$c_4 = .50 \text{ mdyn} \tag{69}$$

With c_4 defined, c_5 (58) and c_3 (63) become

$$c_5 = .374 \text{ mdyn} \tag{70a}$$

$$c_3 = .461 \text{ mdyn} \tag{70b}$$

We can now compute the T_{1u}-T_{2g}, $C_{T_{2g}}$ (39), and T_{1u}-T_{1u}, $C_{T_{1u}}$ (42), coupling constants. These were

$$C_{T_{2g}} = \frac{2c_4^2 \; c_5}{k_5 \Delta\varepsilon_o^{\;2}} \tag{39}$$

$$C_{T_{1u}} = \frac{2c_3 c_4}{k_3 \Delta\varepsilon_o} \tag{42}$$

For the unperturbed T_{2g} and T_{1u} stretch frequences at $V^o_{T_{2g}} = 312 \text{ cm}^{-1}$, $V^o_{T_{1u}\text{ stretch}} = 581 \text{ cm}^{-1}$, the force constants are $k_3(T_{1u}\text{stretch}) =$ 3.78 (mdyn/Å), $k_5(T_{2g}) = .272$ mdyn/Å. The mass (m_3) associated with the $T_{1u}(S_3)$ stretch was approximated as $m_3 = m_F$.[56] The coupling constants $C_{T_{2g}}$ (39) and $C_{T_{1u}}$ (42) are

$$C_{T_{2g}} = .91 \left(\frac{1}{\text{Å}}\right) \tag{71a}$$

$$C_{T_{1u}} = .14 \tag{71b}$$

The $C_{T_{2g}}$ and $C_{T_{1u}}$ coupling constants calculated by electron diffraction were placed at $C_{T_{2g}} = 1.9\ (\frac{1}{\text{Å}})$, $C_{T_{1u}} = .13$. Considering the approximations used in the spectroscopic determination of $C_{T_{2g}}$ and $C_{T_{1u}}$ the agreement with the diffraction work is quite good. The larger discrepancy in the $C_{T_{2g}}$ case is not totally unexpected due to lack of knowledge about the missing component of the split T_{2g} band.

For the reader's convenience the low temperature assignment of the XeF_6 spectrum based on a C_{3v} structure is summarized in Table 4. The symmetry species in parenthesis indicates the origin of the C_{3v} component from a hypothetical octahedral structure. The $E(T_{1u}$ bend) bend is not included in Table 4 because it corresponds to the low frequency, pseudorotation mode. In Table 5, we have collected most of the parameters derived in this section.

3. Ultraviolet Spectrum of XeF_6

The purpose of discussing the ultraviolet spectrum of XeF_6 is to determine which of the observed transitions corresponds to the one of interest, $\Delta\varepsilon_o(^1A_{1g} \rightarrow {}^1T_{1u})$. Before looking at the observed spectrum we should gain a qualitative understanding of what to expect. As a starting point we can study the molecular orbital diagram for XeF_6 (Fig. 2). The lowest electronic transition is from the A^*_{1g} orbital, which has partial 5s (Xe) character, to the T^*_{1u} orbital, which is mostly localized on xenon's 5p orbitals. It is therefore natural to view this transition as a s→p type transition for the purpose of deciding what kinds of states will arise. As a function

of the spin-orbit interaction, the states, in order of energy, with the ground state at the bottom, are[62]

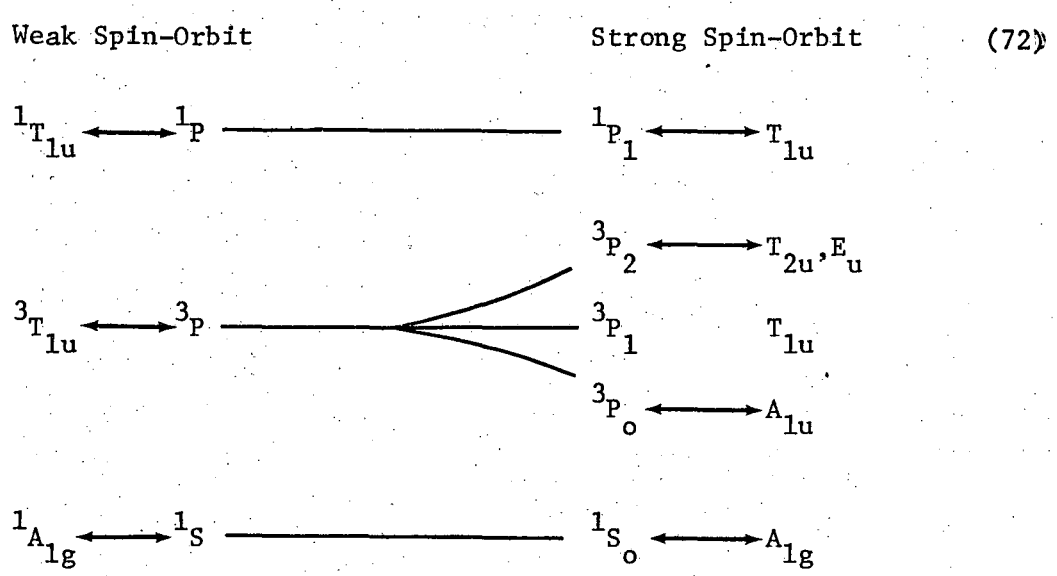

where the symmetry of the atomic state is indicated under the O_h point group. In the weak spin-orbit case the states are approximately a separable product of a spatial and spin part, hence the indication of the spin state is retained in the labeling of the state under the O_h point group. In the strong spin-orbit case the spin and space functions are scrambled together and actually form a direct product state under the full rotation group (D^j). However, to facilitate comparison to the weak spin-orbit case the these states were decomposed into their octahedral (O_h) representations.

First, we can consider the allowed electronic transitions in the weak spin-orbit case. In the O_h point group the dipole moment operator is contained completely in the T_{1u} representation. This means, only transitions from an A_{1g} spatial part to a T_{1u} spatial part can have

intensity. Because the spin of the A_{1g} ground state is singlet, $^1A_{1g}$, there is the additional requirement that the excited state also have a singlet spin in order for the transition to have intensity. In the weak spin-orbit case we see (72) that only one transition is allowed, $^1A_{1g} \rightarrow {}^1T_{1u}$, and the observed spectrum would show only one band at a relatively low energy. The effect of increasing the spin-orbit effect is to give some intensity to the $^1S_o(A_{1g}) \rightarrow {}^3P_1(T_{1u})$ transition, thus producing an additional absorption at lower energy than the $^1P_1(T_{1u})$ band. It should be mentioned that if the molecule undergoes a large amplitude motion, or a permanent distortion from O_h, the $^1S_o(A_{1g}) \rightarrow {}^3P_2(T_{2u},E_u)$ transition will gain some (very little) intensity. We can derive an expression to quantitatively determine the relative strength of the spin-orbit interaction. The spin-orbit interaction will mix the $^1T_{1u}$ and $^3T_{1u}$ basis states of the weak spin orbit case to produce the states[65]

$$|C\rangle = (1-t^2)^{1/2}\,|^1T_{1u}\rangle + t|^3T_{1u}\rangle \tag{73a}$$

$$|A\rangle = -\,t\,|^1T_{1u}\rangle + (1-t^2)^{1/2}\,|^3T_{1u}\rangle \tag{73b}$$

where $|A\rangle$ corresponds to $^3P_1(T_{1u})$ and $|C\rangle$ to $^1P_1(T_{1u})$, and t is a coefficient which indicates the extent of mixing of $^1T_{1u}$ with $^3T_{1u}$.

The ratio of the observed spectral intensity of $|A\rangle$ to $|C\rangle$ is determined by the ratio of the square of their $|^1T_{1u}\rangle$ components.

$$R_{|A\rangle/|C\rangle} = \frac{t^2}{1-t^2} \tag{74}$$

The experimental ultraviolet[60] XeF_6 spectrum (Fig. 11) shows two absorptions, one at 2300 Å (.87 mdyn-Å) and one at 3500 Å (.57 mdyn-Å). The 2300 Å peak is the $A_{1g} \rightarrow T_{1u}$ ($^1p_1$) transition, which is what we have called $\Delta\varepsilon_o$ and is sometimes called the C band. The 3500° Å peak is the $A_{1g} \rightarrow T_{1u}$ ($^3P_1$) transition, called the A band. From the relative intensities (area under the curves) we calculate R at R = .1, which places t at t = .3. This indicates that spin-orbit coupling is not negligible, however the $^1P_1(T_{1u})$ state is mostly $^1T_{1u}$(~ 76%). In principle, spin-orbit effects require that both T_{1u} states ($^1P_1$, $^3P_1$) be included in determining the interaction with the ground electronic state, A_{1g}, via the T_{1u} distortion. To do this would complicate the problem drastically as one would have a 7×7 determinant to diagonalize in resolving the ground state vibrational potential. Because the upper T_{1u} state, $^1P_1$, contains most of the $^1T_{1u}$ component, it is a reasonable approximation to only include it in determining the ground state vibrational potential, which is the approach taken here.

Toyozawa and Inoue[63] have demonstrated that the structure of the $|C\rangle$ band ($^1A_{1g} \rightarrow {}^3T_{1u}$) can be related to $c_5(2d)$, the linear T_{2g} matrix element. Because the $^1T_{1u}$ excited state is spatially degenerate it can undergo a Jahn-Teller distortion in the vibrational modes defined

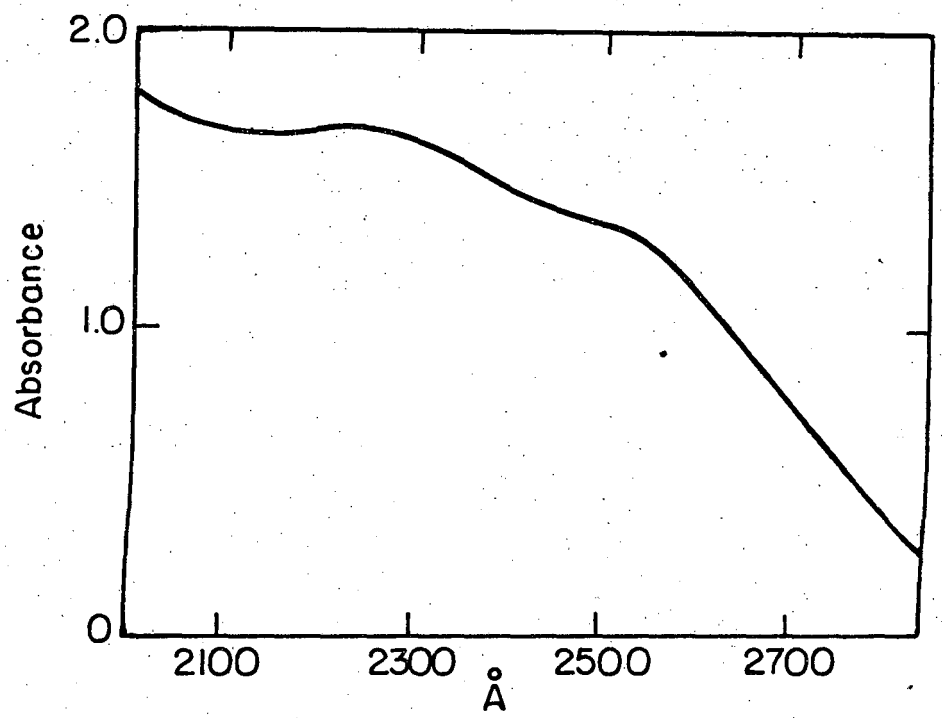

Ultraviolet spectra of XeF_6 at 25°C and 1mm pressure, 10 cm path length

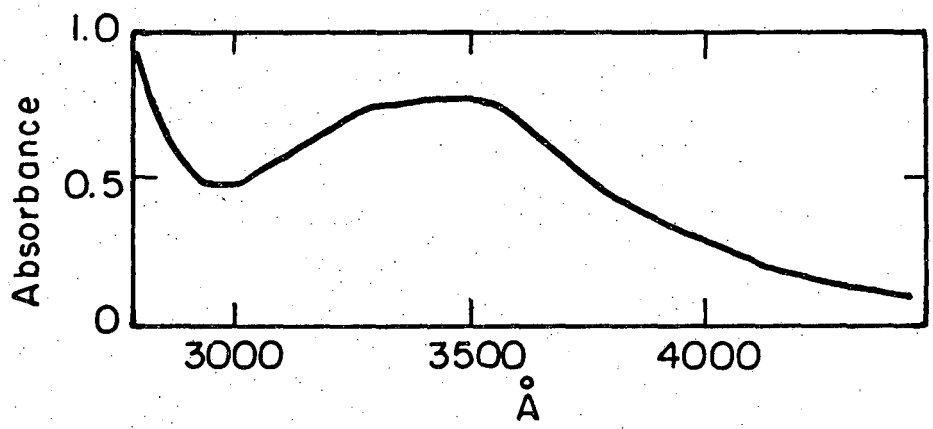

Ultraviolet spectra of XeF_6 at 25°C and 3mm pressure, 10cm path length

XBL 744-6135

Fig. 11. Ultraviolet spectrum of XeF_6 from the work of Claassen, Goodman and Kim.[60]

by $T_{1u} \times T_{1u} = T_{2g} + A_{1g} + E_g + T_{1g}$. For reasons which will not be discussed here, only the T_{2g} mode will lead to an observable splitting of the triply degenerate (T_{1u}) potential surface. This splitting will produce three humps in the $^1A_{1g} \rightarrow {}^3T_{1u}$ band. The symmetrical splitting (ΔE) of these side peaks (humps) relative to the central peak is given by the formula

$$\Delta E = (.91) \left(\frac{2c_5^2}{k_5} kT\right) \tag{75}$$

where k is Boltzman's constant and T is temperature. For XeF_6 ΔE = .107 mdyn-Å (5,000 cm^{-1}), k_5 = .272 (mdyn/Å), and T=298°C. The linear T_{2g} matrix element, c_5, has the value

$$c_5 = .66 \text{ mdyn} \tag{76}$$

This is somewhat larger than c_5 calculated from vibrational spectroscopic data in the previous section where c_5 = .374 mdyn. However, it is encouraging that the two values are reasonably close considering the differences in approaches. There is considerable uncertainty in the value of c_5 just derived because, (1) the components of the C band are very broad making a determination of the exact splitting difficult, and (2) the theoretical formula (75) for the splitting was derived assuming vertical electronic transitions from the $|^1A_{1g}\rangle$ ground electronic state of an MX_6 molecule undergoing harmonic oscillations about an octahedral equilibrium geometry to the $|^1T_{1u}\rangle$ excited electronic state - XeF_6 does not have an octahedral equilibrium geometry in the ground electronic state.

Toyozawa and Inoue[63] also derived theoretical expressions for both c_5 and c_2, the Eg linear matrix element, in terms of molecular constants (see their Eqs. 5.6, 5.7). Although their configuration coordinates, ξ_α, do not correspond exactly to the symmetry coordinates used in this chapter, a comparison of their equations for c_2 and c_5 allows one to estimate the relative size of these parameters.

$$|c_5| \leqslant |c_2| \leqslant 1.5\ |c_5| \tag{77}$$

The range for $|c_2|$, in terms of $|c_5|$, is a reflection of the difference in coordinate systems.

There is an independent way in which we can estimate c_2. It is from the X-ray diffraction work on solid XeF_6 at - 80°C.[64] In the solid, XeF_6 exists in two different environments, (1) a hexameric arrangement of 6 XeF_6 molecules, (2) a tetrameric arrangement of 4 XeF_6 molecules. We will confine our remarks to the tetrameric type XeF_6 molecules because they are considerably less distorted than the hexameric XeF_6, relative to the gas phase XeF_6 molecule. In the tetrameric arrangement each XeF_6 assumes an approximately C_{4v} symmetry, with one of the axial fluorines displaced considerably from its gas phase distance (1.9 Å) to 2.23 Å in the solid. This is due mainly to the lone pair of electrons sitting underneath a fluorine atom in the C_{4v} form, and partly to the attraction of the displaced fluorine to an incompletely shielded xenon nucleus on an adjacent XeF_6 molecule in the tetramer. The potential of each of the equivalent XeF_6 molecules in the tetramer can be idealized as

$$V_{XeF_6\ solid} = V_{T_{1u}\ (gas)} + V' \tag{78}$$

where V' is the potential due to the other three XeF_6 molecules in the tetramer, and $V_{T_{1u}}$ (30) is the potential derived in the XeF_6 theory section for a gas phase XeF_6 molecule. We found that in the gas phase, the C_{3v} configuration was a potential minimum and the C_{4v} structure a potential maximum. The nature of V' must be such as to reverse this behavior because in the solid, XeF_6 assumes a C_{4v} structure. Because the XeF_6 molecules have no net charge, the leading term in V' must be a dipole-dipole interaction between XeF_6 molecules in the tetramer. This implies that each individual XeF_6 molecule in the tetramer is coupled to the other three XeF_6 molecules only through terms involving a T_{1u} symmetry coordinate. This is clear, because only T_{1u} distrotions can generate a dipole moment in XeF_6 (Fig. 1). The effects of this external coupling to the T_{1u} motion are to alter the potential minimum to C_{4v} and also to change the magnitude of the radial (R) minimum. Because the external coupling (V') does not explicity involve the E_g symmetry coordinates (S_2) any geometrical changes in the XeF_6 (C_{4v}) molecule due to an E_g displacement can still be treated through the T_{1u}(bend) - E_g coupling term derived previously (20,21).

The molecular parameters of a tetrameric XeF_6 molecule are indicated in Table 6. If we choose the C_{4v} axis in the "Z" direction, we can see qualitatively that only the T_{1u} bend (S_{4z}) coupled to the T_{1u} stretch (S_{3z}) and E_g coordinate (S_{2a}) will account for the geometry

(C_{4v}) and the distribution of bond lengths. The effect of the $E_g(S_{2a})$ coordinate is to equally shorten the four basal fluorines, and lengthen the apical fluorines. The T_{1u}(stretch) lengthens the Xe-F_{apical} bond directly under the lone pair and shortens the opposite Xe-F_{apical} bond. The net effect of the combined E_g and T_{1u}(stretch) is to significantly lengthen the apical Xe-F bond on top of the lone pair and leave the other apical Xe-F relatively unchanged. The T_{1u}(bend), S_{4z}, gives the molecule the required C_{4v} symmetry.

The F_{apical} - Xe - F_{basal} bond angle of 77.2° corresponds to $\Delta\alpha$ = 12.8° in terms of the S_{4z} coordinate (33b). The value S_{4z} is S_{4z} = 1.16 Å. The relationship between S_{4z} and S_{2a} (E_g) is given by Eq. (20)

$$S_{2a} = \sqrt{\frac{3}{2}} \frac{c_2 c_4^2 \, 2S_{4z}^2}{k_2 \Delta\varepsilon_o^2} \tag{79}$$

where S_{4x}, S_{4y} = 0 for C_{4v} geometry, and k_2, the E_g force constant, is placed at k_2 = 2.86 (mdyn/Å) for $V^o_{E_g}$ = 506 cm^{-1}. The E_g mass (m_2) was assumed equal to 19 amu. In the C_{4v} form the change in basal bond length is Δr = - .04 Å where this is relative to the gas phase bond length of 1.9 Å. This puts the S_{2a} coordinate (33a) at S_{2a} = .092 Å. With previously determined c_4 (.5 mdyn) and $\Delta\varepsilon_o$(.87 mdyn-Å), we can solve Eq. (7a) for c_2.

$$c_2 = .242 \text{ mdyn} \tag{80}$$

where this is slightly lower than our expected range for c_2 (77).

We are now in a position to estimate the parameters b, and c via Eqs. (29b, 29c). These are

$$b = \frac{c_4^{\,4}}{\Delta\varepsilon_o^{\,3}} - \frac{3c_2^{\,2}c_4^{\,4}}{k_2\Delta\varepsilon_o^{\,4}} \tag{29b}$$

$$c = \frac{2c_4^{\,4}c_5^{\,2}}{k_5\Delta\varepsilon_o^{\,4}} - \frac{9c_2^{\,2}c_4^{\,2}}{k_2\Delta\varepsilon_o^{\,4}} \tag{29c}$$

The value of the parameter "a" is fixed exactly by relation (65a).

The estimated ranges for b, and c are

$$.05 \leqslant b \leqslant .09 \ \left(\frac{\text{mdyn}}{\text{Å}^3}\right) \tag{81a}$$

$$0 \leqslant c \leqslant .1 \ \left(\frac{\text{mdyn}}{\text{Å}^3}\right) \tag{81b}$$

The larger range for c is a reflection of the much greater uncertainty in the values of c_2 and c_5 as compared to the relatively accurate determination of c_4 (66,67). A rigorous lower bound for "b" can be calculated from Eq. (65b), by setting c=0. This yields b = .0576 mdyn/Å^3, which is in good agreement with the predicted "b" range. An upper bound for c can be found using Eq. (65b) and setting b = .09. This yields c = .1 mdyn/Å^3, which agrees nicely with the "c" range established by (29c). In summary, we have accomplished two major things in this section, (1) a relatively accurate value of the

$^1A_{1g} \rightarrow {}^1T_{1u}$ transition energy, $\Delta\varepsilon_o$ (.87 mdyn-Å), (2) an initial estimation of the ranges of the potential parameters b and c.

4. Thermodynamics of XeF_6

The heat capacity of XeF_6 has been measured by Schreiner[65] and co-workers from 5 → 350°K. They derived a value of the standard entropy, S^o, of XeF_6 at 335°K which was $S^o_{335°K}$ = 96.22 (cal/deg). Weinstock and co-workers[66] calculated $S^o_{298°K}$ for various static geometries of XeF_6. Their results for a C_1 structure, which because of its low symmetry should have the highest entropy of all static structures, was $S^o_{298°K}$ = 87.72 (cal/deg). The inability of a static structure to approach the experimental entropy indicates that there is either a very low frequency vibration, or even a pseudorotational motion occurring. Thermodynamically, the situation in XeF_6 parallels that of cyclopentane,[35,36] where a free pseudorotational model for cyclopentane reproduced the experimental heat capacity quite well.

If we can somehow extract the entropy associated just with the pseudorotational mode in XeF_6, then it should be possible to use this information to further refine the potential parameters b, and c. This can be accomplished by assigning all the vibrational modes, except the T_{1u}(bend), then calculating the standard entropy by statistical mechanics[67] and subtracting the result from the experimental entropy. The difference will then be the entropy of the T_{1u}(bend) motion.

Before presenting this calculation, it is worthwhile to discuss, in general, the problem of determining thermodynamic functions for molecules having multiminimum vibrations. Pitzer[68] has considered this problem in detail for molecules with a double minimum vibration (NH_3). The difficulty in calculating the entropy of a NH_3- like molecule is in deciding what the rotational symmetry number (σ) should be. If we view the molecule as executing a double minimum vibration, then all of its levels in the inversion mode are doubly degenerate. However, in adopting this point of view we must regard the potential surface as D_{3h}, not C_{3v}, and accordingly the symmetry number will be that for a planar (on the average) D_{3h} molecule, $\sigma = 6$. An alternate treatment would be to view NH_3 as a static C_{3v} structure. This would necessitate lowering the degeneracy of the inversion levels to one, and lowering the symmetry number to $\sigma = 3$, for a C_{3v} molecule. In going from the D_{3h} to the C_{3v} viewpoint we have lost R ln 2 vibrational entropy and gained R ln 2 rotational entropy, for a net change of zero. Thus, regardless of the location of the potential minimum (D_{3h}, or C_{3v}) the entropy can always be calculated by considering the more symmetrical structure.

Although the situation in XeF_6 is more complicated than in NH_3, due to the three dimensional nature of the XeF_6 "inversion" mode, the thermodynamic analysis is quite similar. Table 7 lists the relevant thermodynamic quantities for various assumed XeF_6 geometries. To illustrate the use of Table 7 we will consider XeF_6 to be permanently distorted into a C_{3v} structure. There are eight equivalent C_{3v}

structures. This will lead to an eight-fold degeneracy of the "inversion" levels, $8(C_{3v})$. If we view the molecule as pseudorotating among these eight structures then we must regard the potential surface as O_h, not C_{3v}, which requires a symmetry number of $\sigma = 24$. Alternatively, we can consider the molecule in only one of the C_{3v} potential wells which leads to a vibrational degeneracy of one for the pseudorotation mode and a symmetry number of $\sigma=3$. Thus in transferring from an O_h to C_{3v} viewpoint we loose R ln 8 vibrational entropy and gain R ln 8 rotational entropy, for a net change of zero. If we, in turn, assume XeF_6 to have any of the remaining symmetries (C_{2v}, C_{4v}, C_s) the same conclusion regarding the entropy calculation will be reached. One case which was not included in Table 7 is that of a free pseudorotation. In this case it is clear that the potential must be treated from an O_h point of view since all geometries are equally accessible. The basic result of this discussion is that for any possible conformation of XeF_6 the entropy can always be calculated assuming the most symmetrical structure (O_h).

The assignment of the vibrational modes, except for the T_{1u}(bend), assuming an O_h structure for XeF_6 is found in Table 8. These assignments are based on the room temperature XeF_6 infrared and Raman spectra (Figs. 5,7,8). There is a moderate shifting of the stretching frequencies to lower energy in going from the low temperature to the room temperature spectra (Figs. 5-9). Frequency shifts of this size are commonly observed in going from matrix isolation spectra to gas phase spectra.[69] The range of possible frequencies for the T_{2g} and

T_{2u} modes reflects the large uncertainty of their exact location. The calculated standard entropy of the T_{1u} (bend) motion ($S^{\circ}_{T_{1u}}$) at 335°K is

$$11.24 \leqslant S^{\circ}_{T_{1u}} \leqslant 15.05 \text{ cal/deg} \tag{82a}$$

$$S^{\circ}_{T_{1u}*} = 14.67 \text{ cal/deg} \tag{82b}$$

where the large range of $S^{\circ}_{T_{1u}}$ is a reflection of the large uncertainty of the T_{2g} and T_{2u} assignments. The value $S^{\circ}_{T_{1u}*}$(82b) corresponds to the assignment T_{2g} = 284 cm^{-1} and T_{2u} = 189 cm^{-1} (Table 8).

Now that the experimental entropy associated with the T_{1u} motion is known, we can compare it with calculated entropies based on the T_{1u} potential (30). This comparison should help to narrow the ranges of the potential parameters b, and c established by electron diffraction and spectroscopic considerations. Because the entropy associated with the T_{1u} motion is relatively large (~ 14 cal/deg) we can use a classical approximation to the partition function with which to calculate the entropy. The usual test for the validity of the classical approximation is that the spacings of adjacent energy levels be small compared to kT. Bartell has shown[59] that if one considers XeF_6 to undergo a completely free pseudorotation, the effective pseudorotation "B" value is B = 5 cm^{-1}. For XeF_6 at 335°K (~ 240 cm^{-1}) the classical approximation[67] is reasonable because B(5 cm^{-1}) $\ll$ kT (240 cm^{-1}). In terms of the T_{1u} potential (30) the partition function, $Q_{T_{1u}}$, is

$$Q_{T_{1u}} = \frac{(2\pi m_4 kT)^{3/2}}{h^3} \int_0^{2\pi}\int_0^{\pi}\int_0^{\infty} e^{-(-aR^2+bR^4-cR^4 f(\theta,\phi))/kT} R^2 \sin\theta dR d\theta d\phi \tag{83}$$

where $f(\theta,\phi)$ is an abbreviation for the octahedral field term in the potential (30). The entropy ($S^o_{T_{1u}}$) was calculated by[67]

$$S^o_{T_{1u}} = RT \left(\frac{\partial \ln Q_{T_{1u}}}{\partial T}\right)_{V,N} + R \ln Q_{T_{1u}} \tag{84}$$

where R is the molar gas constant.

The partition function, $Q_{T_{1u}}$ (83), and the related quantity, $(\partial \ln Q_{T_{1u}}/\partial T)_{V,N}$ (84), were evaluated by numerical integration for various values of the potential parameters a, b, and c. In addition, the root mean square displacement, $\langle R^2 \rangle^{1/2}$, was also computed.

$$\langle R^2 \rangle = \frac{\frac{(2\pi m_4 kT)}{h^3} \int_0^{2\pi}\int_0^{\pi}\int_0^{\infty} R^2 e^{-(-aR^2+bR^4-cR^4 f(\theta,\phi))/kT} R^2 \sin\theta dR d\theta d\phi}{Q_{T_{1u}}} \tag{85}$$

The results are tabulated in Table 9. In order to properly evaluate the results in Table 9 let us briefly review what parameters, relevant to the entropy calculation, are known with reasonable accuracy. These are "a" and R_o. The constant "a" is related to the force constant ($K_{C_{3v}}$) for the $A_1(T_{1u}$ bend) vibration by $a = K_{C_{3v}}/4$ (65a). $A_1(T_{1u}$ bend) is the vibrational motion associated with the radial coordinate, R, of the potential function (30). We found in the spectroscopy section that the A_1

(T_{1u} bend) was reasonably assigned to the 302 cm^{-1} peak in the matrix isolation infrared spectrum. This placed "a" at a = .0873 (mdyn/Å). Most likely there will be a shift in frequency for this mode in going from the matrix to the gas phase, however the magnitude and direction of the shift are difficult to predict. With this problem in mind, it is probably reasonable to assume a maximum ± 50 cm^{-1} uncertainty in the location of the A_1 (T_{1u} bend) band, which corresponds to a ± 15% uncertainty in the value of "a". The parameter R_o is the magnitude of the radial distortion, which was calculated from the best static C_{3v} model of the electron diffraction work. The value for R_o(.87 Å) is probably an upper bound to $\langle R^2 \rangle^{1/2}$. This is because the radial potential minimum contracts slightly in going from the C_{3v} radial minimum to the C_{2v} radial minimum, and contracts even more in passing from the C_{2v} radial minimum to the C_{4v} radial minimum (32a, 32b, 32c). In our model calculations, we can safely disregard the potential parameters corresponding to $\langle R^2 \rangle^{1/2}$ greater than .9 Å. The lower bound to $\langle R^2 \rangle^{1/2}$ is more difficult to establish. We will discuss this in more detail somewhat latter in this section in relation to angular barriers.

The potential parameters b, and c for the first eleven entries in Table 9 obey the requirement

$$b = \frac{K_{C_{3v}}}{8R_o^2} + .333c \qquad (86)$$

which was discussed in the spectroscopy section (65). The general effect of increasing b and c according to Eq. (86) is to steepen the potential walls beyond R_o and to increase the angular barriers. This is reflected in the lower entropy and smaller $\langle R^2 \rangle^{1/2}$ for the first eleven entries. In order to sample entropies on the upper end of the experimental range for $S^\circ_{T_{1u}}$ (15.05 cal/deg) we have to considerably soften the potential in the radial (R) direction. This is demonstrated for the remaining entries in Table 9. It is seen that one has to go well beyond the anticipated ± 15% range for "a" just to reach 13 cal/deg. This is an indication that the actual T_{2g} and T_{2u} frequencies occur closer to the lower range indicated in Table 8, which would shorten the experimental $S^\circ_{T_{1u}}$ range to approximately $11.24 \leqslant S^\circ_{T_{1u}} \leqslant 12.5$ (cal/deg).

There is one additional criterion which the potential parameters, particularly c, must follow. This is that the angular potential minimum at the C_{3v} configuration is less than approximately 200 cm^{-1} (room temperature). If the angular barrier was much higher than 200 cm^{-1} XeF_6 should appear as a rigid C_{3v} molecule, which would give relatively sharp spectral features. There are actually three angular barriers, a $C_{3v} \leftrightarrow C_{2v}$ barrier, a $C_{2v} \leftrightarrow C_{4v}$ barrier, and a $C_{3v} \leftrightarrow C_{4v}$ barrier. In order of increasing energy (lowest at bottom) these barriers are

$$\begin{array}{l} \text{——} \quad C_{4v} \\ \text{——} \quad C_{2v} \\ \text{——} \quad C_{3v} \end{array} \qquad (87)$$

The 200 cm^{-1} restriction applies to the $C_{3v} \leftrightarrow C_{2v}$ barrier. In terms of the potential function, the larger the parameter c, the larger the angular barriers will be. For the set of potential parameters (a=.0873, b=.0743, c=.05) (Table 9) the calculated angular barriers are

$$\begin{array}{ll} \underline{360\ cm^{-1}} & C_{4v} \\ \underline{120\ cm^{-1}} & C_{2v} \\ \underline{0\ cm^{-1}} & C_{3v} \end{array} \tag{88}$$

which is consistent with the requirement that $C_3 \leftrightarrow C_{2v} < 200\ cm^{-1}$. If we double the value of c to c=.1 (entry 11, Table 9) the $C_3 \leftrightarrow C_{2v}$ barrier will approximately double to 240 cm^{-1} which is too large. The upper allowed value of c by this reasoning is

$$c = .08\ \left(\frac{mdyn}{Å}\right) \quad .$$

We can estimate the radial barrier, the barrier to the octahedral configuration, from the free pseudorotation potential (a=.0873, b=.0576, c=0) (Table 9). The radial barrier is 1,650 cm^{-1}.

The basic result of this section was to refine the potential parameters to the following ranges

$$a = .0873\ \frac{mdyn}{Å} \pm 15\% \tag{89a}$$

$$.05 \leqslant b \leqslant .075\ \frac{mdyn}{Å^3} \tag{89b}$$

$$0 \leqslant c \leqslant .08\ \frac{mdyn}{Å^3} \tag{89c}$$

5. Electric Field Deflection of XeF_6

The result of the electric field deflection experiment on XeF_6 [70] was negative, that is XeF_6 did not focus. There are two possible interpretations of this behavior. The first, is that the dipole moment in XeF_6 is vanishingly small. The lower limit of detectability in these experiments is .03 D for a static structure. It is unlikely that the sum of the individual Xe-F bond moments and the lone pair moment would have such a low value. The second, and more reasonable proposition, is that the effect of pseudorotation is to drastically reduce the effective interaction of the dipole moment with the inhomogeneous electric field. This is further indication that XeF_6 undergoes a not-too-hindered pseudorotation. The phenomenon of electric field deflection will be discussed fully in the next chapter.

6. Comparison to other Theoretical Approaches

There have been two different theoretical treatments of XeF_6 previously explored, (1) an electronic isomer model,[71] (2) a crystal-field model.[62]

The basic contention of Goodman's[71] electronic isomer model is the existence of several, thermally accessible excited electronic states. These excited states are considered to arise from excitation into the T^*_{1u} molecular orbital. We have discussed the ultraviolet spectrum of XeF_6 in an earlier section and found the lowest lying T_{1u} excited state ($^3P_1$) to be approximately 28,000 cm^{-1} above the ground $^1A_{1g}$ electronic state. This essentially negates the electronic isomers approach, of which we will say no more.

A more first principles type approach was undertaken by Wang[62] in his crystal-field model for XeF_6. He assumed a Xe(+6) ion was surrounded by six point charges, F(-1). The Hamiltonian for this system consisted of the nonrelativistic Hamiltonian for the Xe(+6) ion plus a spin-orbit term, a nuclear repulsion term for the six fluorine ligands, and a crystal-field term expressing the interaction of the valence Xe(+6) electrons with the fluorine ligands as a function of ligand geometry. The ground state vibrational potential was defined by diagonalization of the Hamiltonian in a Russell-Saunders basis on the Xe(+6) ion for different ligand geometries. There are four electronic parameters associated with this model, (1) the energy difference between the xenon 5s and 5p orbitals, (2) the spin-orbit coupling constant for the xenon 5p orbitals (3) two Slater-Condon electron repulsion parameters. Values for these parameters were obtained from entirely empirical considerations.

The basic results of this model, for their assumed best set of parameters, are (1) a radial distortion (R_o) of approximately R_o = .9 Å, (2) a radial barrier of 1860 cm^{-1}, and (3) the following angular barriers

160 cm^{-1}	C_{4v}
40 cm^{-1}	C_{2v}
0 cm^{-1}	C_{3v}

These results compare nicely to this work, which are, (1) a radial distortion of R_o = .87 Å, (2) a radial barrier of approximately 1650 cm^{-1}, and (3) the following angular barriers

360 cm^{-1}	C_{4v}
120 cm^{-1}	C_{2v}
0 cm^{-1}	C_{3v}

where it should be recalled that the exact sizes of the angular barriers were not calculable in this work because the parameter "c" could only be defined within a certain range. The angular barriers quoted above correspond roughly to the midpoint of the allowed range for "c" (.05 mdyn/Å).

Wang's crystal-field model and the approach taken in this work have basically the same origin, although after the first step our approaches taken different routes. In both treatments the first step is to diagonalize a suitable Hamiltonian in an appropriate electronic basis set. Wang carries out the diagonalization numerically by using quantitatively defined electronic wave functions, while we carry out the diagonalization analytically to obtain a general form for the potential, and then use experimental data to refine the parameters of the potential. In principle, both approaches should yield almost identical results if the diagonalization is exact, and the various electronic parameters used in the numerical approach have the correct value for XeF_6.

The excellent agreement between these two approaches is strong evidence for a slightly hindered pseudorotational motion in XeF_6.

Table 1. Structural parameters for the best static C_{3v} configuration

Parameter	Multiplicity	R (Å)	Amplitude (Å)
r_{Xe-F}	3	1.850	0.036
r_{Xe-F}	3	1.941	0.036
adjacent F-F	6	2.498	0.108
adjacent F-F	3	2.535	0.208
adjacent F-F	3	3.106	0.302
long F-F	3	3.757	0.070

In addition

ANG4 = 5.348°

ANG5 = 7.260°

Table 2. Infrared and Raman activities for the fundamentals of a MX_6 molecule of varying geometry

O_h	$A_{1g}(R_p)$	$E_g(R_{dp})$	$T_{2g}(R_{dp})$	$T_{1u}(Ir)$	$T_{2u}(NA)$
C_{3v}	$A_1(Ir,R_p)$	$E(Ir,R_{dp})$	$A_2(NA)$		
C_{4v}	$A_1(Ir,R_p)$	$B_1(R_{dp})$	$B_2(R_{dp})$	$E(Ir,R_{dp})$	
C_{2v}	$A_1(Ir,R_p)$	$A_2(R_{dp})$	$B_1(Ir,R_{dp})$	$B_2(Ir,R_{dp})$	
C_s	$A'(Ir,R_p)$	$A''(Ir,R_{dp})$			

Ir = infrared active

R = Raman active

p = polarized

dp = depolarized

NA = not active

Table 3. T_1u(Bend), T_{2g} and T_{2u} Bending Frequencies for TeF_6.

	T_1u(Bend) (cm^{-1})	T_{2g} (cm^{-1})	T_{2u} (cm^{-1})
TeF_6	323	314	197
PuF_6	206	211	173

Table 4. Assignment of low temperature XeF_6 spectrum based on a C_{3v} geometry

Mode	Frequency (cm^{-1})
$A_1(T_{1u}$ stretch)	630
$A_1(A_{1g})$	624
E (T_{1u} stretch)	557
$E(E_g)$	506
$A_1(T_{1u}$ bend)	302
$E(T_{2g})$	(343)[a]
$A_1(T_{2g})$	252
$A_2(T_{2u})$	(150-200)[b]
$E(T_{2u})$	(150-200)[b]

a. This is a guess (see main text).

b. Based on room temperature far infrared data (Fig. 7).

Table 5. Derived parameters for XeF_6

Parameter	Description	Value
m_3	T_{1u}(stretch) mass	19 (amu)
m_5	T_{2g} mass	4.75 (amu)
m_4	T_{1u}(bend) pseudorotation mass	6.56 (amu)
$K_{C_{3v}}$	Force constant for radial (A_1) motion in C_{3v}	0.349 (mdyn/A°)
k_4	Force constant for "unperturbed" T_{1u} frequency	0.314 (mdyn/A°)
$v^o_{T_{1u}}$(bend)	"Unperturbed" T_{1u} bend frequency	284 (cm^{-1})
$v^o_{T_{1u}}$(stretch)	Unperturbed T_{1u} stretch frequency	581 (cm^{-1})
k_3	T_{1u} stretch force constant	3.78 (mdyn/A°)
$v^o_{T_{2g}}$	Unperturbed T_{2g} frequency	312 (cm^{-1})
k_5	T_{2g} force constant	0.272 (mdyn/A°)
$\Delta\varepsilon_o$	$^1A_{1g} \rightarrow {}^1T_{1u}$ electronic transition energy	0.87 (mdyn/A°)
c_3	T_{1u} stretch linear matrix element	0.461 (mdyn)
c_4	T_{1u} bend linear matrix element	0.500 (mdyn)
c_5	T_{2g} linear matrix element	0.374 (mdyn)
$C_{T_{1u}}$	T_{1u}-T_{1u} coupling constant, spectroscopic determination	0.14
$C_{T_{2g}}$	T_{1u}-T_{2g} coupling constant, spectroscopic determination	0.91 (1/A°)
$C_{T_{1u}}$	Electron diffraction determination	0.13
$C_{T_{2g}}$	Electron diffraction determination	1.9 (1/A°)

Table 6. Molecular parameters for a tetrameric $XeF_6(C_{4v})$ molecule.

Parameter	Value
$r_{Xe-F_{apical}}$	2.23A°
$r_{Xe-F_{apical}}$	1.84A°
$r_{Xe-F_{basal}}$	1.86A°
$\measuredangle F_{apical}-Xe-F_{basal}$	77.2°

Table 7. Thermodynamic parameters for various XeF_6 geometries.

	O_h	C_{3v}	C_{2v}	C_{4v}	C_s
σ(symmetry number)	24	3	2	4	1
Equivalent Structures	1	8	12	6	24
Degeneracy of Inversion Mode	$8(C_{3v})$, $12(C_{2v})$ $6(C_{4v})$, $24(C_s)$	1	1	1	1

Table 8. Room temperature assignment of XeF_6 modes assuming an octahedral geometry

Mode	Frequency (cm^{-1})
T_{1u} (stretch)	580
A_{1g}	588
E_g	513
T_{2g}	284[a] (200-300)[b]
T_{2u}	189[a] (150-200)[b]

a. estimate based on TeF_6 and PuF_6

b. Possible range of values

Table 9. Calculated entropy of the T_{1u} potential function ($V_{T_{1u}}(R,\theta,\phi)$) at 335°K.

$a(\frac{mdyn}{A°})$	$b(\frac{mdyn}{A°^3})$	$c(\frac{mdyn}{A°^3})$	$S^o_{T_{1u}}(\frac{cal}{deg})$	$\langle R^2\rangle^{1/2}$ (A°)
0.0873	0.0576	0.00	11.82	0.878
0.0873	0.0610	0.01	11.77	0.869
0.0873	0.0643	0.02	11.70	0.862
0.0873	0.0676	0.03	11.62	0.856
0.0873	0.0710	0.04	11.54	0.850
0.0873	0.0743	0.05	11.46	0.846
0.0873	0.0776	0.06	11.38	0.841
0.0873	0.0810	0.07	11.30	0.838
0.0873	0.0843	0.08	11.24	0.834
0.0873	0.0876	0.09	11.14	0.832
0.0873	0.0910	0.10	11.07	0.829
0.088	0.0306	0.00	13.1	1.205
0.088	0.0306	0.015	12.97	1.286
0.088	0.0306	0.03	12.14	1.424
0.081	0.03	0.00	13.06	1.168
0.0432	0.02	0.00	13.21	1.054
0.027	0.01	0.00	14.1	1.184
0.108	0.04	0.00	12.78	1.167

VII. ELECTRIC FIELD DEFLECTION OF MOLECULES WITH LARGE AMPLITUDE MOTIONS

A. Introduction to Electric Field Deflection

In this chapter we will consider the behavior of molecules in inhomogeneous electric fields. As an introduction to this area we will discuss the behavior of a permanent dipole in an inhomogenous electric field. A schematic diagram of a typical experimental arrangement[72] is found in Fig. 1, where a molecule with dipole moment $\vec{\mu}$ is ejected from the source (oven) into the inhomogeneous electric field $\vec{E}$. The electric field $\vec{E}$ is assumed to have radial symmetry about the axis drawn (dashed line).. We chose the dipole moment aligned parallel to the electric field, and we also assume that the molecule is not rotating. The potential of interaction of the dipole with the field is

$$W = -\vec{\mu} \cdot \vec{E} \tag{1}$$

Because the electric field is inhomogeneous (its gradient is non zero) the molecule will experience a force, $\vec{F}$, given by

$$\vec{F} = -\frac{\partial W}{\partial |\vec{E}|} \nabla |\vec{E}| \tag{2}$$

For the alignment of the dipole pictured, the molecule will experience a force directed into the center of the apparatus. Initially the molecule will be accelerated downwards, then when it reaches its

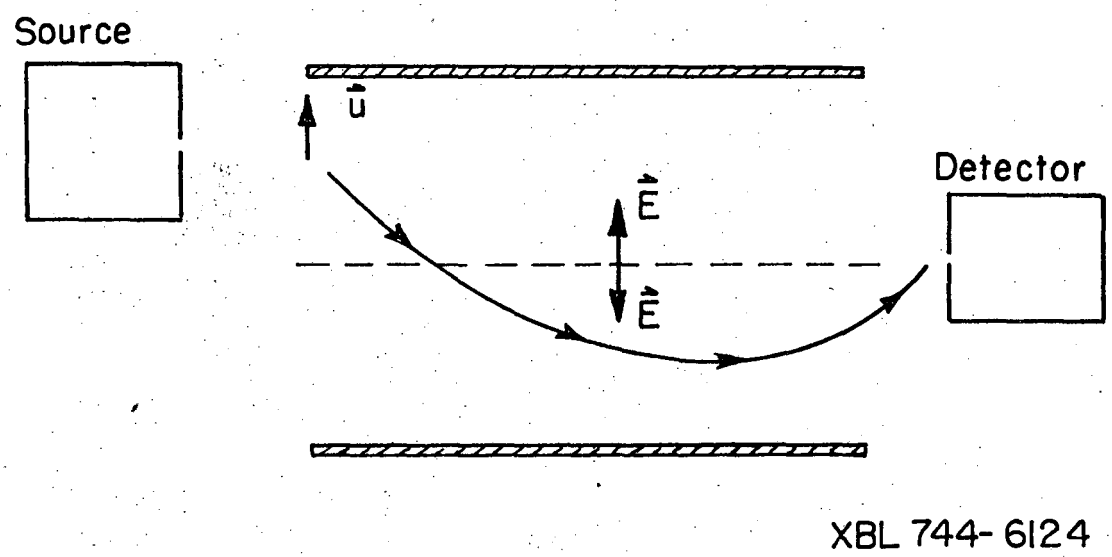

Fig. 1. Schematic diagram of apparatus used in electric field focusing experiments.

mirror image position on the bottom half it will be accelerated upward until it reaches its initial position, whereupon the cycle will repeat itself. Concurrently the molecule is translating across the apparatus towards the detector (mass spectrometer). If the oscillation about the symmetry axis of the field occurs at just the right frequency the molecule can actually enter the detector as is pictured in Fig. 1. This is called refocusing, or sometimes just focusing. If we pick the alignment of the dipole opposite to that pictured it would always experience a force directed away from the center of the apparatus, and obviously it could not focus. It should be stressed that simply aligning the dipole parallel to the electric field, $\vec{E}$, will not insure focusing. The velocity of the molecule has to be related to the frequency of oscillation such that the molecule is crossing the center of the apparatus at the precise instant it reaches the detector. In principle there are an infinite number of velocities for which a given dipole can focus. The exact value of these velocities is of course dependent on the electric field strength $|\vec{E}|$, and the magnitude of the dipole moment, $|\vec{\mu}|$.

We can now allow the molecule to rotate and see what effect this will have on its focusing properties, The basic complication introduced by allowing the molecule to rotate is that its interaction with the field (1) must be averaged over the rotational state of the molecule.

$$W_1 = - |\vec{\mu}| \; |\vec{E}| \; C(n_R) \tag{3}$$

The quantity $C(n_R)$ represents a particular function of the rotational quantum numbers, n_R, of the rotational state over which Eq. (1) was averaged. The specific form of $C(n_R)$ will depend on the symmetry of the molecule - symmetric top, spherical top, etc. The subscript of one on $W_1(3)$ is to indicate that this is known as a first order Stark effect. The force the rotating dipole will experience is

$$\vec{F} = C(n_R)\ |\vec{\mu}|\ \nabla|\vec{E}| \tag{4}$$

The electric field can be represented as[70]

$$\vec{E} = \left(\frac{V}{R^2}\right) r\ \hat{r} \tag{5}$$

where V is the voltage applied to the apparatus, R is the radius of the apparatus, r is the radial coordinate, and $\hat{r}$ is the unit radial vector. Substitution of $\vec{E}(5)$ into Eq. (4) gives

$$\vec{F} = C(n_R)\ |\vec{\mu}|\ \left(\frac{V}{R^2}\right) \hat{r} \tag{6}$$

When $C(n_R)$ is negative the molecule will experience a force directed into the center of the apparatus, hence it can focus. For $C(n_R)$ positive the molecule will not focus. From Eq. (6) we see that for a first order Stark effect, $W_1(3)$, it is the rotational state, $C(n_R)$, which completely determines a molecule's potential for focusing.

We can add yet another complication to this system by allowing the molecule to have a nonstatic dipole moment. Specifically, we mean a molecule undergoing relatively unhindered, large amplitude

motions carrying it through a variety of geometries, and simultaneously changing the orientation of the dipole moment relative to a molecule fixed reference frame. We must now average the interaction of the dipole with the field (1) over both the rotational motion and the internal motion. The effect of this averaging process will be to yield a second order stark effect, W_2, instead of a first order effect, W_1. As we will see later, this is due to the symmetry of the internal motion. The second order stark effect will have the form

$$W_2 = \frac{|C(n_R,n_I)|\ |\vec{\mu}_{eff}|^2\ |\vec{E}|^2}{\Delta E_I} \tag{7}$$

where $\vec{\mu}_{eff}$ is the effective dipole moment associated with the internal motion, $C(n_R,n_I)$ is a function of the rotational, n_R, and internal, n_I, quantum numbers, and ΔE_I is an energy difference between the energy levels of the internal motion. The force that the molecule will experience is

$$\vec{F} = -\frac{|C(n_R,n_I)|\ |\vec{\mu}_{eff}|^2\ \left(\frac{V}{R^2}\right)^2 r\,\hat{r}}{\Delta E_I} \tag{8}$$

From the force Eq. (8) we find that for $\Delta E_I > 0$ the molecule can focus, while molecules with $\Delta E_I < 0$ cannot focus. The most interesting feature of the second order Stark effect (7) is that a molecule's potential for focusing is determined solely by its internal quantum state, in contrast to the first order Stark effect (3) where the rotational state was the deciding factor. Equation (8) can be viewed compactly as

$$\vec{F} = -K\,r\hat{r} \tag{9}$$

where K is defined as

$$K = \frac{|C(n_R,n_I)|\ |\vec{\mu}_{eff}|^2\ (\frac{V}{R^2})^2}{\Delta E_I} \tag{10}$$

The form of Eq. (9) shows that a molecule with a second order Stark effect (7) behaves as a harmonic oscillator[73] with force constant K (10).

For a typical electric field deflection apparatus[70] the radius, R, is R = .3 cm, the average field, $|\vec{E}_{ave}|$, at maximum voltage (35 KV) is $|\vec{E}_{av}| = 180\ (\frac{\text{statvolts}}{\text{cm}})$, and the length of the apparatus (source to detector) is approximately 20 cm. If we inject a molecule with $|\vec{\mu}_{eff}| = 1D$, $\Delta E_I = 1\ \text{cm}^{-1}$, and mass equal to 20 amu (this hypothetical molecule is similar to NH_3) into the apparatus at T = 300°K, with $|\vec{E}| = |\vec{E}_{av}|$ then we can estimate its period of oscillation and its time of flight. The most probable velocity of the molecule is calculated by

$$\frac{1}{2}mv^2 = kT \tag{11}$$

For T = 300°K the most probable velocity is $v = 10^4$ cm/sec, which gives an average time of flight from source to detector of 10^{-3} sec. The approximate period of oscillation, which is determined by the force constant, K(10), is 10^{-3} (sec/cycle). This molecule is seen to be a strong focuser because its period of oscillation is comparable to the average time of flight. If on the other hand, (μ_{eff}) is much

smaller, or ΔE_1 much larger, or both, then the period of oscillation would be greatly reduced and only those molecules with a velocity substantially less than v(11) could focus (a very few molecules). Generally speaking it is the ratio of $|\mu_{eff}|^2$ to ΔE_I which will determine whether or not a given molecule, in a given state, is a strong or weak focuser.

B. Stark Effect for MX_3 Molecules Undergoing a Double Minimum Vibration

The wavefunction for the inversion notion in MX_3 molecules is characterized by two quantum numbers,[74]

$$\Psi_{inversion} = |n,p\rangle \qquad \begin{array}{l} n = 0,1,2 \ldots \\ p = \pm 1 \end{array} \tag{12}$$

where "n" denotes the level and "p" its parity (±). The dipole moment associated with the inversion coordinate, $S_2(A_2'')$ (see Chap. 1, Fig. 2), can be expressed as

$$\vec{\mu} = cS_2\hat{K} \tag{13}$$

where c is a constant which takes geometric (bond length, bond angles) and electronic (partial charge) factors into account and $\hat{K}$ is the molecule fixed axis defined by the three fold rotation axis through the central (M) atom. The dipole-field interaction (1) becomes

$$W = -cS_2 |\vec{E}| \cos\beta \tag{14}$$

where β is the angle between the molecule fixed $\hat{K}$ axis and the space fixed unit radial vector, $\hat{r}$, which for simplicity we will consider as the $\hat{Z}$ axis, because the experiment essentially takes place in a single plane. The presence of the linear coordinate, S_2, in the interaction term (14) precludes any first order Stark effect due to the parity ($\pm$) of the inversion wavefunctions (12). This requires the use of second order perturbation theory to evaluate W(14). The rotational wavefunctions which we will use throughout this chapter are the symmetric top wavefunctions.[74] These are characterized by

$$\Psi_{rotation} = |JKM\rangle \tag{15}$$

where J is the total angular momentum quantum number, K is the component of J along the molecular symmetry axis, and M is the component of J along a space fixed axis, in this case the field direction, $\vec{E}(\hat{Z})$.

To second order, the interaction term W(14) is

$$W_2 = |\vec{E}|^2 \sum_{|JKMnp\rangle \neq |J'K'M'n'p'\rangle} \frac{\langle JKMnp|cS_2 \cos\beta|J'K'M'n'p'\rangle\langle J'K'M'n'p'|cS_2 \cos\beta|JKMnp\rangle}{(E_{JKM} - E_{J'K'M'}) + (E_{np} - E_{n'p'})} \tag{16}$$

where E_{JKM} is the energy of the $|JKM\rangle$ rotational state and E_{np} is the vibrational energy of the $|np\rangle$ inversion state. The relevant matrix elements are

$$\langle np|S_2|n'p'\rangle \neq 0 \quad p'\neq p \tag{17a}$$

$$\langle JKM|\cos\beta|J'K'M'\rangle \neq 0 \quad J'=J,\ J\pm1 \quad K'=K \quad M'=M \tag{17b}$$

If we restrict our attention to the focusing properties of the ground state inversion levels in $MX_3(C_{3v})$ molecules then we can effectively ignore the contribution of higher vibrational levels ($n\gtrsim1$) in the denominator of the Stark expression (16). This is because the n=1 inversion levels occur in the range of 800-1000 cm^{-1} above the n=0 levels for the NH_3 series, while the ground state doublet splitting has a maximum value of only .66 cm^{-1} in NH_3. If we were dealing with a low inversion barrier it is possible that higher vibrational levels would contribute to $W_2(16)$ and accordingly, must be included. $W_2(16)$ simplifies to

$$W_2 = |\vec{E}|^2 c^2 |\langle 0-|S_2|0+\rangle|^2 \sum_{J'} \frac{\langle JKM|\cos\beta|J'KM\rangle\langle J'KM|\cos\beta|JKM\rangle}{(E_J - E_{J'}) + (E_{o-} - E_{o+})} \tag{18}$$

where we have picked $|0-\rangle$ as the reference vibrational state. Choosing $|0+\rangle$ as the reference state would just change the sign of the vibrational energy difference in the denominator (18). We can identify the term, $c^2|\langle 0-|\ S_2\ |0+\rangle|^2$, as the effective dipole moment squared, μ^2_{eff}. Equation (18) becomes

$$W_2 = \mu^2_{eff}\ |\vec{E}|^2 \sum_{J'} \frac{\langle JKM|\cos\beta|J'KM\rangle\ \langle J'KM|\cos\beta|JKM\rangle}{(E_J - E_{J'}) + (E_{o^-} - E_{o^+})} \tag{19}$$

There are two different limiting situations to this expression for the Stark effect, W_2(19). These are

$$E_{o^-} - E_{o^+} \gg E_J - E_{J'} \tag{20a}$$

$$E_J - E_{J'} \gg E_{o^-} - E_{o^+} \tag{20b}$$

In the MH_3 series (NH_3, PH_3, AsH_3, SbH_3) the rotational constant, B, is on the order of $B \approx 10\ cm^{-1}$, and the ground state inversion splitting ($E_{o^-} - E_{o^+}$) has a maximum value of $.7\ cm^{-1}$ for NH_3. Thus for the MH_3 molecules the second limiting case (20b) is seen to apply. We will see later that for the MX_7 molecules and XeF_6 the first limit (20a) applies because the rotational constants are much smaller due to larger moments of inertia, and the pseudorotational spacings are larger than the ground state MH_3 inversion doublets. We will consider both limits for the MX_3 system.

If we assume the first limit (20a) to apply then Eq. (19) simplifies approximately to

$$W_2 = \frac{\mu_{eff}^2 \, |\vec{E}|^2}{E_{o^-} - E_{o^+}} \sum_{J'} \langle JKM|\cos\beta|J'KM\rangle\langle J'KM|\cos\beta|JKM\rangle \tag{21}$$

If we sum over a complete $|J'K'M\rangle$ basis, and use the identity

$$\sum_{\substack{\text{sum over}\\ \text{all states}}} |J'K'M'\rangle\langle J'K'M'| = 1 \tag{22}$$

then Eq. (22) becomes

$$W_2 = \frac{\mu_{eff}^2 \, |\vec{E}|^2 \, \langle JKM|\cos^2\beta|JKM\rangle}{E_{o^-} - E_{o^+}} \tag{23}$$

The error in W_2(23) caused by neglecting the $E_J - E_{J'}$ term is approximately

$$\delta W_2 = \frac{\mu_{eff}^2 \, |\vec{E}|^2}{E_{o^-} - E_{o^+}} \cdot \frac{2JB}{E_{o^-} - E_{o^+}} \left(|\langle JKM|\cos\beta|J+1, KM\rangle|^2 - |\langle JKM|\cos\beta|J-1, KM\rangle|^2\right) \tag{24}$$

where δW_2 must be small compared to W_2(23) because our initial assumption was essentially $2JB \ll E_{o^-} - E_{o^+}$ (20a).

If the second limiting situation (20b) is applicable, the Stark effect, W_2 (19), becomes

$$W_2 = \frac{\mu_{eff}^2 \, |\vec{E}|^2 \, |\langle JKM \,|\cos\beta|\, JKM \rangle|^2}{E_{o-} - E_{o+}} = \frac{\mu_{eff}^2 \, |\vec{E}|^2 \, M^2 \, J^2}{J^2(J+1)^2 \, (E_{o-} - E_{o+})} \tag{25}$$

where the J=J' rotational state is the major contribution to W_2(19) in this limit. The error in W_2(25) from neglecting $J'=J\pm1$ is

$$\delta W_2 = \frac{\mu_{eff}^2 \, |\vec{E}|^2}{2JB} \left(|\langle JKM|\cos\beta|J-1,KM \rangle|^2 - |\langle JKM|\cos\beta|J+1, KM \rangle|^2 \right) \tag{26}$$

where δW_2 should be much smaller than W_2(25) because our initial assumption was $2JB \gg E_{o-} - E_{o+}$ (20b).

Both limiting Stark effects, W_2(23,25), have been written in terms of the inversion state which can focus, $|0-\rangle$. If the molecule were in the lower ground state inversion doublet, $|0+\rangle$, the denominator of W_2(23,25) would be negative, thus this state cannot focus (8).

C. Stark Effect in MX_7 (IF_7, ReF_7) Molecules

In the MX_7 chapter we found the IF_7 and ReF_7 could be considered as undergoing a free pseudorotation, which was analogous to a rotating-vibrating diatomic molecule restricted to rotate in a plane. The wave functions for this type of motion are[29]

$$\Psi_{\text{pseudorotation}} = R_n(\rho)\, e^{i2m\phi} = |n,m\rangle$$
$$n = 0, 1, 2, \ldots \qquad (27)$$
$$m = 0, \pm 1, \pm 2, \ldots$$

where the factor of two on the angular function arises from the boundary condition, $\psi(0) = \psi(\pi)$, in five membered rings.[36] The energy of the pseudorotational mode is

$$E_{nm} = (n + \tfrac{1}{2})\, h\nu_\rho + m^2 B_\phi \qquad (28)$$

where ν_ρ is the frequency of the radial motion (ρ) and B_ϕ is the effective rotational constant associated with the pseudorotation.

In the MX_7 molecules the dipole moment lies in the plane of the hypothetical five membered ring formed by a planar arrangement of the equatorial fluorines. The origin of the dipole moment is the coupling of the axial bend (E_1') to the puckering motion (E_2'')[48] (MX_7 chapter, Eqs. (12,13)). The dipole moment will have the form

$$\vec{\mu} = c\rho^2[\cos 4\phi\hat{i} + \sin 4\phi\hat{j}\,] \qquad (29)$$

where the ρ^2 dependence and the 4ϕ dependence of the dipole on the pseudorotational phase angle are both determined by the $E_1' - E_2''$ coupling,[48] and $\hat{i}$, $\hat{j}$ are molecule fixed axes in the equatorial plane. The dipole-field interaction will look like

$$W = c|\vec{E}|\rho^2 \, [\cos 4\phi \, \sin\beta \, \cos\gamma - \sin 4\phi \, \sin\beta \, \sin\gamma] \tag{30}$$

where β, and γ are Euler angles,[75] relating the molecule fixed axes to the space fixed $\hat{Z}$ axis ($\vec{E}$).

Because of the 4ϕ dependence of W(30) there will be both a first and a second order Stark effect. The origin of the first order effect is that the terms, $\cos 4\phi$ and $\sin 4\phi$, connect the degenerate wavefunctions $e^{\pm i2\phi}$ to each other. The remaining states ($m \neq \pm 2$) can be treated by second order perturbation theory.

The rotational constants for IF_7 and ReF_7 are in the neighborhood of $B \approx .6 \text{ cm}^{-1}$,[52] while the effective pseudorotational constant, B_ϕ, is approximately $B_\phi \approx 5 \text{ cm}^{-1}$ in both molecules.[48,49] This indicates that IF_7 and ReF_7 can be treated under the limiting situation in Eq. (20a), because $B_\phi \gg B$. The second order Stark effect will have the form

$$W_2 = \frac{\mu_{eff}^2 \, |\vec{E}|^2 \, \langle JKM| \, \sin^2\beta |JKM\rangle}{B_\phi \, (8m^2-2)} \qquad m \neq \pm 2 \tag{31}$$

This demonstrates that the pseudorotational ground state, m=0, will not focus (W_2 is negative) while all the remaining states are focusable (W_2 is positive).

The derivation of the first order Stark effect for the degenerate $m = \pm 2$ states is rather complicated because the angular terms ($\sin\beta$, $\cos\gamma$, $\sin\gamma$, $\cos\gamma$) connect many of the (near) degenerate M,K levels for a given value of J. While we will not solve this problem

here we can comment on the nature of the expected Stark effect. That is, we saw earlier (3), that for a first order Stark effect some states will focus and some will not, depending on the specific set of rotational quantum numbers.

D. Stark Effect in XeF_6 (Free Pseudorotation Limit)

If we consider XeF_6 to undergo a free pseudorotation then its behavior will be analogous to a rotating-vibrating diatomic molecule. The wavefunctions for the free pseudorotation are[74]

$$\Psi_{\text{pseudorotation}} = R_n(R)P_\ell^{|m|}(\cos\theta)e^{im\phi} = |n\ell m\rangle$$

$$m = 0, \pm 1, \pm 2 \ldots$$

$$\ell = |m|, |m| + 1 \ldots$$

$$n = 0, 1, 2 \ldots$$

The energy levels are

$$E_{n\ell} = (n + \tfrac{1}{2})h\nu_R + B_{\theta,\phi}\,\ell(\ell+1) \tag{33}$$

where ν_R is the frequency of the radial motion, R, and $B_{\theta,\phi}$ is the effective pseudorotational constant.

In terms of the spherical coordinate system defined in the XeF_6 chapter we can write the dipole moment as

$$\vec{\mu} = cR(\sin\theta\cos\phi\hat{i} + \sin\theta\sin\phi\hat{j} + \cos\theta\hat{k}) \tag{34}$$

where $\hat{i}, \hat{j}, \hat{k}$ are molecule fixed axes, which correspond to the S_{4x}, S_{4y} and S_{4z} directions respectively (XeF_6 Chap., Fig. 1). The dipole-field interaction has the form

$$W = c|\vec{E}|R\ (\sin\theta\ \cos\phi\ \sin\beta\ \cos\gamma - \sin\theta\ \sin\phi\ \sin\beta - \cos\theta\ \cos\beta) \tag{35}$$

where β, γ are Euler angles.[75] For XeF_6, $B_{\theta\phi} \approx 5\ cm^{-1}$ [59] and the rotational constant is similar to the MX_7 case, which means XeF_6 can also be handled in the limit $B_\phi \gg B$ (20a). The second order Stark effect for XeF_6 is

$$W_2 = \frac{\mu^2_{eff}\ |\vec{E}|^2}{4B_{\theta,\phi}} \sum_{\ell'=\ell\pm1} (\langle JKM|\sin^2\beta|JKM\rangle \{|\langle \ell^m|\sin\theta|\ell^{m+1}\rangle|^2 + |\langle \ell^m|\sin\theta|\ell^{m-1}\rangle|^2\}$$

$$+ \langle JKM|\cos^2\beta|JKM\rangle \{|\langle \ell^m|\cos\theta|\underline{\ell}^m\rangle|^2\})/(\ell(\ell+1) - \ell'(\ell'+1)) \tag{36}$$

where this expression for W_2(36) is considerably more complicated than those for MX_7(31) and MX_3(23). The reason for this is that the dipole moment is not restricted to any particular direction or plane with respect to the molecule fixed frame, which is why both a $\sin^2\beta$, and a $\cos^2\beta$ term are present in Eq. (36). The ground pseudorotational state, ℓ=0, does not focus (W_2 is negative). The disposition of the higher states is difficult to ascertain from Eq. (36) without explicitly evaluating it for each specific set of $|JKM\ell m\rangle$ quantum numbers,

however it is probably safe to say that some, if not all, of the higher states ($\ell>0$) are focusable.

E. Stark Effect in XeF_6 (Low Angular Barrier Limit)

In the XeF_6 chapter it was concluded that XeF_6 was undergoing either a free pseudorotation or a slightly hindered pseudorotation (low angular barrier). We have just considered the focusing properties of a free pseudorotation, and will now investigate the effect of adding a small angular barrier corresponding to a C_{3v} potential minimum. There is another limiting case one could study, which is the high angular barrier limit. This would yield a rigid C_{3v} structure with a first order Stark effect, where one would expect to observe appreciable focusing.[70]

We will assume the angular barrier is small enough so that the "inversion" multiplet spacings are still large compared to the overall rotational spacings. In effect, we are working with the limiting case in Eq. (20a). The first step in this problem is to calculate the spacings of the lower "inversion" multiplets. This was done by taking appropriate linear combinations (representations of O_h) of ground state harmonic oscillator functions (ψ_n, n=1-8) located in each of the eight C_{3v} potential minima and evaluating the Hamiltonian (H) corresponding to a slighty hindered pseudorotation in this basis set. The resulting spacings are

$$
\begin{array}{ll}
|A_{2u}\rangle & \\
 & 16b - 32c + 16d \\
|T_{2g}\rangle & \\
 & 16b - 16d \\
|T_{1u}\rangle & \\
 & 16b + 32c + 16d \\
|A_{1g}\rangle &
\end{array}
\qquad (37)
$$

$$b = \langle \psi_n | H | \psi_{adjacent} \rangle \qquad (38a)$$

$$c = \langle \psi_n | H | \psi_{adjacent} \rangle \qquad (38b)$$

$$d = \langle \psi_n | H | \psi_{opposite} \rangle \qquad (38c)$$

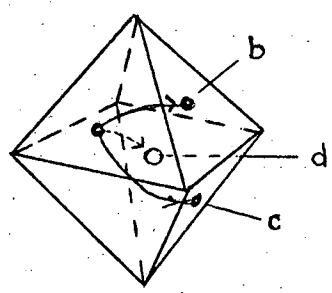

The largest matrix element should be "b" (38a) since this is the overlap of localized oscillators in adjacent C_{3v} minima of the nearest type (see drawing above). Then, for simplicity, the spacings of the levels (37) are approximately equal, $\Delta E \approx 16b$.

The expression for the Stark effect differs from state to state in this limit. The resulting expressions are

$$W_{2,|A_{1g}\rangle} = \frac{3\,\mu_{eff}^2\,|\vec{E}|^2\,|\langle A_{1g}|\,X\,|T_{1ux}\rangle|^2}{-16|b|} \qquad (39a)$$

$$W_{2,|T_{1u_x}\rangle} = \frac{\mu_{eff}^2\,|\vec{E}|^2}{16|b|}\,\{\langle JKM|\sin^2\beta\,\cos^2\gamma|JKM\rangle\,|\langle T_{1u_x}|\,X\,|A_{1g}\rangle|^2 \qquad (39b)$$

$$- (\langle JKM|\,\sin^2\beta\,\sin^2\gamma|JKM\rangle + \langle JKM|\cos^2\beta|JKM\rangle)\,|\langle T_{1u_x}|Y|T_{2g_{xy}}\rangle|^2\,\}$$

similar expressions for $|T_{1u_y}\rangle$, $|T_{1u_z}\rangle$

$$W_{2;|T_{2g_{xy}}\rangle} = \frac{\mu^2_{eff}\,|\vec{E}|^2}{16|b|}\,\langle JKM|\sin^2\beta|JKM\rangle\,|\langle T_{2g_{xy}}|\,X\,|T_{1_{uy}}\rangle|^2 \tag{39c}$$

similar expressions for $|T_{2g_{xz}}\rangle$, $|T_{2g_{yz}}\rangle$

$$W_{2,|A_{2u}\rangle} = 0 \tag{39d}$$

From these results we see that the vibrational ground state, $|A_{1g}\rangle$, does not focus, and the $|A_{2u}\rangle$ state does not focus, while the $|T_{2g}\rangle$ states can focus. It is not obvious what the focusing properties of the $|T_{1u}\rangle$ states are. One might speculate that some $|JKM\rangle$ states will lead to focusing of the $|T_{1u}\rangle$ states will other $|JKM\rangle$ states will exhibit defocusing.

F. Comparison of Theory to Experiment

Calculation of absolute focusing intensities is a complicated problem which interrelates the molecular velocity distribution to the distribution of internal and rotational states.[70] While we will not attempt to do this here it is still possible to get a good idea of the relative focusing power of a given molecular species simply by evaluating its Stark effect (W_2). A large Stark effect means the effective force constant, K (10), for the oscillatory motion is large.

We saw earlier that for K sufficiently large, molecules with a velocity near v(most probable), which includes must of the molecules, had a good chance of focusing. When K was small, only those molecules on the low end of the velocity distribution, which includes very few molecules, were focusable. Simply by comparing "K" for different molecules one can arrange those molecules in order of focusing ability. This can be further simplified to a comparison of the factor in K(10) which varies most from molecule to molecule, which is

$$R = \frac{\mu_{eff}^2}{\Delta E_I} \tag{40}$$

where R is the ratio of the effective dipole moment squared to the separation of internal (pseudorotational) levels. For the molecules studied here the "R" factors are

$$R_{MX_3} = \frac{\mu_{eff}^2}{E_{o^-} - E_{o^+}} \tag{41a}$$

$$R_{MX_7} = \frac{\mu_{eff}^2}{8B_\phi} \tag{41b}$$

$$R_{XeF_6} \text{ (free pseudorotation)} = \frac{\mu_{eff}^2}{8B_{\theta,\phi}} \tag{41c}$$

$$R_{XeF_6} \text{ (low angular barrier)} = \frac{\mu_{eff}^2}{16|b|} \tag{41d}$$

In order to quantitatively evaluate R one needs values for μ_{eff} and ΔE_I. The effective pseudorotational constants for IF_7, ReF_7, and XeF_6 have been estimated by Bartell in the electron diffraction studies of these molecules.[48,49,59] The value of the doublet splitting in the NH_3 ground vibrational state is known. We have performed energy level calculations in a three dimensional harmonic oscillator basis for the low angular barrier limit of XeF_6 and have found the separation of the lower multiplet levels to be approximately $|16b| \approx 1\ cm^{-1}$. Determination of μ_{eff} for IF_7, ReF_7 and XeF_6 is somewhat of a problem. The approach taken here was to estimate the partial negative charge on the fluorines, which in turn fixes the partial positive charge on the central atom. Then one can use structural information provided by the electron diffraction studies to determine the effective dipole in the system of interest. In XeF_6 there was an additional problem, in that the lone pair contributes a significant moment due to its directional preference (partial "p" character). Interestingly, the lone pair moment is in the opposite direction to the "geometric" moment caused by the partial charges. We have calculated the total XeF_6 dipole moment to be $\mu_{eff} \approx .1$ D, where the uncertainty of the calculation leads to a probable range of $0 \leqslant \mu_{eff} \leqslant .3$ D.

The values of the effective dipole (μ_{eff}), ΔE_I, and R for the molecules considered here are found in Table 1. The results demonstrate that the order of focusing ability, from highest to lowest, is $NH_3 \gg ReF_7 > IF_7 > XeF_6$. This same ordering is experimentally observed.[55,70]

There is one additional experimental observation which can be understood in terms of the models presented here. For ReF_7 and to a lesser degree, IF_7, a very strong temperature dependence was found, with the focusing intensity increasing dramatically as the temperature was decreased.[55] We saw that all the pseudorotational states of IF_7 and ReF_7, with the exception of the ground state, were potentially focusable. In addition there was a $1/m^2$ (31) dependence to the Stark effect, where m was the pseudorotational quantum number. As the temperature is increased, higher m levels will gain appreciable population, and because $1/m^2$ is a rapidly decreasing function of m, the higher m states will show a rapidly decreasing focusing ability. The reverse process, of course, will lead to repopulation of the lower m levels where the focusing is strongest.

Although XeF_6 did not focus in the region around room temperature, it might show focusing at lower temperatures because its R value in the low angular barrier regime is similar to that of IF_7, which shows focusing at ~ 150°K. The main problem in the low temperature focusing experiments is to get a significant number of molecules in the gas phase (XeF_6 boils at 347°K).

Falconer and co-workers[70] have derived an expression for the Stark effect in XeF_6 through an analogy to the one dimensional inversion of $MX_3(C_{3v})$ molecules. They reasoned that although the "inversion" motion in XeF_6 is described by a triply degenerate coordinate system one could view the inversion along one of the degenerate coordinates and then the problem becomes formally analogous to the inversion of

$MX_3(C_{3v})$ molecules. Their derived Stark coefficient (what we have called the "R" factor here) is

$$R = \frac{\mu^2}{\Delta} \tag{42}$$

where μ is the effective dipole moment and Δ is the separation of inversion levels. This expression is formally identical to the ones we derived for XeF_6 (41c,41d), however the meaning of Δ (42) is quite different from our parameters, $B_{\theta,\phi}$ (41c) and "b" (41d). By restricting XeF_6 to invert in only one dimension it must tunnel through the central barrier in order to reach an equivalent configuration. Therefore Δ must be the usual doublet separation between inversion levels. For a particle with a relatively large mass tunnelling through even a moderate barrier the doublet separation in the lower levels will be negligible. This will lead to a very large R factor (42) unless the effective dipole moment is almost zero. Thus Falconer and co-workers concluded that for XeF_6 the central barrier must be quite low in order to make Δ relatively large and thus make R(42) relatively small for reasonable values of "μ". They argued that the possibility of "μ" being almost zero was very unlikely.

By restricting the "inversion" in XeF_6 to occur in only one dimension the molecule has no choice but to tunnel through the central barrier. However, by allowing the motion to take place in the full three dimensions it can reach the other side of the central barrier by pseudorotating around it. The effect of the pseudorotational motion is to allow the presence of a high central barrier while still permitting a large energy separation between "inversion" states. Our conclusion for XeF_6 is that the pseudorotation is either completely

free or slightly hindered, because if the angular barriers were quite large then the pseudorotational "inversion" multiplets would be very small, leading to a very large R(41d) factor.

Falconer and co-workers[70] derived the following expression for the upper limit for lack of observation of refocusing in symmetric top molecules with one dimensional inversion

$$\frac{\mu}{\Delta^{1/2}} < .1 \frac{D}{(cm^{-1})^{1/2}} \tag{43}$$

Due to the similarity in the form of the Stark effect among one, two, and three dimensional "inversion" motions we can generalize (43) to

$$\frac{\mu}{\Delta E_I^{1/2}} < .1 \frac{D}{(cm^{-1})^{1/2}} \tag{44}$$

where ΔE_I is the doublet separation in the one dimensional inversion and is related to the pseudorotational constant in the two and three dimensional cases. We can use Eq. (44) and previous knowledge about ΔE_I (Table 1) to predict a limiting value for "μ". For IF_7 and ReF_7 the value of "μ" corresponds to a lower limit for the actual dipole moment because these molecules focus, while for XeF_6 "μ" is an upper limit because XeF_6 does not focus. The results can be found in Table 2. It is pleasing that the predicted dipole moments (μ_{eff}) are properly bound by the limiting dipole moments ($\mu_{limiting}$) from Eq. (44) (Table 2). We see that for XeF_6 the upper limit for the dipole moment is .4D (low angular barrier case) in agreement with our earlier prediction

that $\mu_{eff} \approx .1D$ with the probable range of μ_{eff} being, $0 \leqslant \mu_{eff} \leqslant .3D$. It is interesting that for IF_7, which focuses weakly, the predicted dipole ($\mu_{eff} = .7D$) is just slightly larger than the lower limit (.63D) which still permits focusing, while for ReF_7, which focuses considerably stronger than IF_7, the predicted dipole ($\mu_{eff} = 1.5D$) is much larger than the lower limit (.59D).

In conclusion, we have derived expressions for the Stark effect in several molecules exhibiting large amplitude internal motions, and have demonstrated semi-quantitatively that these expressions account for the observed focusing behavior of the molecules. We have completely ignored the coupling of rotational and vibrational motion which will undoubtedly be significant for large amplitude motions. However, this additional complication is not required to explain the origin of the focusing effects.

Table 1. Relative focusing strengths of various molecules with large amplitude internal motions.

		μ_{eff}(D)	ΔE_I(cm^{-1})	R (normalized to RNH_3)
NH_3	$E_{o^-} - E_{o^+} = .7\ cm^{-1}$	1.5	.7	1
ReF_7	$B_\phi = 4.4\ cm^{-1}$	1.5	35.2	.02
IF_7	$B_\phi = 5.\ cm^{-1}$	.7	40	.0038
XeF_6 (free pseudorotation)	$B_{\theta,\phi} = 5.\ cm^{-1}$	.1	40	.000078
XeF_6 (low angular barrier)	$16\|b\| = 1.\ cm^{-1}$	.1	1	.0031

Table 2. Limiting Dipole Moments Based on Equation (44).

	$\Delta E_I (cm^{-1})$	$\mu_{limiting}$ (D)	μ_{eff} (D)
NH_3	.7	.084 (lower limit)	1.5
ReF_7	35.2	.59 (lower limit)	1.5
IF_7	40	.63 (lower limit)	.7
XeF_6 (free pseudorotation)	40	.63 (upper limit)	.1
XeF_6 (low angular barrier)	1	.4 (upper limit)	.1

ACKNOWLEDGEMENTS

I wish to thank Professor Kenneth S. Pitzer, my research director, for suggesting this project and for his continual help and encouragement. I am grateful to the other members of the research group, Janice Kim, Jerry Vogt, Leonard Silvester, and Yoon Lee for extending their friendship to myself and my wife, Ellen.

My appreciation is extented to Professor Kenneth Hedberg and his wife, Dr. Lise Hedberg, for collaborating with Professor Pitzer and myself on the XeF_6 electron diffraction work, and also for making my brief visit to Corvallis (Oregon State University) most enjoyable. Professor W. D. Gwinn and the members of his group have been very kind in supplying me with various computer programs and assisting me with their use. I thank Professor Herbert L. Strauss for many helpful discussions pertaining to my thesis project.

I thank Gloria Pelatowski for preparing the thesis diagrams and also Alice Ramirez and Shirley Ashley for typing the thesis.

I thank all my friends, especially Gary Schwartz, for making our stay in Berkeley enjoyable.

I express my deepest gratitude to my wife, Ellen.

This work was done under the auspices of the U. S. Atomic Energy Commission.

APPENDIX 1.

High Frequency Approximation in Calculating the Mass for the Inversion Motion in $MX_3(C_{3v})$ Molecules

The G-matrix element for the symmetrical stretch (A_1) is

$$G_{11} = \frac{1}{m_x} + \frac{(1+2\cos\alpha)}{m_M} \tag{1}$$

where m_x, m_M are the masses of atoms x, and M respectively, and α is defined in Fig. 4. The G-matrix element for the symmetric bend (A_1) is

$$G_{22} = 2\left(\frac{1+2\cos\alpha}{1+\cos\alpha}\right)\left(\frac{1}{m_x} + \frac{2(1-\cos\alpha)}{m_M}\right) \tag{2}$$

The cross term is

$$G_{12} = -\frac{2(1+2\cos\alpha)(1-\cos\alpha)}{m_M \sin\alpha} \tag{3}$$

The high frequency approximation becomes

$$G^o_{22} = G_{22} - \frac{G^2_{12}}{G_{11}} \tag{4}$$

The inversion mass can now be defined as

$$m_2^{\Delta\alpha} = (G^o_{22})^{-1} \tag{5}$$

APPENDIX 2

High Frequency Approximation in Calculating the Mass for the Exchange Motion in $MX_5(D_{3h})$ Molecules

The relavant G-matrix elements are defined in the following matrix

$$
\begin{array}{c}
 \\ S_5 \\ S_6 \\ S_7
\end{array}
\begin{array}{c}
\begin{array}{ccc} S_5 & S_6 & S_7 \end{array} \\
\begin{pmatrix}
\frac{3}{2m_M} + \frac{1}{m_x} & \frac{3\sqrt{3}}{2} \cdot \frac{1}{m_M} & -\frac{3}{2}\sqrt{2} \cdot \frac{1}{m_M} \\
\frac{3\sqrt{3}}{2} \cdot \frac{1}{m_M} & 3(\frac{3}{2m_M} + \frac{1}{m_x}) & -\frac{3}{2}\sqrt{6} \cdot \frac{1}{m_M} \\
-\frac{3}{2}\sqrt{2} \cdot \frac{1}{m_M} & -\frac{3}{2}\sqrt{6} \cdot \frac{1}{m_M} & \frac{3}{2}(\frac{2}{m_M} + \frac{1}{m_x})
\end{pmatrix}
\end{array}
\qquad (1)
$$

where m_M and m_x are the masses of atoms M and x respectively. The high frequency approximation becomes

$$G^{o}_{77} = \frac{3}{2}\left(\frac{2}{m_M} + \frac{1}{m_x}\right) - \frac{\left(-\frac{3}{2}\sqrt{2}\cdot\frac{1}{m_M} - \frac{3}{2}\sqrt{6}\cdot\frac{1}{m_M}\right)\begin{pmatrix}\frac{9}{2}\cdot\frac{1}{m_M} + \frac{3}{m_x} & -\frac{3}{2}\sqrt{2}\cdot\frac{1}{m_M} \\ -\frac{3}{2}\sqrt{2}\cdot\frac{1}{m_M} & \frac{3}{2}\cdot\frac{1}{m_M} + \frac{1}{m_x}\end{pmatrix}\begin{pmatrix}-\frac{3}{2}\sqrt{2}\cdot\frac{1}{m_M} \\ -\frac{3}{2}\sqrt{6}\ \frac{1}{m_M}\end{pmatrix}}{\left(\frac{3}{2}\cdot\frac{1}{m_M} + \frac{1}{m_x}\right)\left(\frac{9}{2}\cdot\frac{1}{m_M} + \frac{3}{m_x}\right) - \left(\frac{3}{2}\sqrt{3}\,\frac{1}{m_M}\right)^2} \tag{2}$$

This eventually simplifies to

$$G^{o}_{77} = \frac{3}{m_M} + \frac{3}{2}\cdot\frac{1}{m_x} - \frac{9}{m_M}\cdot\frac{\left[\frac{.275}{m_M} + \frac{1}{m_x}\right]}{\left[\frac{m_M}{m_x^2} + \frac{3}{m_x}\right]} \tag{3}$$

The reduced mass for the exchange motion is therefore

$$m_7 = (G^{o}_{77})^{-1} \tag{4}$$

APPENDIX 3

Wave Functions of a Two Dimensional Isotropic Harmonic Oscillator

It is well known that solutions of the quadratic potential

$$V = a\rho^2 \tag{1}$$

can be expressed as

$$\Psi = R_{nK}(\rho)\, e^{\pm im\theta} \tag{2}$$

where the following conditions apply to m, n, K

$$n, m, K = 0, 1, 2, \ldots \tag{3a}$$

$$n = m + 2K \tag{3b}$$

The relation (3b) can be expressed in tabular form as

Dengeneracy	n	m	K
1	0	0	0
2	1	1	1
3	2	2	0
	2	0	1
4	3	3	0
	3	1	2

APPENDIX 4

High Frequency Approximation in Calculating the $T_{1u}(S_4)$ Mass

The relevant G-matrix is

$$\begin{array}{c} \\ S_3 \\ S_4 \end{array} \begin{array}{c} \begin{array}{cc} S_3 & S_4 \end{array} \\ \begin{pmatrix} \frac{2}{m_{Xe}} + \frac{1}{m_F} & \frac{4}{m_{Xe}} \\ \frac{4}{m_{Xe}} & \frac{8}{m_{Xe}} + \frac{2}{m_F} \end{pmatrix} \end{array} \tag{1}$$

where m_{Xe} is the mass of the xenon (Xe) atom and m_F is the mass of a fluorine atom (F). The high frequency approximation becomes

$$G^o_{44} = \frac{8}{m_{Xe}} + \frac{2}{m_F} - \frac{16m_F}{2m_{Xe}m_F+m^2_{Xe}} \tag{2}$$

The reduced mass (m_4) for the $T_{1u}(S_4)$ distortion coordinate is

$$m_4 = (G^o_{44})^{-1} \tag{3}$$

which for XeF_6 has the value m_4 = 6.56 amu.

REFERENCES

1. U. Öpik, M. H. L. Pryce, Proc. Roy. Soc. A., 238, 425 (1957).
2. H. C. Longuet-Higgins, U. Öpik, M. H. L. Pryce, Proc. Roy. Soc. A., 244, 1 (1958).
3. J. H. Van Vleck, J. Chem. Phys., 7, 72 (1939).
4. W. L.Clinton, B. Rice, J. Chem. Phys., 30, 542 (1959).
5. R. G. Body, D. S. McClure, E. Clementi, J. Chem. Phys., 49, 4916 (1968).
6. J. M. Lehn, B. Munsch, Chem. Comm., 1327 (1969).
7. C. M. Humphries, A. D. Walsh, P. A. Warsop, Disc. Faraday Soc., 35, 148 (1963).
8. A. E. Douglas, Disc. Faraday Soc., 35, 158 (1963).
9. M. Halmann, J. Chem. Soc., 2853 (1963).
10. T. Shimanouchi, I. Nakagawa, J. Hiraishi, M. Ishi, J. Mol. Spectry., 19, 78 (1966).
11. E. B. Wilson, Jr., J. Chem. Phys., 9, 76 (1941).
12. Kazuo Nakamoto, Infrared Spectra of Inorganic and Coordination Compounds (John Wiley and Sons, Inc., New York, 1963), App. II, p. 265.
13. G. DeAlti, G. Costa, V. Galasso, Spectrochim. Acta, 20, 965 (1964).
14. M. F. Manning, J. Chem. Phys., 3, 136 (1935).
15. J. D. Swalen, J. A. Ibers, J. Chem. Phys., 36, 1914 (1962).
16. R. R. Newton, L. H. Thomas, J. Chem. Phys., 16, 310 (1948).
17. H. Selig, A. Reis, E. L. Gasner, J. Inorg. Nucl. Chem., 30, 2087 (1968).
18. H. Selig, J. H. Holloway, J. Tyson, H. H. Claassen, J. Chem. Phys., 53, 2559 (1970).

19. Joseph B. Mann, Atomic Structure Calculations (I), LA-3690, July 1967.

20. T. R. Dyke, A. A. Muenter, W. Klemperer, W. E. Falconer, J. Chem. Phys., 53, 3382 (1970).

21. K. W. Hansen, L. S. Bartell, Inorg. Chem., 4, 1775 (1965).

22. L. C. Hoskins, R. C. Lord, J. Chem. Phys., 46, 2402 (1967).

23. V. H. Siebert, Z. Anorg. Allg. Chem., 265, 303 (1951).

24. G. V. Romanov, V. P. Spiridonov, Zhurnal Strukturnoi Khimii, 7, 882 (1966).

25. G. V. Romanov, V. P. Spiridonov, Vestn. Mosk. Univ. Khim., 5, 7 (1968).

26. S. Berry, M. Tamres, C. J. Ballhausen, H. Johansen, Acta. Chem. Scand., 22, 231 (1968).

27. R. R. Holmes, Sr., R. M. Deiters, J. A. Golen, Inorg. Chem., 8, 2612 (1969).

28. R. S. Berry, J. Chem. Phys., 32, 933 (1960).

29. E. Merzbacher, Quantum Mechanics (John Wiley and Sons, Inc., New York, 1970), p. 213.

30. J. D. Witt, L. A. Carreira, J. R. Durig, J. Mol. Structure, 18, 157 (1973).

31. D. O. Harris, H. W. Harrington, A. C. Luntz, W. D. Gwinn, J. Chem. Phys., 44, 3467 (1966).

32. J. W. Raymonda, W. T. Simpson, J. Chem. Phys., 47, 430 (1967).

33. F. H. Watson, Jr., A. T. Armstrong, S. P. McGlynn, Theoret. Chim. Acta (Berl.), 16, 75 (1970).

34. F. H. Watson, Jr., S. P. McGlynn, Theoret. Chim. Acta (Berl.), 21, 309 (1971).

35. K. S. Pitzer, W. E. Donath, J. Am. Chem. Soc., 81, 3213 (1959).

36. J. E. Kilpatrick, K. S. Pitzer, R. Spitzer, J. Am. Chem. Soc., 69, 2483 (1947).

37. S. Lipson, A. Warshell, J. Chem. Phys., 49, 5116 (1968).

38. J. R. Hoyland, J. Chem. Phys., 50, 2775 (1969).

39. N. L. Allinger, J. A. Hirsch, M. A. Miller, I. J. Tyminski, F. A. Van-Catledge, J. Am. Chem. Soc., 90, 1199 (1968).

40. J. R. Durig, W. Wertz, J. Chem. Phys., 49, 2118 (1968).

41. S. I. Chan, J. Zinn, W. D. Gwinn, J. Chem. Phys., 34, 1319 (1961).

42. T. R. Borgers, J. W. Russell, H. L. Strauss, W. D. Gwinn, J. Chem. Phys., 44, 1103 (1966).

43. T. R. Borgers, H. L. Strauss, J. Chem. Phys., 45, 947 (1966).

44. J. Laane, R. C. Lord, J. Chem. Phys., 47, 4941 (1967).

45. C. S. Blackwell, R. C. Lord, Vibrational Spectroscopy and Structure, edited by J. R. Durig, (Dekker, New York, 1972), and references therein.

46. W. J. Adams, H. J. Geise, L. S. Bartell, J. Am. Chem. Soc., 92, 5013 (1970).

47. R. L. Oakland, G. H. Duffey, J. Chem. Phys., 46, 19 (1967).

48. E. J. Jacob, L. S. Bartell, J. Chem. Phys., 53, 2235 (1970).

49. W. J. Adams, H. B. Thompson, L. S. Bartell, J. Chem. Phys., 53, 4040 (1970).

50. R. K. Khana, J. Mol. Spec., 8, 134 (1962).

51. H. H. Claassen, H. Selig, J. Chem. Phys., 43, 103 (1965).

52. H. H. Eysel, K. Seppelt, J. Chem. Phys., 56, 5081 (1972).

53. H. H. Claassen, E. L. Gasner, H. Selig, J. Chem. Phys., 49, 1803 (1968).

54. H. H. Claassen, G. L. Goodman, J. H. Holloway, H. Selig, J. Chem. Phys., 53, 341 (1970).

55. E. W. Kaiser, J. S. Muenter, W. Klemperer, W. E. Falconer, J. Chem. Phys., 53, 53 (1970).

56. G. Nagarajan, Bull. Soc. Chim. Belg., 72, 276 (1963).

57. Kenneth Hedberg (Chemistry Department, Oregon State University, Corvallis Oregon) private communication. All experimental electron diffraction results for XeF_6 quoted in this thesis are based on Hedberg's results as Bartell has indicated that his sample of XeF_6 was probably contaminated with $XeOF_4$.

58. R. M. Gavin, Jr., L. S. Bartell, J. Chem. Phys., 48, 2460 (1968).

59. L. S. BArtell, R. M. Gavin, Jr., J. Chem. Phys., 48, 2466 (1968).

60. H. H. Claassen, G. L. Goodman, H. Kim, J. Chem. Phys., 56, 5042 (1972).

61. H. Kim, H. H. Claassen, E. Pearson, Inorg. Chem., 1, 616 (1968).

62. S. Y. Wang, L. L. Lohr, Jr., J. Chem. Phys., (to be published).

63. Y. Toyozawa, M. Inoue, J. Phys. Soc. Japan, 21, 1663 (1966).

64. R. D. Burbank, G. R. Jones, Science, 168, 248 (1970).

65. F. Schreiner, D. W. Osborne, J. G. Malm, G. N. McDonald, J. Chem. Phys., 51, 4838 (1969).

66. B. Weinstock, E. Eugene Weaver, C. Piknop, Inorg. Chem., 5, 2189 (1966).

67. T. L. Hill, Introduction to Statistical Thermodynamics (Addison-Wesley Publ. Co., Inc., Readings, Mass., 1960).

68. K. S. Pitzer, J. Chem. Phys., 1, 251 (1939).

69. G. C. Pimental, S. W. Charles, J. of Intern. Union of Pure and Applied Chem., 7, 111 (1963).

70. W. E. Falconer, A. Büchler, J. Stauffer, W. Klemperer, J. Chem. Phys., 48, 312 (1968).

71. G. L. Goodman, J. Chem. Phys., 56, 5038 (1972).

72. A. Büchler, J. L. Stauffer, W. Klemperer, L. Wharton, J. Chem. Phys., 39, 2299 (1963).

73. R. A. Berg, L. Wharton, W. Klemperer, A. Büchler, J. L. Stauffer, J. Chem. Phys., 43, 2416 (1965).

74. C. J. H. Schutte, The Wave Mechanics of Atoms, Molecules, and Ions (Edward Arnold, Ltd., London, 1968), Chaps. III, IV.

75. M. E. Rose, Elementary Theory of Angular Momentum (John Wiley and Sons, Inc., New York, 1967), Chap. IV.

LEGAL NOTICE

This report was prepared as an account of work sponsored by the United States Government. Neither the United States nor the United States Atomic Energy Commission, nor any of their employees, nor any of their contractors, subcontractors, or their employees, makes any warranty, express or implied, or assumes any legal liability or responsibility for the accuracy, completeness or usefulness of any information, apparatus, product or process disclosed, or represents that its use would not infringe privately owned rights.

TECHNICAL INFORMATION DIVISION
LAWRENCE BERKELEY LABORATORY
UNIVERSITY OF CALIFORNIA
BERKELEY, CALIFORNIA 94720